NASA
Technical Memorandum 103184

AVSCOM
Technical Memorandum 89-C-007

Current Research in Cavitating Fluid Films

Edited by

D.E. Brewe
Propulsion Directorate
U.S. Army Aviation Systems Command
Lewis Research Center
Cleveland, Ohio

J.H. Ball
Waukesha Bearings Corp.
Waukesha, Wisconsin

and

M.M. Khonsari
University of Pittsburgh
Pittsburgh, Pennsylvania

Prepared for the
Cavitation Symposium—1988 Society of Tribologists and Lubrication Engineers Annual Meeting
Cleveland, Ohio, May 9-12, 1988

NASA

US ARMY AVIATION SYSTEMS COMMAND
AVIATION R&T ACTIVITY

CURRENT RESEARCH IN CAVITATING FLUID FILMS

Edited by

D.E. BREWE, STLE Member
U.S. Army Propulsion Directorate
NASA Lewis Research Center
Cleveland, Ohio 44135

J.H. BALL, STLE Member
Waukesha Bearings Corporation
Waukesha, Wisconsin 53187

M.M. KHONSARI, STLE Member
Dept. of Mechanical Engineering
University of Pittsburgh
Pittsburgh, Pennsylvania 15261

ABSTRACT

The 1988 STLE Annual Meeting held a two-session symposium on cavitation in fluid films. This paper is an edited review of the current research as discussed by the invited participants. Phenomena and experimental observations included gaseous cavitation, vapor cavitation, and gas entrainment. Cavitation in flooded, starved, and dynamically loaded journal bearings, as well as squeeze-film dampers was reviewed. Observations of cavitation damage in bearings and the possibility of cavitation between parallel plates with microasperities were discussed. The session on theoretical modeling summarized the transcavity fluid transport process, meniscus motion, and geometry, or form, of the film during rupture and reformation. Performance effects were related to heat-transfer models in the cavitated region and hysteresis influences on rotor-dynamic coefficients. Contributors presented a number of cavitation algorithms together with solution procedures using the finite-difference and finite-element methods. Although Newtonian fluids were assumed in most of the discussions, the effect of non-Newtonian fluids on cavitation was also discussed.

INTRODUCTION

This paper is a survey of the state-of-the-art in research in cavitating fluid-film bearings and seals based on a symposium held at the STLE Annual Conference in Cleveland, Ohio, in May 1988. The purpose of this article is to discuss the fundamental issues, experimental observations, theoretical modeling techniques, and further research needed in this field. It is hoped that this paper can serve as a reference publication for both the experienced researcher and those who are becoming interested in this area. Nevertheless, this article is not a general review paper, as it is largely based on the viewpoints of the participants in the symposium. Each participant provided a short position paper covering his presentation from which the editors have drawn freely.

This article is divided into three parts. In the first part, we present experimental results to provide the reader with the observed phenomena as well as some of the pertinent measurements; the second part of the paper deals with theoretical modeling techniques. Part III consists of the editor's summary.

In the text that follows, different types of cavitation are described:

Gaseous Cavitation

The lubricating oil often contains some dissolved air and/or other gases. It is, therefore, likely that these gases could come out of the solution if the fluid pressure falls below the saturation pressure of the dissolved gases (nearly atmospheric pressure). This type of cavitation is called gaseous cavitation. In journal bearings under steady-state conditions, one would generally expect gaseous cavitation to take place in the divergent region where the mating surfaces tend to pull the lubricant apart, thus creating the condition in which the gases could emerge from the solution and give rise to "atmospheric pressure". Side entrainment is another manifestation of gaseous cavitation when bubbles at the ambient pressure of the sides are drawn into the negative pressure regions of the bearing.

Vapor Cavitation

If the local pressure of the fluid coincides with that of the vapor pressure, then the boiling of the fluid by pressure reduction causes the formation of a so-called vapor cavitation. This type of cavitation normally occurs in dynamically loaded bearings used in common machinery.

Understanding the mechanism of the formation and collapse of cavitation bubbles is of fundamental importance since it is known to affect the performance of the bearing. Furthermore, it is the vapor cavitation that is known to be harmful as the bubbles violently collapse against the bushing surfaces, resulting in cavitation damage.

CONTENTS

	Page
PART I -- FUNDAMENTAL AND EXPERIMENTAL OBSERVATION	1
Nomenclature to Part I	3
Experimental Studies in Cavitation H. Heshmat	4
Cavitation in Journal Bearings and Squeeze Film Dampers: Experimental B. Jacobson	9
Categorization of Cavitation Types and Onset Conditions D.W. Parkins	11
Cavitation in Microsperity Lubrication A.O. Lebeck	15
Cavitation Erosion Damage in Engine Bearings F.A. Martin	17
References to Part I	21
PART II -- THEORETICAL MODELING AND PERFORMANCE	23
Introduction	25
Nomenclature to Part II	27
Development and Evaluation of a Cavitation Algorithm T.G. Keith and D. Vijayaraghavan	29
Fundamental Issues Concerning the Moving Boundary Coda H.T. Pan and Jean Frene	34
Geometry and Motion of the Meniscus Jean Frene, Luc Launay, and Coda H.T. Pan	37
Classic Cavitation Models for Finite Element Analysis J.F. Booker	39
Mathematical Models and Related Algorithms in Cavitation Problems C. Bayada, M. Chambat, M. El Alaoui	41
Non-Newtonian Effects in Film Cavitation A.Z. Szeri, K.R. Rajagopal, and Zhang	43
Cavitation Modeling for Analysis of Fluid Film Journal Bearings L.E. Barrett and L.A. Branagan	47
A Model for Cavitation in Dynamic Systems John A. Tichy and C.P. Ku	49
The Influence of Cavitation on Journal-Bearing Rotordynamic Characteristics M.L. Adams	52
Cavitation in Journal Bearings and Squeeze-Film Dampers: Analytical B. Jacobson	54
References to Part II	57
PART III -- EDITORS SUMMARY	61

PART I

FUNDAMENTAL AND EXPERIMENTAL OBSERVATION

NOMENCLATURE

b	Pad width, m
C	Bearing radial clearance, m
D	Bearing diameter, m
d	Depth of oil, m
e	Eccentricity, m
F	Force, N
f	Frequency of load (Hz), s^{-1}
G	Duty parameter, [μUb/W]
h	Film thickness, m
h_a	Amplitude of oscillation, m
L	Length of bearing in z-direction, m
N	Shaft rotational frequency, rev/min
P	Unit loading (W/LD)
p_s	Oil supply pressure, m^3/s
Q	Volumetric oil flow, m^3/s
$\overline{Q}$	Q/(0.5 UCL)
R	Bearing or journal radius, m
t	Time, s
U	Linear velocity, m/s
u	Velocity of the fluid in the circumferential direction, m/s
W	Load on bearing, N
x	Coordinate in circumferential direction, m
y	Coordinate in radial or normal direction, m
y_o	Initial film thickness, m
z	Coordinate in axial direction, m
β	Fluid film arc, rad
ε	Eccentricity ratio of bearing (e/c)
θ	Coordinate in plane of rotation, rad
θ_o	Angle of line of centers, rad
μ	Viscosity, Ns/m^2
μ_t	Coefficient of friction
σ	Shear stress, N/m^2
τ	Period of dynamic load, s
φ	Attitude angle, $(\theta_o - \pi)$, rad
ω	Angular velocity of shaft, rad/s

Subscripts:

B	Beginning of bearing pad
d	Dynamic
E	End of bearing pad
F	Full fluid film
min	Minimum
S	Starvation
s	Static, supply
st	Steady
1	Start of fluid film
2	End of fluid film

EXPERIMENTAL STUDIES IN CAVITATION

H. HESHMAT[1]

The experiments cited here deal primarily with the flow and formation of oil streamlets in cavitated regions.

FLOODED BEARINGS

Consider Fig. 1, which depicts a hydrodynamic journal bearing. As shown, the fluid film ends at θ_2 after which it cavitates; the space at $\theta > \theta_2$ is filled with oil streamlets, released gasses, ambient air, and possibly oil vapor. In the absence of hydrodynamic positive pressures in the region $\theta_2 - \theta_E$, the amount of flow (θ_2) leaving Q_2 remains constant at all $\theta > \theta_2$. If one observes the cavitation region through the bearing t ansparent shell, one sees fluid film streamlets in the manner shown in view B of Fig. 1. A sample of such experimentally observed streamlets seen through a transparent bearing shell is shown in Fig. 2 (cf. (1)). This figure reveals that the oil adhering to the stationary surface is in narrow strips. The fluid film emerging from a cavitated region beyond the physical end of the pad θ_E is shown in Fig. 3. The pattern of ridges and troughs indicates that next to the shaft is a sublayer of fluid that completely covers the rotating shaft. This is unlike the stationary surface. The fluid as it emerges from the bearing pad does not leave the shaft but adheres to it even when the film is not restrained by an upper bearing surface but is open to the atmosphere. The streamlets thus will adhere to the shaft even when they cross an oil groove. The streamlets emerge at the top of the picture from a cavitated zone and cross an axial groove before entering the downstream pad. As seen, neither the axial distribution nor the individual width of the streamlets changes in crossing the groove, thus indicating adhesion of the entire flow (Q_2) to the moving surface.

The above discussion suggests that the shape of the fluid film in the cavitated region is in the form depicted in Fig. 4. The fluid adheres in thin strips to the stationary surface, but forms a continuous sublayer on the moving surface. This pattern prevails as long as there is an upper pad and a thin spacing gap between shaft and bearing surface. Upon termination of the pad, the tips detach, and the entire flow (Q_2) adheres to the shaft in the manner shown in Fig. 3. This "detached pattern" also prevails in the oil groove, whose dimensions are two to three orders of magnitude larger than the thickness of the film layer and is thus equivalent to an open space. The detached pattern reveals that there is a very weak bond between moving streamlets and stationary surface, permitting side entrainment of gas to take place in cavitated regions.

[1]Mechanical Technology, Inc., Latham, NY.

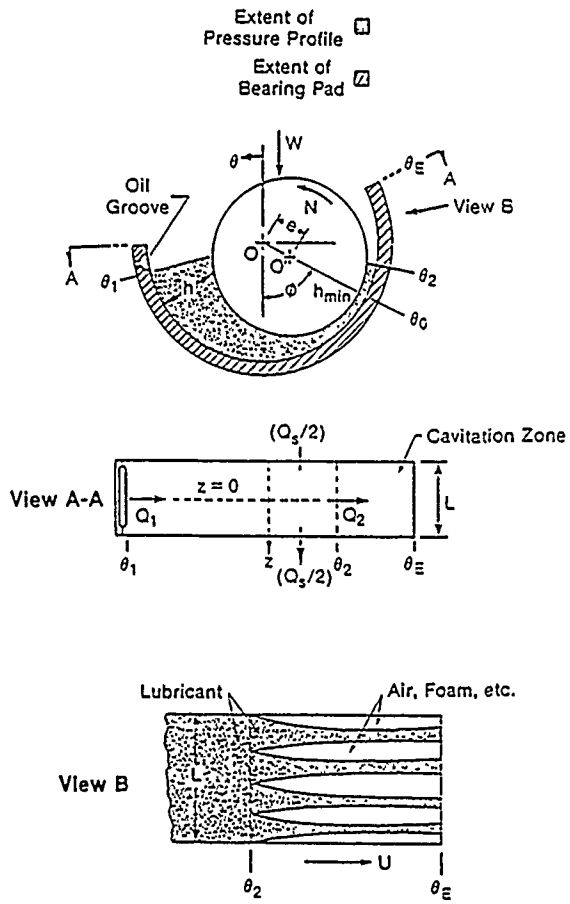

Fig. 1. - Cavitation in journal bearings.

TEMPERATURE EFFECTS

The next topic pertains to the temperatures of the hot layer (Q_2). Numerous tests have shown that the temperatures of the fluid film in the cavitated region are more or less constant. This is true despite seemingly further energy dissipation, which takes place due to viscous shear over the extent of the cavitated region. Figure 5 shows, for five sets of experimental operating conditions, that the temperatures of the cavitated region remained constant even though this region extended over nearly 80°. A possible explanation for this phenomenon is that the entrainment of ambient air separates the fluid from the bearing surface and causes less heat conduction to the thermocouples; i.e., thermocouple tips are exposed to gas rather than hot oil. A partial explanation has also been given in terms of released gases and oil vaporization, which requires high enthalpies. However, even in cases where the subambient pressure is not low enough to cause oil vaporization, a constant temperature has been observed. To this end, the

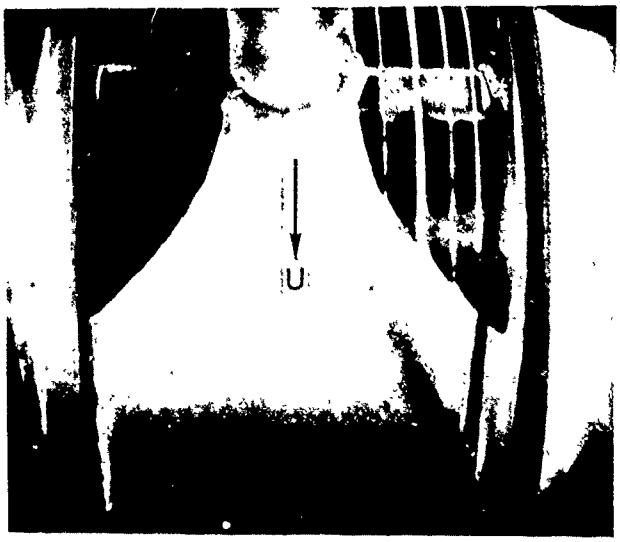

L/D = 1; N = 1000 rpm; P = 60 psi
$(C/R) = 2 \times 10^{-3}$; P_s = 0.5 psi

Fig. 2. - Flow of oil streamlets over groove.

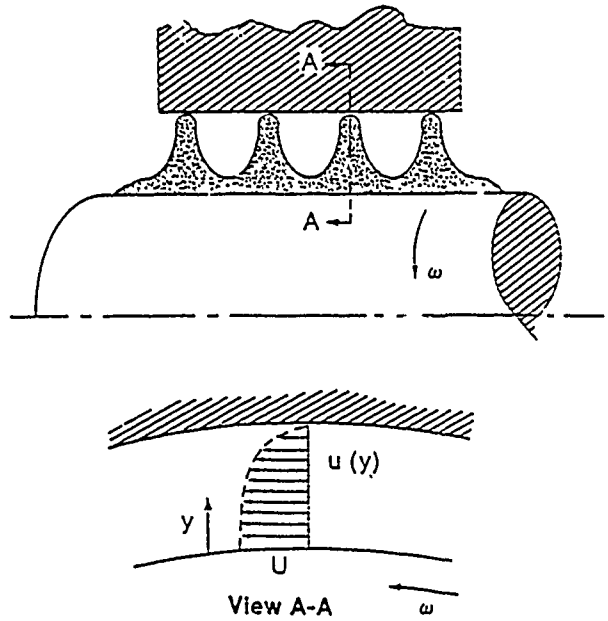

Fig. 4. - Oil streamlets in cavitated regions or journal bearings.

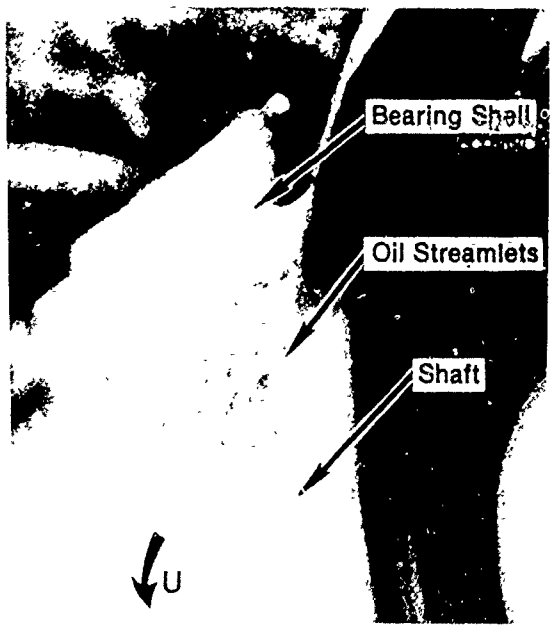

D × L × C = 5.4375 × 5.4375 × 0.0055 in.
N = 1800 rpm; P = 100 psi; P_s = 0.1 psi

Fig. 3. - Adhesion of oil streamlets to rotating shaft.

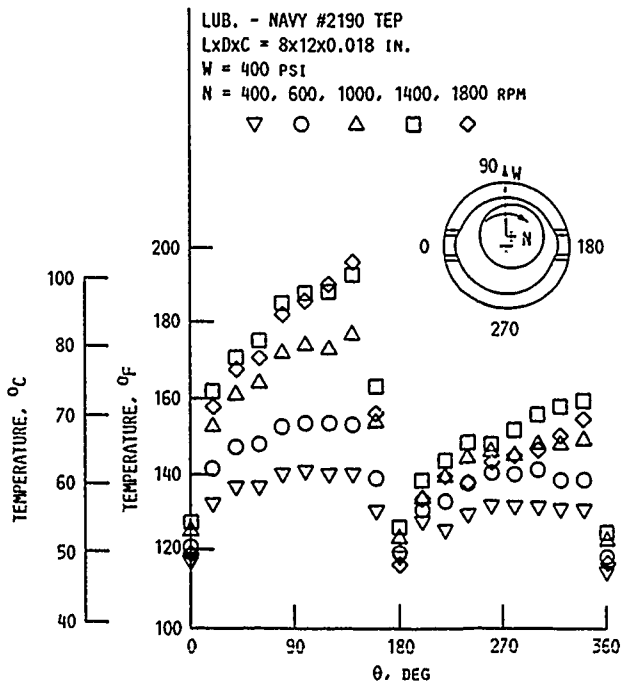

FIGURE 5.

Fig. 5. - Constant temperatures in cavitated regions; P = 2.76 MPa.

shape of the fluid film as postulated in Fig. 4 offers an explanation of the role of gas entrainment and constancy of temperature in the cavitated region. The lower part of Fig. 4 shows the transverse velocity distribution in the oil streamlets. As seen, most of the oil moves with a velocity very near the journal speed (U); the principal strain thus occurs near the stationary surface. Since the power dissipation is related to the stress $\sigma = \omega(du/dy)$ at the moving surface and since, here $(du/dy) = 0$, the losses would be negligible. Consequently, there would be no rise in temperature.

To show that oil generally adheres to the moving surface, a series of tests was conducted with a tapered-land thrust bearing with reverse rotation. The apparatus and the experimental procedures are described by Heshmat (2). The test bearing was instrumented with pressure taps and thermocouples to monitor the fluid film pressure as well as temperature. Rotation was opposite to the customary direction so that only the flat portion was loaded. Figure 6 gives some of the results obtained with this series of tests. The noteworthy points pertinent to the cavitation are the following:

1. The pressure cap (located at the center of the flat portion of the pad) response attests to the presence of a hydrodynamic film, not boundary lubrication over the pad at the onset.

2. In the diverging portion of the film, the temperatures actually tend to drop (Fig. 6). This further supports the view that, in the diverging film with cavitation, temperature rise is negligible because of the negligible power losses mentioned earlier. Furthermore, the end flow and streamlets in the cavitation region - induced by the diverging wedge configuration - basically adhere to the moving surface independent of surface geometry (journal or flat collar).

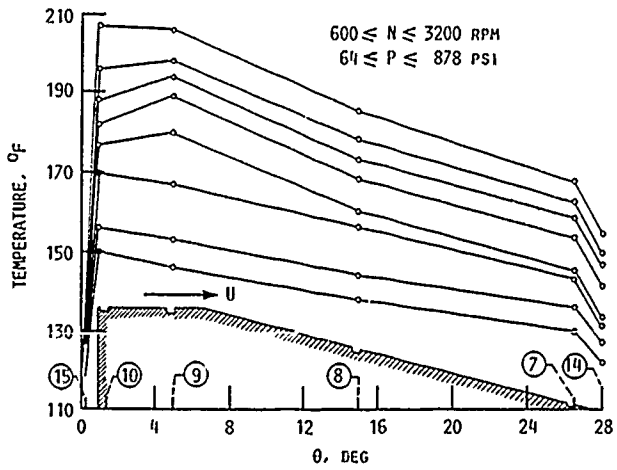

Fig. 6. - Temperature profiles in a flat, divergent bearing.

STARVED BEARINGS

An experimental study documenting the performance of journal bearings for conditions ranging from full hydrodynamic lubrication to states of extreme lubricant starvation is described by Heshmat and Pinkus (3). The effects of an incomplete fluid film on the extent of the film and the formation of cavitation will be reviewed here as functions of the amount of lubricant available to the bearing.

Figure 7 presents the hydrodynamics of a starved bearing vis-a-vis a full film or flooded condition. For a fixed speed and supply oil temperature, the deviations of a starved bearing from one operating with a full fluid film are as follows:

1. The film starts later and terminates earlier, i.e, $\theta_1 > \theta_{1F}$ and $\theta_2 < \theta_{2F}$, producing, in essence, something similar to a partial bearing - though the upstream, and sometimes also the downstream, boundary conditions are different.

2. The decrease in the fluid film extent in starved bearings is shown in Fig. 8 and is pretty close to the theoretical values reported elsewhere. The start and end of the film was ascertained by means of pressure probes which located the points of the commencement and termination of the hydrodynamic pressures.

3. The behavior of the fluid film in the starvation zone ($\theta_B - \theta_1$) was observed via a transparent bearing shell. Its appearance is

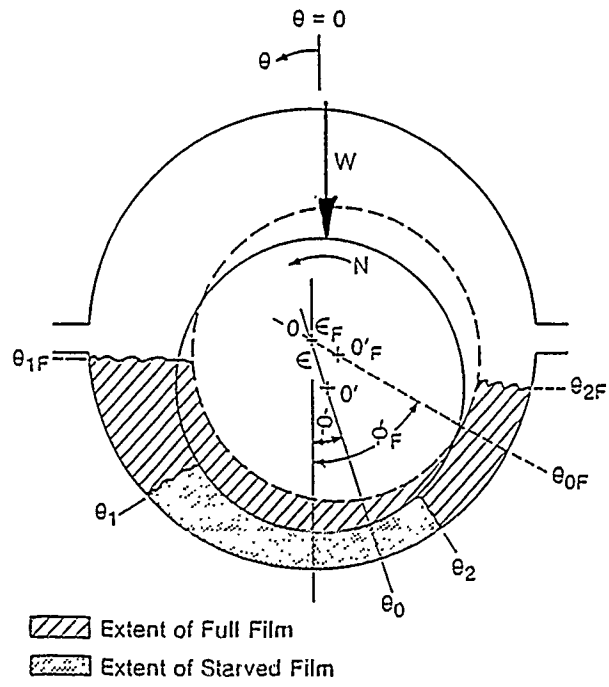

Fig. 7. - Full and starved fluid films.

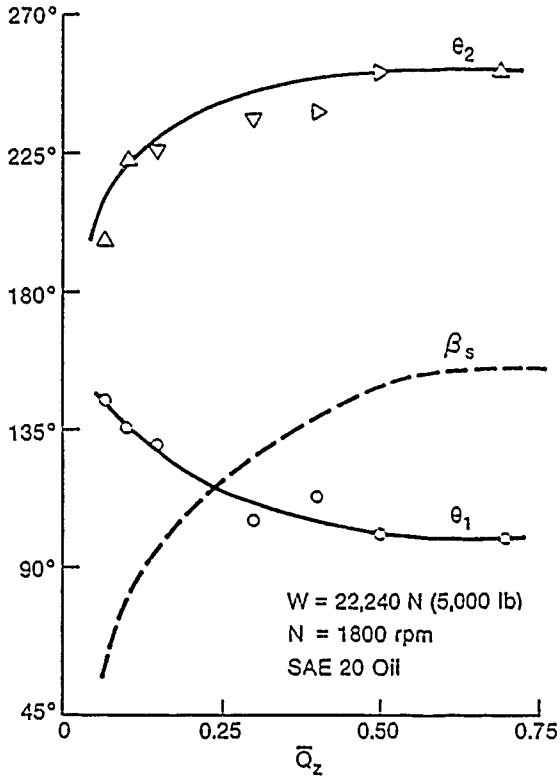

Fig. 8. - Extent of fluid film in starved bearings.

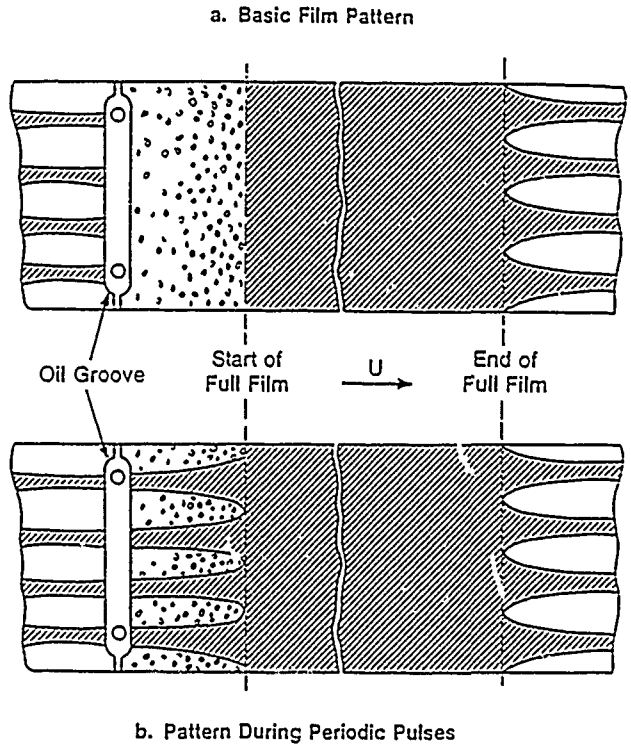

Fig. 9. - Fluid film pattern in starved bearings.

sketched in Fig. 9. As seen, the full film under starved conditions started at more or less a constant angle, $\theta_1 \approx \theta_{1F}$ and did not vary along z. The starved zone between the start of the pad and θ_{1F} underwent cyclic changes in appearance. Most of the time, the zone $\theta_B \leqq \theta \leqq \theta_1$ was filled with an amorphous mixture of oil, foam, and gas bubbles (Fig. 9(a)). However, every 0.5 to 1.0 s, a pulse, originating from the cavitated zone downstream ($\theta > \theta_2$), transformed this region into a pattern of oil streamlets (Fig. 9(b)) similar to the conventional downstream cavitation. The pulse frequency was checked against the journal's rotational frequency, but no relation nor connection was found between them. However, the pulsating streamlets and their frequency were related to the degree of starvation. The higher the degree of starvation, the longer the period of pulse frequency.

4. The upstream portion of the starved bearing $\theta_B \geqq \theta \geqq \theta_1$ filled with an oil and gas mixture is shown schematically in Fig. 9(a). Although gaseous bubbles were visible through the transparent bearing, they disappeared in the film and had no effect on the streamlets' patterns in the cavitated zone.

Based on these observations, the model provides a reasonably accurate prediction as given in the literature (1,4-6).

DYNAMICALLY LOADED BEARINGS

Film rupture in dynamically loaded bearings has been experimentally observed (7-24) to occur in two general patterns: (1) film rupture always exists through the load cycle, and (2) occurrence and disappearance of the film rupture are repeated every load cycle. In the case of a nutating squeeze-film damper, the ruptured film travels circumferentially ahead of the minimum film thickness (25).

Recent studies by Nakahara et al. (18), Nakai et al. (14), and Natsumeda and Someya (26), all of whom used special pressure transducers (semiconductor strain gauge type) mounted in the test journal and bearing, report the existence of a sharp negative pressure except under a lightly loaded condition. Negative pressure (tensile) up to -1.2 MPa, as shown in Fig. 10, was reported by Natsumeda and Someya et al. (26). It is concluded that the heavier the dynamic load, the greater the negative pressure. Such a large value has been scarcely reported by others. Dyer and Reason (11) reported tensile stress with a maximum value of 0.64 MPa. However, their experimental results showed that the magnitude of tensile stress decreases as the eccentricity ratio is increased. Nakahara et al. (18) concluded from their experiments that cavity pattern changes were caused by the cavity growth due to the diffusion of dissolved gas in oil under constant speed. Furthermore, as reported recently by Walton et al. (25),

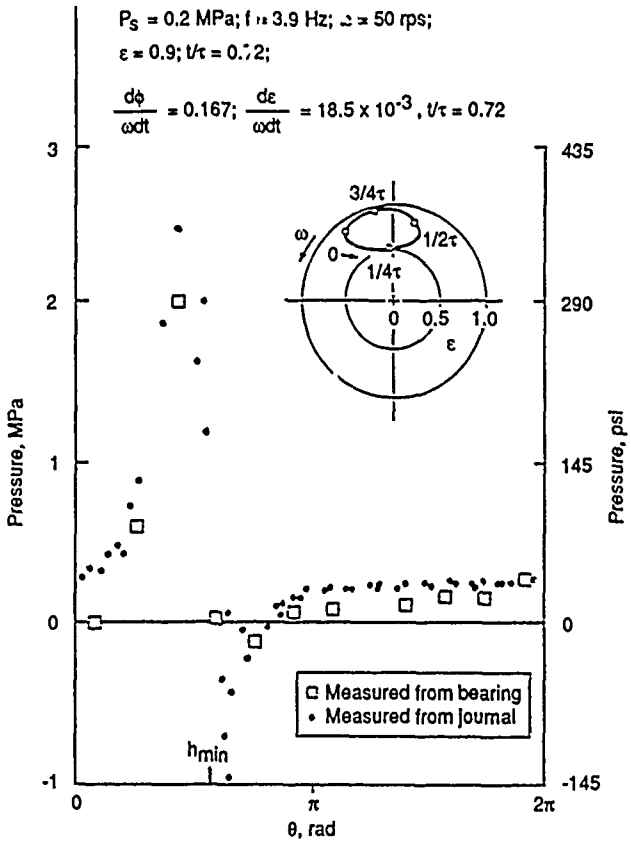

Fig. 10. - Circumferential pressure distribution of journal bearing under dynamic load (26).

cavity patterns changed with the change of cavity locations. Both subcavity pressure and radial flow resistance across the circumferential groove changed discontinuously (traveling pressure wave up to five times that of supplied pressure).

Depending on the apparatus and test operating conditions, five or more modes of transitional phenomena with cavity change were categorized by the investigators. Various boundary conditions have been used to predict dynamically loaded bearing performance. These are Sommerfeld conditions for light load, Reynolds conditions for heavy load, separation boundary condition for detecting tensile stress in the oil-film region downstream of the minimum film thickness position, and others in order to suit the fulfillment of the experimental data pattern. While the agreement between analysis and test is of the right order of magnitude (depending on the test and boundary conditions assumed) in predicting the extent of the film rupture zone, analysis does not adequately reflect the noted variations in the boundary conditions observed and does not account for the change in the shape of the film rupture zone with increasing speed.

In a review of experimental results described by Walton et al. (25), pressure variations in the damper grooves exhibited significant flow reversals (circumferential feed and drain grooves in the sealed squeeze film damper). Also, the grooves, instead of being full of oil, appeared to experience film rupture, which contradicts the boundary condition assumption that the groove acts as a large sink. The flow fluctuations in the damper oil grooves, while not fully explainable, do affect damper performance and various stages of cavitation formation.

It is believed that side entrainment of gas takes place in most of those tribological test apparatus and sets up various cavitation configurations. These discrepancies could be attributed, at least partially, to the differences in the interpretation of the various observations.

CONCLUDING REMARKS

Based on the review of the literature and results of an experimental investigation, the following remarks are made:

1. Side entrainment of the surrounding gas to the bearing gap at the downstream position is conceivable.

2. The shape of the fluid film in the cavitated region is in the form given by Fig. 4. The fluid adheres by means of weak thin strips to the stationary surface, but forms a continuous sublayer on the moving surface. This pattern prevails as long as there is an upper pad. Upon termination of the pad, the tips detach, and the entire exit flow adheres to the moving surface. In this region there would be no rise in temperature.

3. Negative pressure (tensile stress) has been detected experimentally on the order of 1.2 MPa (absolute).

4. To fully understand and explain a sharp dent of negative pressure, one needs to consider the lubricant as a two-phase liquid consisting of oil and bubbles of gas and to take into account the surface-dilation effect of the surface tension together with tensile strength of the film in the governing equation of motion.

5. Under dynamic conditions, other types of pressure distributions exist and further experimentation and exploration are needed to quantify the nature of the formation of film rupture.

6. Careful pressure measurements (from moving and stationary surfaces) of both the statically and the dynamically loaded journal bearing (although it is a difficult task) should be complemented by film temperature measurements in order to elucidate some of the unresolved aspects of cavitation.

CAVITATION IN JOURNAL BEARINGS AND SQUEEZE FILM DAMPERS: EXPERIMENTAL

B. JACOBSON[2]

EXPERIMENTAL INVESTIGATIONS

In nonstationary bearings, where the minimum film thickness moves during vibration, vapor cavitation can appear. This type of cavitation is a breakage of the oil or oil-bearing interface caused by tensile stresses in the lubricant. It can appear anywhere in the oil film -- not just at the outlet where the film thickness is increasing in the direction of the sliding speed.

Vapor cavitation has recently been studied by Jacobson and Hamrock (27,28) and Brewe et al. (29-31) experimentally, theoretically, and numerically. The experiments show that the cavitation is influenced by the vibration amplitude, the vibration frequency, and the sliding velocity in the bearing. The clear influence of the surface energy of the bearing surfaces is also apparent; cavitation seems to start at the bearing surface, if it is made of PTFE (polytetrafluoroethylene), or in the middle of the film, if the surface is made of steel or PMMA (polymethylmethacrylate).

In experiments vapor cavitation occurs when the tensile stress applied to the oil exceeds the tensile strength of the oil or the binding of the oil to the surface. The physical situation necessary for vapor cavitation to occur is a squeezing motion within a bearing. This implies that the minimum film thickness is constantly changing in size and location as a result of the motion tangential and normal to the surfaces.

Experiments showing vapor cavitation were first made at Luleå Technical University in the Machine Elements Laboratory and later at NASA Lewis Research Center.

The geometry of the two test setups was the same, but the NASA Lewis test apparatus was stiffer and more precise, both in the measures of the bearings and also in the motion of the PMMA tube and the shafts. Figure 11 shows the NASA test apparatus with the high-speed camera and the driving motors for the rotation and vibration motions. The high-speed motion picture camera could take up to 11 000 frames per second with ordinary 16-mm motion picture film. In the experiments here, the framing rates were 1000 and 2000 frames per second.

The test bearing was lubricated by gravity feed from a can placed approximately 600 mm above the bearing. The test lubricant was a nondegassed Dexron II automatic transmission fluid with a viscosity of 0.066 N·s/m^2 under atmospheric conditions. The lubricant passed from the can, through

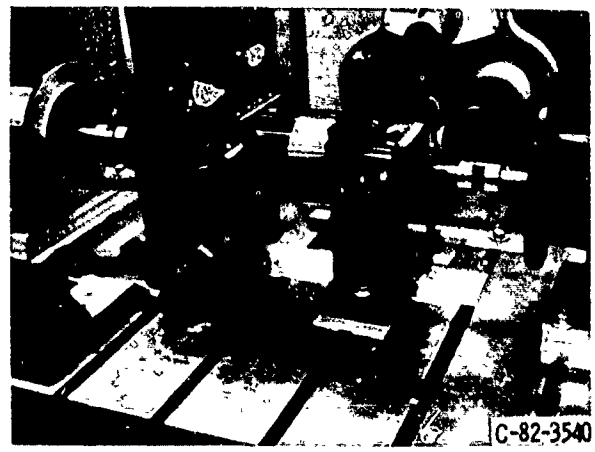

Fig. 11. - Test apparatus.

a line and entered the bearing at the top left of the PMMA bearing (Fig. 11). On the right of the test bearing is the motor that gives the sliding velocity to the roller, and on the left is the motor that gives the squeeze velocity to the bearing. The speeds of these identical 0.5 kW motors can vary continuously from 0 to 250 rad/s.

Figure 12 shows the PMMA bearing, which can vibrate in a circular motion keeping the axis of vibration parallel to the axis of rotation. A special mechanism was manufactured to keep the centerlines of the bearing and shaft parallel and is also shown in this figure.

The dynamic eccentricity mechanism can be adjusted to give dynamic eccentricity ratios between 0 and 1 or in actual measures from 0 to 0.5 mm. The static eccentricity ratio is set by moving the motor with the shaft horizontally so that the centerlines of the two motors are offset.

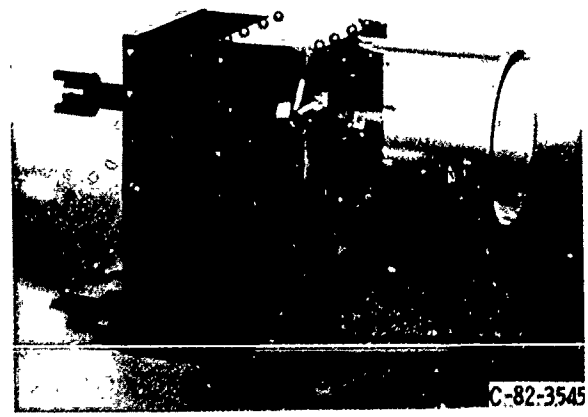

Fig. 12. - PMMA-tube and eccentric.

[2]Chalmers University of Technology, Goteborg, Sweden, and SKF Engineering and Research Centre, Nieuwegein, The Netherlands.

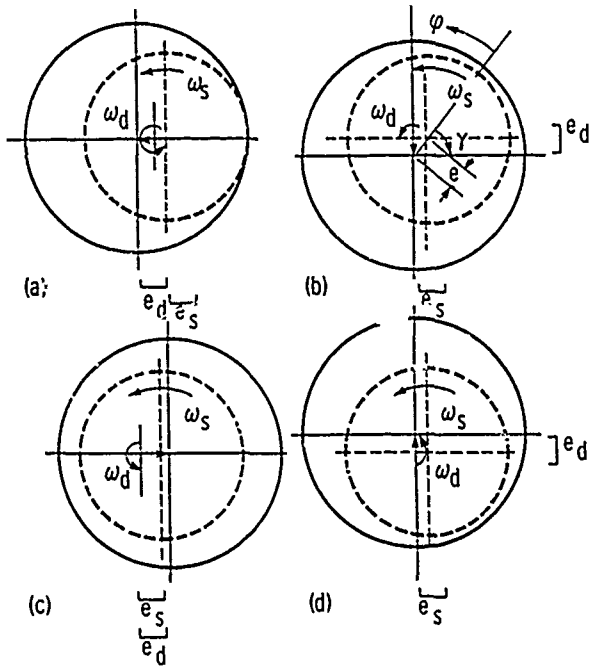

Fig. 13. - Bearing geometries at four different times; $\varepsilon_s = 0.4$; $\varepsilon_d = 0.6$

The static eccentricity can be between 0 and 0.5 mm. The offset of the center of vibration from the center of the journal gives a static load, and the amplitude of vibration can be varied.

Figure 13 shows four positions of the journal relative to the bearing for a dynamically loaded journal bearing. The static eccentricity ratio ε_s is set at 0.4, and the dynamic eccentricity ratio ε_d is set at 0.6.

EXPERIMENTAL RESULTS

Figure 14 presents seven frames from the high-speed film showing the formation and collapse of

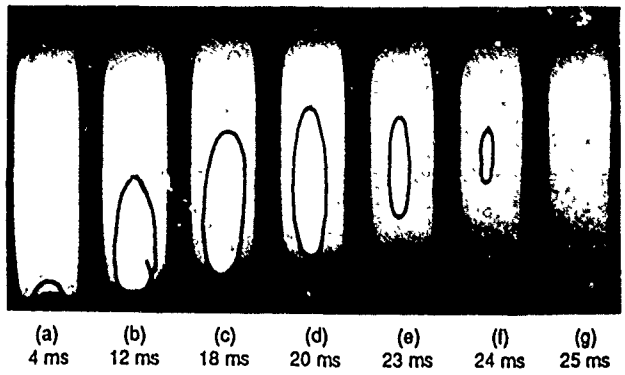

Fig. 14. - Dynamic cavitation bubble developed ($\varepsilon_s = 0.34$, $\varepsilon_d = 0.66$, $\omega_s = 19.5$ r/s, and $\omega_d = 92.7$ r/s).

vapor cavitation in a journal bearing. The experimental conditions in Fig. 14 are length to diameter ratio, 1/4; static eccentricity, 0.34; dynamic eccentricity, 0.66; rotational speed, ω_s, 19.5 rad/s; and vibration speed, ω_d, 92.7 rad/s. The journal surface, was made of PTFE, and the camera framing rate was 2000 frames per second. The time from the first frame to the last frame in Fig. 14 is less than 25 ms, indicating how rapidly the vapor cavitation forms and collapses.

Experiments with steel journals and with PTFE journals show a difference in the cavitation pattern. For steel journals cavitation bubbles start in different parts of the low pressure region, depending on where the largest bubble or dirt particle is located. For PTFE journals, the cavitation seems to start from the same position of the journal for each vibration, which indicates a rupture of the oil-PTFE interface.

The eccentricity ratios have a big influence on the size of the cavitation region and the duration of this region from start to collapse. For small dynamic eccentricities (compared with the minimum oil film thickness), no vapor cavitation is found.

CATEGORIZATION OF CAVITATION TYPES AND ONSET CONDITIONS

D.W. PARKINS[3]

Oil films in dynamically loaded journal bearings are subject to both translatory and oscillatory squeeze motion of their containing surfaces. This discussion deals with oscillatory squeeze motion only. The principal aim of all work described here is to understand squeeze-film phenomena - simplified by removing the translational component. It is important to distinguish sustained oscillatory squeeze motion from "single-shot movements" in which the oil film containing surfaces approach or separate. This paper deals with the former case. Some published work (32,33) deals with oscillatory motion in the frequency range of 1 to 2 Hz and only the transient first few cycles. Other works consider the radial squeeze motion of two circular surfaces, as, for example, in the application of squeeze-film dampers to the outer race of rolling-element bearings. This discussion deals with oscillatory normal motion of parallel surfaces at frequencies in the range likely to be met in machinery, say 5 to 50 Hz, and for fully established behavior.

Two of the important aspects of the more recently identified behavior are

1. A steady force is generated by the oil film subject to normal oscillatory motion of its containing surfaces. The possibility was first suggested by Kauzlarich (34) who gave a theoretical treatment for a circular pad using a liquid lubricant and a harmonic displacement input. He concluded that inertial forces in the fluid created the steady force. Kauzlarich conducted a qualitative experiment to verify this finding. Subsequent experimental work by others (35-37) using nonharmonic oscillatory motion of a square plate has confirmed that such a steady force is generated, and - over a limited range of parameters - determined the influence thereon of the initial oil film thickness, the oscillatory amplitude, and frequency of oscillation. Most recently, Kang (38) used a numerical solution to the Navier-Stokes equation to compute values of the steady force.

2. Various regimes of cavitation appearing in the oil film due to the oscillatory squeeze motion have been identified and characterized, together with the location of the conditions that determine the onset of cavitation. Reference 39 gives an initial classification and Ref. 36 fuller descriptions, all for behavior of an oil film contained in a square plate. Rodriques (40) predicted the growth and collapse of central cavitation patterns in a circular plate. His supporting experiments were conducted at only one frequency, approximately 1.0 Hz - but appear to show cavitation patterns which conform exactly to the characteristics of that which was later (39) defined as regime 2.

[3]Cranfield Institute of Technology, College of Manufacturing, Bedford, MK43 Oal, England.

STEADY FORCE GENERATED BY THE OIL FILM

Figure 15 contains data on the magnitude and direction of the steady force (F_{st}) for eight cases and from three sources (35,36,41). Each source used the same basic equipment, but otherwise worked completely independently. Some curves show data obtained with invariant vibratory amplitude (h_a); one curve shows data obtained with invariant frequency; and one shows amplitude and frequency varying together. The data of Fig. 15 are for initial film thicknesses (y_o) from 0.11 to 0.73 mm, vibratory amplitudes from 0.0055 to 0 5 mm, frequencies from 5 to 50 Hz, three values of viscosity. Two values of oscillating surface area (A) are included. The use of the steady

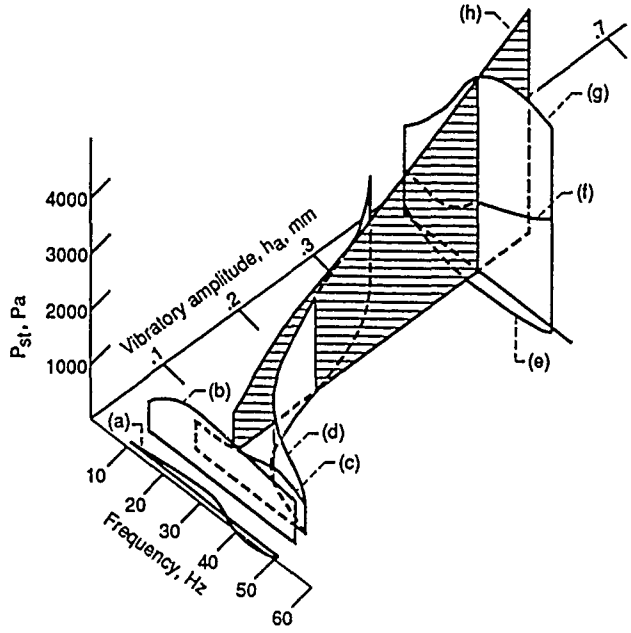

Curve	Ref.	Amplitude of oscillation h_a, mm	Initial film thickness, y_o, mm	Frequency, Hz	Pod area, mm^2	Lubricant kinematic viscosity, CS
(a)	35	0.0055	0.11	10 to 50	625	313
(b)	35	.0275	.11	10 to 50	625	313
(c)	41	.044	.22	20 to 50	2500	750
(d)	41	.044 to .66	.22	10 to 50	2500	313
(e)	36	.4	.73	5 to 45	2500	370
(f)	36	.4	.5	5 to 45	2500	370
(g)	36	.4	.25	5 to 45	2500	370
(h)	36	.07 to .47	.25	25	2500	370

Fig. 15. - Measured steady oil film pressure.

pressure $P_{st} = F_{st}/A$ allows for its effect. Reference 42 gives additional values covering wider ranges. These include data for a third value of oscillatory surface area A and from a fourth source (43,44). It is reassuring to observe that all the curves in Fig. 15 form a coherent pattern, even though they originate from separate sources. It is also reassuring to note that the additional data of Ref. 42 would also fit the coherent pattern if Fig. 15 were vastly extended. However, the data sparsely cover the parameter range. It is analogous to attempting to determine the picture of a jigsaw puzzle when only a few scattered parts are completed. Clearly, there remains the vital task of conducting a complete parametric study over a full range of variables.

Data from Fig. 15 and Ref. 42 show that, depending on conditions, the steady force may either increase or decrease the surface separation. These data also show that the principal influences on the steady force are initial film thickness (y_o), oscillatory amplitude (h_a), and frequency. The steady force varies directly with h_a and inversely with y_o. Cavitation appeared in many of the cases reported.

CAVITATION REGIMES

It is widely established that cavitation may arise in such oscillating squeeze films. Rodriques (40) measured and computed cavitation patterns with a circular plate oscillating at 1 Hz. May-Miller (39,41) identified three cavitating behavioral regimes, which he named regimes 1, 2, and 3. Each regime is characterized by a distinct method of feeding the bubbles and by the location of the bubbles in the displacement and pressure time histories. Extension of the concept (36,45) shows that regime 3 could take several forms. Figure 16 shows a typical displacement and pressure time history with cavitation of an oscillatory cycle for a harmonic force input. The pressure-time history is not harmonic. It shows a rapid increase to maximum pressure followed by a fall to the minimum value. Regime 2 appears in this part of the cycle. A very rapid rise from the minimum pressure to near atmospheric is followed by a relatively long period near atmospheric pressure before the sharp rise again to maximum pressure. Regime 3 appears in this part of the cycle. The near atmospheric shoulder in the pressure curve of Fig. 16 shows a small positive gradient in the versions arising when regime 2 alone appears.

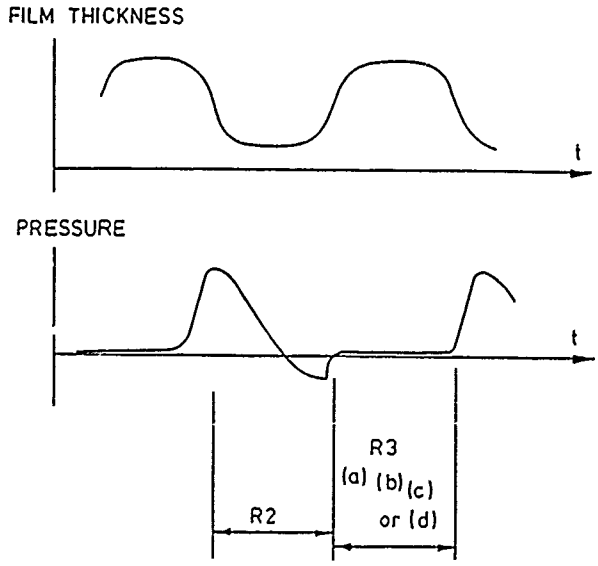

Fig. 16. - Typical oil film thickness and pressure-time history (with cavitation).

The regimes and their subdivisions are

Regime 1. No cavitation at any time in the oscillatory cycle.

Regime 2. Cavitation bubbles fed from within the film. Figure 17 is a photograph of a typical fully developed regime 2 cavitation bubble pattern. The bubbles may contain dissolved gas extracted from the solution or vapor of the liquid, or a mixture of both.

Regime 3. Cavitation bubbles fed from outside the film. Cavitation patterns in this regime may take several forms.

(a) Edge fed: This form is characterized by smoothly curved bubbles entering simultaneously from all edges of the square plate. A typical example is shown in Fig. 18. Some bubbles therein show the smooth periphery of the bubble breaking into striations which lead to the form described in under 3(b).

(b) Leaf pattern: This form is characterized by a leaf pattern supplied through a "trunk" that grows inward from the plate edge (see Fig. 19). Usually one,

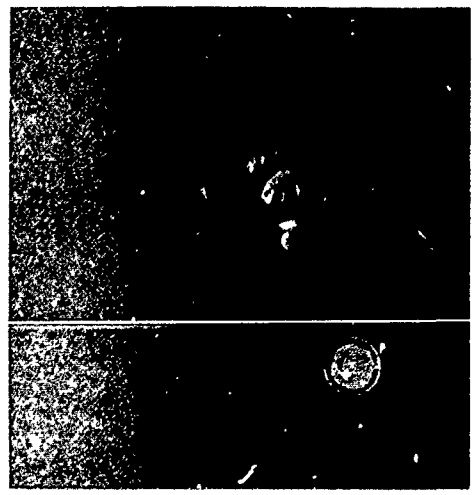

Fig. 17. - Regime 2 cavitation pattern.

Fig. 18. - Regime 3(a) cavitation bubble pattern.

but sometimes more such trees appear. Moreover, the tree may grow from a different side on different cycles of the same condition. References 36 and 45 illustrate both of these points.

(c) Leaf pattern with square parameter: The leaf pattern extends to cover all the oscillating plate surface except for a uniform border around three sides (see Fig. 20).

(d) Stream fed: This form is characterized by a leaf pattern whose perimeter follows that of the oscillating plate, but with a relatively wide (b/4) clear perimeter. This central leaf pattern is fed by a number of diagonal streams. Figure 21 is a photograph of the fully developed pattern.

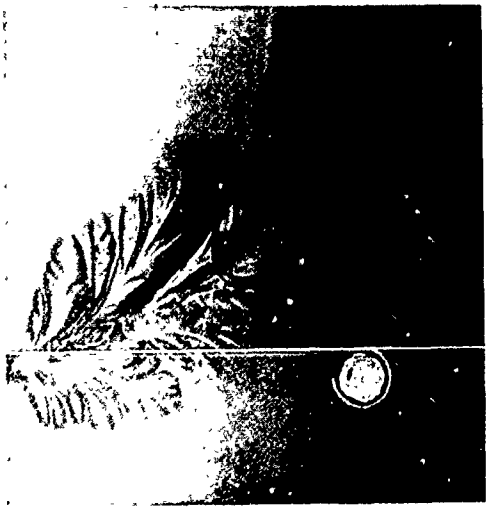

Fig. 19. - Regime 3(b) cavitation bubble pattern.

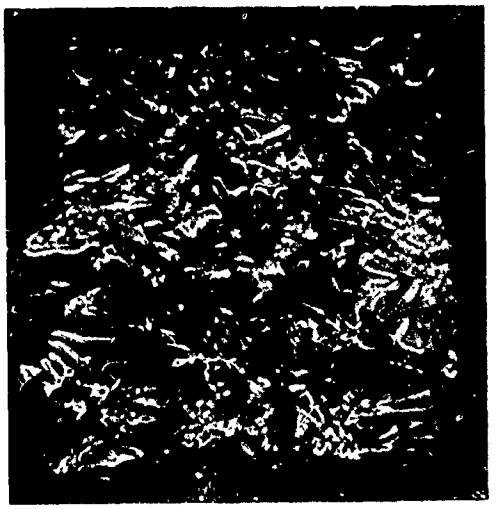

Fig. 20. - Regime 3(c) cavitation bubble pattern.

Fig. 21. - Regime 3(d) cavitation bubble pattern.

Reference 36 gives a sequence of photographs of cavitation patterns at a series of identified points in the oscillating cycle for regimes 3(a), 3(b), and 3(d). In each case the designated cavitation pattern exists for approximately 0.4 of the cycle time. The film is free of bubbles for a similar period. Bubbles advance and withdraw in the remaining time. With regime 3 (whatever subregime) each rapid increase in film pressure arises when the bubble front crosses the pressure transducer. The increase from minimum to atmospheric pressure occurs as the bubble front advances, and that from atmospheric to maximum pressure as the bubbles withdraw. An important finding in this work (39,41) was the extremely rapid movement of the bubble front in both advance and withdrawal.

Oil depth has a marked effect upon the onset cavitation patterns (36,45) . Figure 22, which illustrates this effect, shows the value of

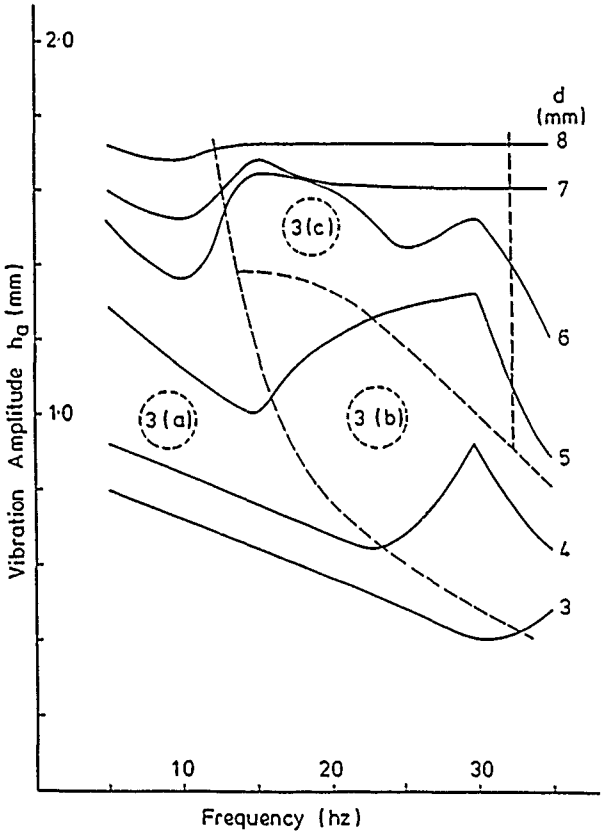

Fig. 22. - Effect of oil depth on onset of regime 3 cavitation (Y_o = 0.7 mm).

vibration amplitude (h_a) for a given frequency and oil depth (d) at which regime 3 occurs. Zones enclosed by dashed lines indicate which subregime will appear. For example, if a frequency, say, of 20 Hz is set and if amplitude is increased from zero, then, with d = 3 mm, regime 3(a) would appear at h_a = 0.57 mm, regime 3(b) at h_a = 0.75 mm, and regime 3(c) at h_a = 1.3 mm. It is interesting to note that one bubble in Fig. 18 (regime 3(a)) shows its curved edge changing into embryo leaf patterns characteristic of regime 3(b). A similar exercise at a frequency of 10 Hz, d = 3 mm would show regime 3(a) cavitation at h_a = 0.7 mm with no change therein occurring as amplitude h_a is increased further. Alternatively, for a frequency of 20 Hz and d = 5 mm, increasing amplitude h_a from zero would show regime 3(b) cavitation at onset at h_a = 1.2 mm.

Figure 16 shows how regimes 2 and 3 occupy different parts of the cycle. Consequently, it is possible for both regimes 2 and 3 to appear together in the same cycle. Indeed, Ref. 36 gives an example of regimes 2 and 3(a) appearing together. Cavitation onset, of whichever regime, is influenced by the geometry of the containing surfaces, A, y_o, and vibration frequency and amplitude h_a. However, evidence suggests that the onset of regime 3 is markedly affected by oil depth (d). The onset of regime 2 however, is influenced by the dissolved gas content in the liquid. These are independent effects; therefore, it is possible to have many different combinations and sequences. It is possible to transform from regime 1 (no cavitation) to any of the variants of regime 3 with, or without, regime 2 appearing. It is also possible to transform between the subdivisions of regime 3. Alternatively, it is possible to transform from regime 1 to regime 2 without regime 3 appearing.

This large number of possible forms of behavior make a confused picture when observed over a small range of variables, which renders it difficult to formulate classifications. There is a need for observation to be taken under a full range of all variables.

CONCLUDING REMARKS

It is now well established that an oil film subject to an oscillatory squeeze motion may generate a force with steady and vibrating components. The steady force component has been measured separately and shown thereby to act - according to circumstances - either to increase or decrease the oil film thickness. Theoretical models that include fluid inertia have been shown to predict this steady force. Measurements have shown that the initial film thickness, vibratory amplitude, and frequency influence the magnitude of the steady force.

Three cavitation regimes - including subregimes - have been identified and characterized according to the method of feeding the bubble. Each regime has a characteristic form of displacement and pressure-time history. Regimes 2 and 3 may coexist in the same oscillatory cycle. A limited knowledge is available about the conditions which determine the onset of a particular regime or subregime and its subsequent transformation into another subregime.

On both aspects, steady force and cavitation regimes, current knowledge is scanty, but sufficient to establish the existence of the listed features. More work needs to be done on both fronts before a full picture can be established.

CAVITATION IN MICROASPERITY LUBRICATION

A.O. LEBECK[4]

It is well known that, even when sliders are made parallel and slide parallel in a lubricating film, fluid pressure load support develops so as to support some or all of the load and reduce friction. Lebeck (46,47) reviewed this behavior, the experimental data, and the mechanisms in detail.

A typical example of such behavior is shown in Fig. 23. The friction of carbon graphite pins sliding on tungsten carbide in water was measured using the apparatus shown in Fig. 24. The friction coefficient at first decreases with increasing duty parameter and then later increases. The decrease is caused by what are apparently hydrodynamic pressures building up and reducing contact friction. The later increase is, of course, caused by viscous friction.

For many years it has been thought that microasperities serve as a source of fluid pressure load support in mechanical seals and parallel sliding lubricated contacts as reported in the experiments by Kojabashian, Richardson (48), and Hamilton (49). Figure 25 shows how microasperities produce load support. Cavitation at the downstream side is essential to get a net load support. As Kojabashian and Richardson (48) show, one can predict that a theoretically significant load support will develop on a seal-like surface which has many microasperities.

Experimental tests of this idea show that, if the ambient pressure is raised well above the cavitation pressure, no net load support results (Fig. 26). It follows that friction should

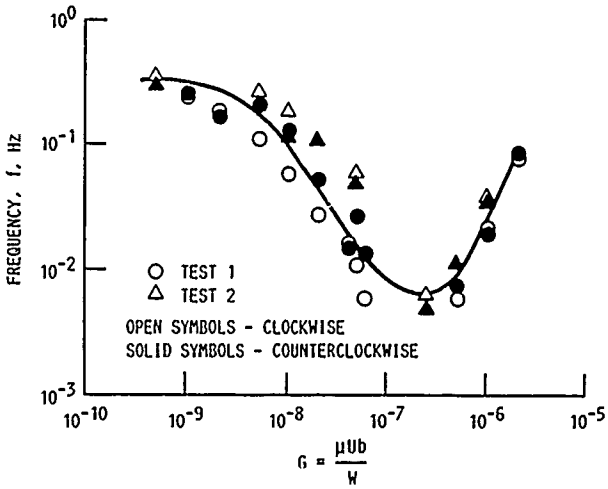

Fig. 23. - Parallel sliding in water.

[4]Mechanical Seal Technology Inc., Albuquerque, NM.

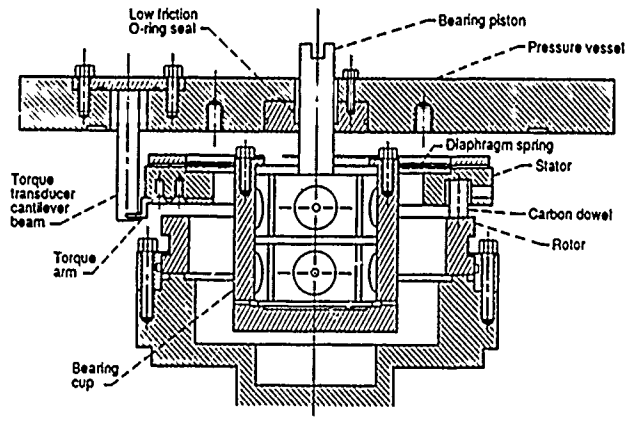

Fig. 24. - Hydrostatic bearing assembly diagram.

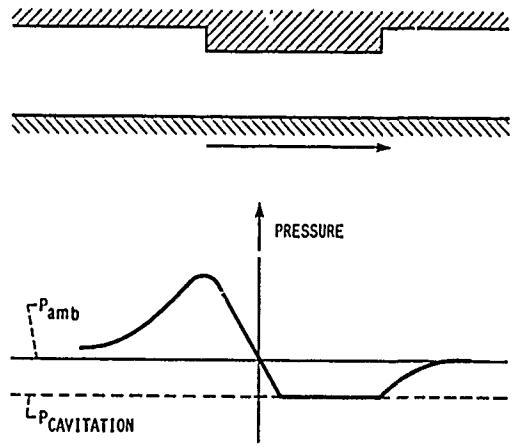

Fig. 25. - Truncated asperity pressure distribution.

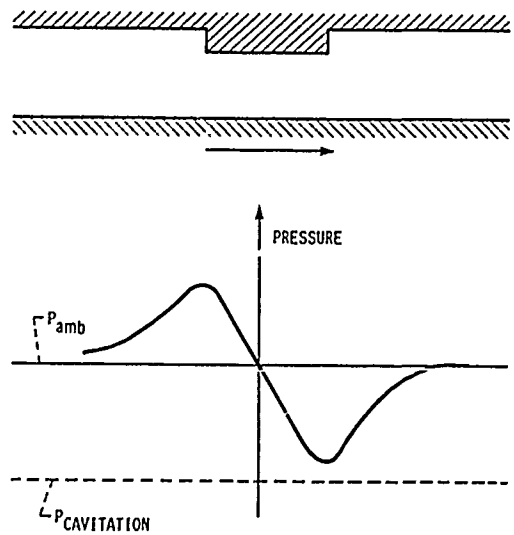

Fig. 26. - Zero load support.

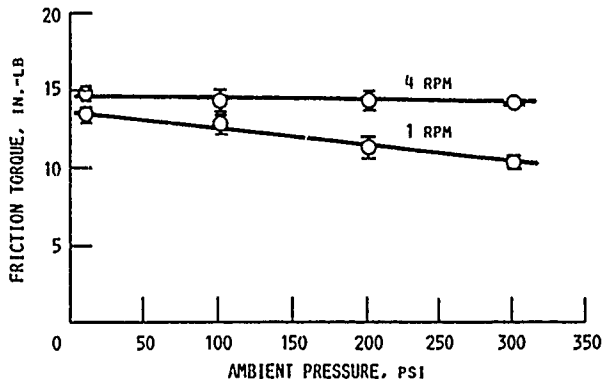

Fig. 27. - Friction torque versus ambient pressure. Carbon pressure, 300 psi. Each point represents an average of 450 samples.

increase because a lower fraction of the load is being supported by microasperities. This can be verified using the theory of Hamilton et al. (50). To test this hypothesis, Kanas (51) ran a series of experiments, using the apparatus shown in Fig. 24, where friction was carefully measured as a function of ambient pressure. His results (see Fig. 27) show no significant increase in friction with increasing ambient pressure. Similar results were obtained at higher speeds.

Thus, in water, under the sliding conditions noted, and at a condition of (from Fig. 23) considerable fluid pressure load support, microasperity lubrication, or any other mechanism that relies on cavitation, does not appear to be a primary source of load support.

CAVITATION EROSION DAMAGE IN ENGINE BEARINGS

F.A. MARTIN[5]

The experiences discussed in the 1979 paper, "Cavitation Erosion Damage in Engine Bearings: Theory and Practice," by Garner, James, and Warriner (52) still reflect much of the current view on the subject. A few selected extracts from that paper are presented here. These include examples of typical cavitation erosion damage, together with suggested mechanism of damage. Commonly applied palliatives and their effectiveness, based on engine experience, are also discussed.

"Cavitation erosion in engine bearings is a phenomenon which has assumed increasing significance during the past...years, probably as result of the design trends towards higher rotational speeds and, in some cases, higher rates of change of cylinder pressure...

"...Damage is seen predominantly in diesel engine bearings, and on the rare occasions when damage occurs in gasoline engines it is normally as a result of operating under [incorrect conditions].

"In many cases the damage is restricted to local attack of the overlay and the performance of the bearing is virtually unaffected... However, in more extreme cases extensive loss of overlay and interlayer material occurs, and the consequential adverse effects upon oil film conditions will reduce the service reliability and life of the bearings...

"The fact that diesel engine bearings are more prone to cavitation erosion damage is attributed to the more severe combustion conditions, and, additionally, to the necessity for more complex oil feeding arrangements with greater chance of flow discontinuities."

Garner et al. state that cavitation erosion damage is associated with the collapse of vaporous cavities near to the bearing surface and suggest that the mechanism is the impingement by micro-jets of fluid. They describe a possible sequence of events in the collapse of vaporous cavities leading to the formation of high intensity micro-jets (see Fig. 28). Let us now look at the result of this in terms of actual damaged bearings.

LARGE-END BEARING DAMAGE PREDOMINANTLY ASSOCIATED WITH OIL IN CONNECTING ROD DRILLING

"The commonest form of damage occurring in large end bearings appears at first sight to be due more to flow erosion than to cavity collapse, but detailed examination of the damage confirms a cavitation effect. This can occur in either fully grooved or partially grooved bearings.

[5]Tribology Consultant to The Glacier Metal Company, Limited, Middlesex, England.

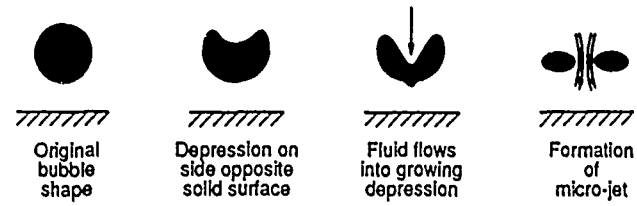

Fig. 28. - Mechanism of micro-jet formation (52).

"In fully grooved bearings, the damage occurs predominantly at the groove edges, but can ultimately spread into the bearing lands. There is strong evidence that the damage is caused by inertia effects on the column of oil in the connecting rod drilling which is supplied from the large-end bearing groove to provide top end lubrication and piston cooling..."

The damage may be cured by restricting the back flow from the rod drilling into the bearing (fitting a nonreturn valve has been one solution). In other cases, "the damage was diminished when the groove cross-sectional areas in both the main and large-end bearings were increased, thus allowing the oil column fluctuation to be better absorbed by the oil in the grooves....

"On partially grooved large end bearings damage frequently occurs at the groove run-out, either at the end of the partial groove, or at the side of the run-out, [Fig. 29]. The problem occurs at the end of the partial groove in the direction of shaft rotation, regardless of the position of the oil feed connection to the rod drilling. In the example shown in [Fig. 29], in which the damage had occurred within 400 hours,

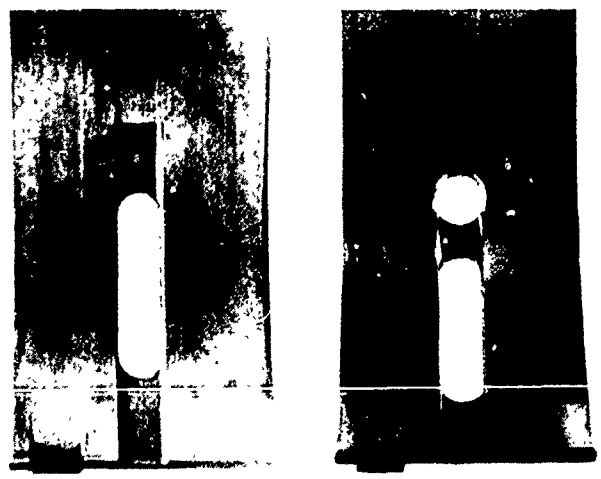

Fig. 29. - Cavitation damage associated with groove run-out in large-end bearing, together with effective solution (52).

the oil feed to the rod was adjacent to the damaged groove ending. The problem was overcome by the simple expedient of drilling a radial hole in the run-out section, as shown by the lower bearing in [Fig. 29] which had run for 1500 hours. Several other cases of similar damage have been successfully treated, ...either by provision of a radial hole or by terminating the groove conveniently at the end of a bridge-piece slot."

MAIN BEARING DAMAGE PREDOMINANTLY ASSOCIATED WITH OIL IN CRANKSHAFT DRILLING

"The majority of modern medium speed diesel engines use partially grooved main bearings in which the ungrooved arc is symmetrically placed in the bottom half, and is approximately 120° in extent. Such bearings provide an acceptable oil film thickness within the narrow confines dictated by the overall design, but, at today's high ratings, are those most likely to suffer from cavitation erosion damage. This occurs downstream of but usually close to, the groove runout and typically takes the form shown in [Fig. 30].

"In this instance, the damage was found after only 400 hours of operation, and was restricted to the soft overlay plated surface of the bearing, which was of the order of 0.03 mm thick. The stronger bearing lining underneath had not been attacked. This form of damage is characterized by a crescent form... In the particular example shown, after the initial short term damage, further progression

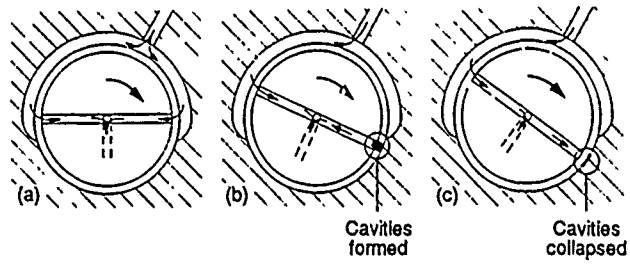

Fig. 31. - Cavity formation associated with interaction between journal drilling and partial groove (52).

was slow. Bearings in this condition after several thousand hours operation may quite safely be refitted. However, in some instances the damage can be much more severe...

"It is probable that as the oil drilling in the shaft traverses the groove run-out, cavities are formed at the intersection of groove run-out edge and the oil hole blend radius, as depicted diagrammatically in [Fig. 31]."

"Various palliatives have been tried on different engine types to alleviate this type of damage. These have usually consisted of modifications to the end of the partial groove. The most effective palliative so far adopted has been a tangential blend from groove to bearing surface with a square profile ([Fig. 32])."

Fig. 30. - Mild overlay damage in partially grooved main bearing (52).

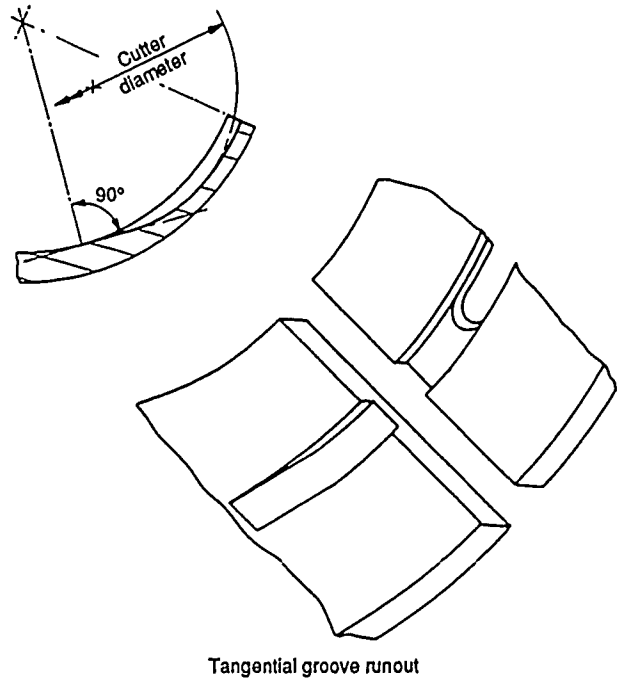

Fig. 32. - Design detail of successfully applied modification to groove ending (52).

Fig. 33. - Suction damage in large-end bearing associated with large clearance (52).

MAIN AND LARGE END BEARING DAMAGE PREDOMINANTLY ASSOCIATED WITH RAPID SHAFT MOTION

Cavitation erosion damage of the type shown in [Fig. 33] (commonly referred to as suction cavitation erosion) occurs in the center of the lands in some fully grooved bearings. It is due to rapid shaft movement away from the bearing surface and is worse with large clearances. It occurs in the upper half of high-speed diesel main bearings (and also in a large end bearing during a series of development tests on a medium speed two stroke engine).

Prediction of the journal orbit and examination of the hydrodynamic conditions within the bearing helps to pinpoint the area of likely damage. It also enables the designer to quickly examine the relative merits and disadvantages of various designs. "For the purposes of balancing loads and integrated pressures, i.e., in predicting the journal center orbit, it has been assumed, as is common practice, that negative pressures cannot be sustained by the lubricant. However, it is considered that predicted negative pressures will indicate the position and intensity of any cavity formation."

This method was used to examine the hydrodynamic conditions of a center main bearing showing the same type of damage as shown in Fig. 33. "The load diagram and resulting orbit are shown in [Fig. 34(a)], and it can be seen

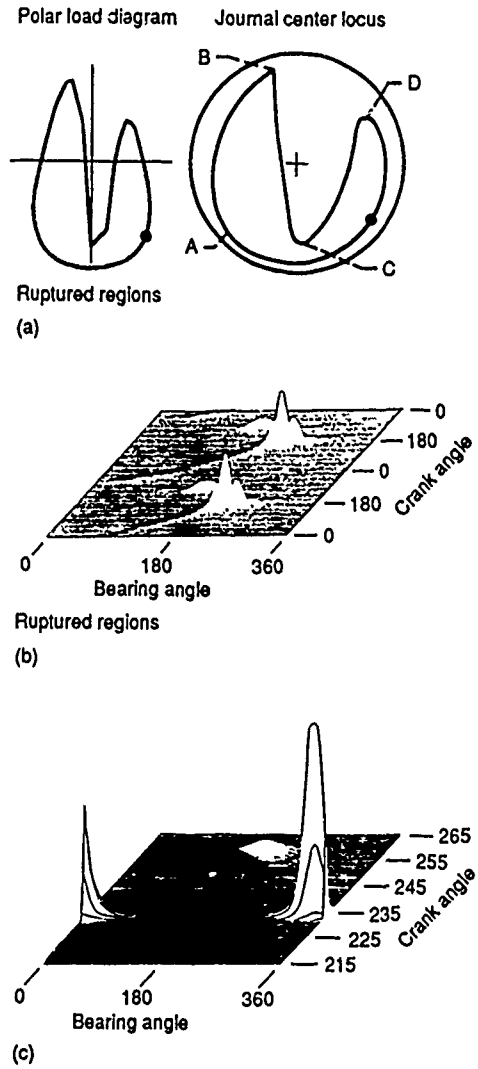

Fig. 34. - Predicted hydrodynamic conditions associated with occurrence of cavity damage (52).

that a rapid journal movement takes place between points B and C. Whilst experience suggests that rapid fluctuations in pressure are associated with such movements, the initial plot of rupture zones within the bearing ([Fig. 34(b)]) failed to show anything significant at the top of the bearing (0 or 360°) where damage occurred. It was only when the time step of the solution was refined (from 10° to 1° crank angle) that intense "negative" pressure zones were predicted ([Fig. 34(c)])." The position of the maximum negative pressure corresponded to the position of cavitation damage on the bearing surface, thus indicating that the cause of the damage was cavity formation (and subsequent collapse). The palliative here was to reduce the bearing clearance which alleviated the damage. However, it may be necessary in other instances to modify the polar load diagram. For example, the counterweights could be changed.

CONCLUDING REMARKS

Cavitation erosion damage in diesel engine bearings appears to fall broadly into three categories, associated with

1. Oil in crankshaft drillings and bearing oil feed features

2. Effects of the oil within the connecting rod drillings

3. Journal movements within the bearing clearance space leading to adverse oil film conditions.

Relatively simple modifications to the detail design of the bearing and its associated components can usually obviate problems from the first two categories, but often not from the third. However, these more intractable problems do seem to show some correlation with predicted oil film conditions. A more detailed theory than that considered here will probably be needed before damage can be reliably predicted at the design stage.

REFERENCES

1. Cole, J.A., and Hughes, C.J., "Oil Flow and Film Extent in Complete Journal Bearings," Proc. Inst. Mech. Eng., 170, 499-510 (1956).

2. Heshmat, H., "On the Mechanism of Operation of Flat Land Bearings," Interface Dynamics, D. Dowson, C.M. Taylor, M. Godet, and D. Berthe, eds., Elsevier, New York, 149-160 (1988).

3. Heshmat, H., and Pinkus, O., "Performance of Starved Journal Bearings with Oil Ring Lubrication," J. Tribology, 107, 23-31 (1985).

4. Articles, A., and Heshmat, H., "Analysis of Starved Journal Bearings Including Temperature and Cavitation Effects," J. Tribology, 107, 1-13 (1985).

5. Heshmat, H., "Theoretical and Experimental Investigation of Oil Ring Bearings," EPRI, Rotating Machinery Dynamics, Bearing and Seals Symposium, September (1986).

6. Heshmat, H., and Pinkus, O., "Mixing Inlet Temperatures in Hydrodynamic Bearings," J. Tribology, 108, 231-248 (1986).

7. Jakobsson, B., and Floberg, L., "The Finite Journal Bearing, Considering Vaporization," Trans. Chalmers Univ. Technology, Goteborg, Sweden, 190 (1957).

8. Olsson, K., "Cavitation in Dynamically Loaded Bearings," Trans. Chalmers Univ. Technology, Goteborg, Sweden, 308 (1965).

9. Wakuri, Y., Tsuge, M., Nitta, Y., and Sanui, Y., "Oil Flow in Short-Bearing with Circumferential Grove," Bull. JSME, 16, 441-446 (1973).

10. Fall, C., "A Study of Cavitation, and the Phenomenon of Ribbing, in Steady, Hydrodynamic Thin-Film Flow," Ph.D. Thesis, Leeds University, (1976).

11. Dyer, D. and Reason, B.R., "A Study of Tensile Stresses in a Journal-Bearing Oil Film," J. Mech. Eng. Sci., 46-52 (1976).

12. Savage, M.D., "Cavitation in Lubrication; Part 1. On Boundary Conditions, and Cavity-Fluid Interfaces; Part 2. Analysis of Wavy Interfaces," J. Fluid Mech., 80, 743-768 (1977).

13. Pan, C.H.T., "An Improved Short Bearing Anaiysis for the Submerged Operation of Plain Journal Bearings and Squeeze-Film Dampers," J. Lubr. Technol., 102, 320-332 (1980).

14. Nakai, M., Kazamaki, T., and Hatake, T., "Study on Pressure Distribution in the Range of Negative Pressure in Sliding Bearings (1st report) -- The Relation Between the Behavior of Cavities and the Pressure Distribution Curve," J. Jpn. Soc. Lubr. Eng., 27, 837-844 (1982).

15. Pan, C.H.T., "Dynamic Analysis of Rupture in Thin Fluid Films. I - A Noninertial Theory," J. Lubr. Technol., 105, 96-104 (1983).

16. Parkins, D.W., and May-Miller R., "Cavitation in an Oscillatory Oil Squeeze Film," J. Tribology, 106, 360-367 (1984).

17. Kawase, T., and Someya, T., "An Investigation into the Oil Film Pressure Distribution in Dynamically Loaded Journal Bearing," 4th European Tribology Congress, Vol. II, 5.2.3. (1985).

18. Nakahar, T., Terasawa, T., and Aoki, H., "Transition PHenomena of Gaseous Cavitation in Thin Oil Film Betwee Non-Parallel Flat Surfaces," Proc. JSLE Intern. Tribology Conf., Vol. 3, Elsevier, New York, 1097-1102 (1985).

19. Brewe, D.E., "Theoretical Modeling of the Vapor Cavitation in Dynamically Loaded Journal Bearings," NASA TM-87076/USAAVSCOM TR 85-C-15, and J. Tribology, 108, 628-637 (1986).

20. Hashimoto, H., and Wada, S., "The Effects of Fluid Inertia Forces in Parallel Circular Squeeze Film Bearings Lubricated with Pseudo-Plastic Fluids," J. Tribology, 108, 282-287 (1986).

21. Elrod, H.G., "A Cavitation Algorithm, "J. Lubr. Technol., 103, 350-354 (1981).

22. Orcutt, F.K., "An Investigation of the Operation and Failure of Mechanical Face Seals," J. Lubr. Technol., 91, 713-725 (1969).

23. Hughes, W.F., Winowich, N.S., Birchak, M.J., and Kennedy, W.C., "Phase Change in Liquid Face Seals," J. Lubr. Technol., 100, 74-80 (1978).

24. Findlay, J.A., "Cavitation in Mechanical Face Seals," J. Lubr. Technol., 90, 356-364 (1968).

25. Walton, J.F., II, Walowit, J.A., Zorzi, E.S., and Schrand, J., "Experimental Observation of Cavitating Squeeze-Film Dampers," J. Tribology, 109, 290-295 (1987).

26. Natsumeda, S., and Someva, T., "Negative Pressures in Statically and Dynamically Loaded Journal Bearings," Fluid Film Lubrication - Osborne Reynolds Centenary, D. Dowson, C.M. Taylor, M. Godet, and D. Berthe, eds., Elsevier, New York, 65-72 (1988).

27. Jacobson, B.O., and Hamrock, B J., "High-Speed Motion Picture Camera Experiments of Cavitation in Dynamically Loaded Journal Bearings," J. Lubr. Technol., 105, 446-452 and NASA TM-82798 (1983).

28. Jacobson, B.O., and Hamrock, B.J., "Vapor Cavitation in Dynamically Loaded Journal Bearings," 2nd Intern. Conf. on Cavitation, Mechanical Engineering Publications, England, 113-140 and NASA TM-83366 (1983).

29. Brewe, D.E., Hamrock, B.J., and Jacobson, B.O., "Theoretical and Experimental Comparison of Vapor Cavitation in Dynamically Loaded Journal Bearings," Intern. Symp. on Cavitation, Sendai, Japan, Apr. 16-19 and NASA TM-87121/USAAVSCOM-TR-85-C-19 (1986).

30. Brewe, D.E., and Jacobson, B.O., "The Effect of Vibration Amplitude on Vapour Cavitation in Journal Bearings," Wear, 115, 63-73 and NASA TM-88826/USAAVSCOM-TR-86-C-26 (1987).

31. Brewe, D.E., and Khonsari, M.M., "Effect of Shaft Frequency on Cavitation in a Journal Bearing for Noncentered Circular Whirl," Tribology Trans., 31, 54-60 (1980).

32. Kuroda, S., and Hori, Y., "An Experimental Study on Cavitation and Tensile Stress in a Squeeze Film," J. Jpn. Soc. Lubr. Eng., 23, 436-442 (1978).

33. Hays, D.F., "Squeeze Films for Rectangular Plates," J. Basic Eng., 85, 243-246 (1963).

34. Kauzlarich, J.J., "Hydraulic Squeeze Bearing," ASLE Trans., 15, 37-44 (1972).

35. Parkins, D.W., and Stanley, W.T., "Characteristics of an Oil Squeeze Film," J. Lubr. Technol., 104, 497-503 (1982).

36. Parkins, D.W., and Woollam, J.H., "Behavior of an Oscillating Oil Squeeze Film," J. Tribology, 108, 639-644 (1986).

37. Parkins, D.W., and Kahangwa, B., "Forces Generated by an Oil Squeeze Film," ASME Paper 80-C-2 Lub-39, (1980).

38. Kang, Byung-Hoo, "Prediction of an Oscillatory Oil Squeeze Film Behavior." M.Sc. Thesis, Cranfield Institute of Technology, (1986).

39. Parkins, D.W., and May-Miller, R., "Cavitation in an Oscillatory Oil Squeeze Film," J. Tribology, 106, 360-367 (1984).

40. Rodriques, A.N., "An Analysis of Cavitation in a Circular Squeeze Film and Correlation with Experimental Results," Ph.D. Thesis, Cornell University, June (1970).

41. May-Miller, R., "An Investigation of Cavitation in a Liquid Squeeze Film," MSc Thesis, Cranfield Institute of Technology (1982).

42. Parkins, D.W., "Oscillatory Oil Squeeze Films," Proc. Institute of Mechanical Engineers, London, Tribology - Friction, Lubrication and Wear - 50 Years On, Vol. 1, Mechanical Engineering Publications, Suffolk, England, 27-36 (1987).

43. Stanley, W.T., "Dynamic Characteristics of an Oil Squeeze Film," MSc Thesis, Cranfield Institute of Technology (1981).

44. Kahangwa, B., "Squeeze-Film Forces in Oil Films," M.Sc. Thesis, Cranfield Institute of Technology (1979).

45. Woollam, J.H., "An Analysis of the Vibratory Characteristics of an Oil Squeeze Film," M.Sc. Thesis, Cranfield Institute of Technology (1984).

46. Lebeck, A.O., "Parallel Sliding Load Support in the Mixed Friction Regime, Part 1 - The Experimental Data," J. Tribology, 109, 198-195 (1987).

47. Lebeck, A.O., "Parallel Sliding Load Support in the Mixed Friction Regime, Part 2 - Evaluation of the Mechanisms," J. Tribology, 109, 196-206 (1987).

48. Kojabashian, C., and Richardson, H.H., "A Micropad Model for the Hydrodynamic Performance of Carbon Face Seals," Proc. Third Intern. Conf. on Fluid Sealing, Cambridge, England, BHRA, Paper E4 (1967).

49. Hamilton, D.B., "Final Summary Report on the Dynamic Behavior of Liquid Lubricated Face Seals to the Rotary Shaft Seal Research Group," Battelle Memorial Institute, Columbus, OH, Feb. 22, 14 (1965).

50. Hamilton, D.B., Walowit, J.A., and Allen, C.M., "A Theory of Lubrication by Microirregularities," J. Basic Eng., 88, 177-185 (1966).

51. Kanas, P.W., "Microasperity Lubrication in a Boundary Lubricated Interface," Masters Thesis, Mechanical Engineering Dept., Univ. of New Mexico (1984).

52. Garner, D.R., James, R.D., and Warriner, J.F., "Cavitation Erosion Damage in Engine Bearing: Theory and Practice," J. Eng. Power, 102, 847-857 (1980).

PART II

THEORETICAL MODELING AND PERFORMANCE

INTRODUCTION

In part I, we were made aware of the numerous ways that cavitation could be manifested and of the categorization thereof. In particular, cavitation can either be the result of (a) dissolved gas coming out of solution or (b) evaporation (flashing) of the fluid. Both types of cavitation are commonly observed in journal bearings, squeeze-film dampers, connecting rod bearings, and pistons. Both have a pronounced effect on their operation. The occurrence of cavitation in journal bearings (1) results in reduced power loss, friction coefficient, bearing torque, and load capacity. Dowson and Taylor (2), in an excellent review of cavitation, point out that cavitation need not have a deleterious effect on the load-carrying capacity of bearings. Horsnell's calculations (3) on load capacity for steady-state conditions show that, if cavitation is not considered, the load can increase threefold over the predicted load.

In recent years imposing higher loads and speed together with more complicated loading cycles resulted in bearings experiencing cavitation erosion damage, as discussed in the article by F.A. Martin in part I. In addition to the cavitation damage, there is the damage that can occur due to self-excited instabilities that are encountered under dynamic loading. These instabilities can be manifested as a whirling or whipping motion (4) of the journal center. Large vibrational amplitudes can result in large forces being transmitted to the system. A designer can circumvent that problem, or at least the severity of it, by knowing the speed threshold at which it occurs. This information is often obtained by referring to "stability maps" (5,6). Stability maps require the determination of hydrodynamic force terms coupled to the dynamical equations of motion.

The calculation of the hydrodynamic force components is dependent on the film model used, especially at high eccentricities. Many of the film models that are used to generate stability maps involve theories that are overly restrictive (e.g., narrow bearing theory, infinite bearing theory) and treat the cavitation in a very superficial way. Notable of these is the π-film cavitation theory in which positive pressures extend through half the circumference of the bearing and the other half is regarded as cavitated. This boundary condition violates the conservation of mass. Specifying zero-pressure gradient and cavitation pressure at the boundary (i.e., Reynolds or Swift-Stieber boundary conditions) represents the conditions for film rupture in a reasonable way but does not properly represent the conditions when the film is reestablished. While this boundary condition may yield satisfactory results for a steadily loaded bearing, it leads to inaccuracies in situations where the bearing is dynamically loaded (7). In actual practice, the Swift-Stieber conditions are often compromised as a matter of convenience by neglecting the implementation of the zero-pressure gradient condition. This is much like the Gümbel conditions in which solutions were obtained to the Reynolds equation, and the cavitation was determined by disallowing the existence of subambient pressures. However, dynamic loading causes changes in the local film thickness, which leads to nonstationary cavitation; that is, the cavitation boundary is in motion. This motion is manifested as the growth and collapse of the bubble as well as downstream transport from the minimum film position. The appropriate boundary condition may require a condition other than a zero-pressure gradient at the boundary. The studies of Olsson (8,9) suggest that the usual Swift-Stieber film-rupture condition is adequate for dynamic situations if the cavitation boundary moves at a speed that is less than half the journal surface speed. It seems highly unlikely that this condition would be met during the initial stages of growth and the last stages of bubble collapse.

Jakobsson-Floberg (1) and Olsson (8) formulated boundary conditions for a moving boundary that conserved mass within the cavitated region as well as at the boundary (commonly referred to as the JFO cavitation theory). It was assumed that liquid was convected through the cavitated region in the form of striations extended to both surfaces in the film gap. There is evidence that some liquid is transported in the form of an adhered layer to the faster surface (10,11). Pan (12) has broadened the JFO theory to accommodate those situations in which the mass transport through the cavitated region is not necessarily via liquid striations. For moderately to heavily loaded bearings (i.e., for a load-carrying capacity much greater than the surface tension forces of the lubricant), the adhered layer can be neglected (10). The striated flow in the JFO theory is necessarily a Couette flow because of a constant-pressure assumption within the cavitated region. Jakobsson and Floberg's experimental findings (1) support the constant-pressure assumption.

However, Etsion and Ludwig (11) have measured pressure variations of the order of 50 kPa inside a gaseous cavitation bubble. To resolve this apparent contradiction, one must know whether the cavitation bubble is gaseous or vaporous. Etsion (11) provides a plausible mechanism for determining this, based on liberation and reabsorption rates between a gas and a liquid. The same arguments for pressure variation within a vapor bubble would not apply (13). In view of this discussion, the constant pressure assumption for vapor cavitation seems reasonable. Despite some of the controversy and certain lack of understanding, the JFO theory perhaps represents one of the best accounts of a dynamical theory to date of moderately to heavily loaded journal bearings and/or dampers. It is an improvement over the Swift-Stieber conditions, even for steady-state solutions, because it provides for film reformation as well as film rupture. Both rupture and reformation require a knowledge of the pressure gradient and fractional film content at the interface to determine its location. Unlike a rupture boundary, the reform-

ation boundary is subjected to a pressure flow (i.e., nonzero pressure gradient).

Furthermore, the fractional film content at the boundary is determined by a residual fluid within the cavitated region that has been released at a rupture boundary (earlier in time) and governed by the fluid transport law. Which condition (reformation or rupture) prevails depends on the relative motion of the boundary with the motion of the convected fluid normal to the boundary. Typically, under steady-state cavitating conditions, the rupture boundary occurs along the upstream boundary, and the reformation boundary occurs along the downstream end. Under dynamic loading and nonstationary cavitation, rupture or reformation conditions may be required at either the upstream or the downstream boundary. The programming task to effect these conditions in a computational algorithm is exceedingly tedious. In current practice this discourages their implementation.

The Elrod and Adams (14) computation scheme, which mimics the JFO theory, avoids the complex programming required to trace the moving boundary between grid points and to evaluate the required pressure derivative. Later, Elrod (15) modified it and presented it in more detail. Rowe and Chong (16) improvised the Elrod algorithm so that pressure is the dependent variable rather than fractional film content. Provision was made for pressure sources as well as automatic switching for full and cavitated regions. Miranda (17) was one of the first to apply this method for steadily loaded axial groove journal bearings. The full potential of the algorithm did not materialize until Brewe (7) applied it to nonstationary cavitation in a journal bearing undergoing noncentered circular whirl. For other bearing and seal applications using the Elrod algorithm, the reader is referred to in (18-26).

This work represents a summary of the state-of-the-art and is by no means complete. Recently newer ideas and methodologies have emerged that contribute to the present methods and techniques of numerical modeling. We are sincerely grateful to the contributors of this composition in presenting many of their innovations, ideas, and insights to this complicated problem.

NOMENCLATURE

$\tilde{A}_1$ First Rivlin-Ericksen tensor, s^{-1}

$\tilde{A}_2$ Second Rivlin-Ericksen tensor, s^{-2}

C Bearing radial clearance, m

C_{ij} Damping matrix, N·s/m

D Bearing diameter, m

e Eccentricity, m

F Total fluid force, N

F(s) Deformation gradient history

f Dynamic fluid force, N

f_A Adhered-film fill factor

g Switch function

H Nondimensional film thickness, (h/C)

H_A Nondimensional adhered film thickness

h Film thickness, m

h_C Film coeficient of heat transfer for condensing oil vapor at low flow velocity, W/m·°C

I Last grid point

i Grid point index

K_{ij} Stiffness matrix, N/m

L Length of bearing in z-direction, m

L' Axial halflength (L' = 1/2L), m

l_v Heat of vaporization, kJ/kg

N Total number of time steps

n Iteration level

n Unit normal vector of the internal boundary

O_B Bearing center

O_j Journal center

P Nondimensional pressure, $p/\mu\omega(C/R)^2$

p Fluid pressure, N/m^2

p_{vap} Vapor pressure, N/m^2

p_a Atmospheric pressure, N/m^2

$\vec{Q}$ Sweeping flux vector, m^2/s

Q_{ZL} Nondimensional axial flow

R Bearing or journal radius, m

r Radius of flat bubble, m

s Marking parameter in time, s

T Temperature, °C

$\Delta T_{v,l}$ Temperature change from oil vapor to liquid, °C

$\tilde{T}$ Stress tensor

t Time, s

U Surface velocity in x direction, and/or sliding velocity, m/s

u Velocity of the fluid in the circumferential direction, m/s

V Collapse velocity of the bubble, m/s

$\vec{v}$ Velocity vector, m/s

W Applied static load on bearing, N; width of cavitation bubble, m

X Nondimensional x-coordinate, x/R

x Coordinate in circumferential direction, m; instantaneous position coordinate relative to journal center, m

x_s Vertical displacement of journal center relative to bearing center, m

$\bar{x}$ Instantaneous position coordinate relative to bearing center, m

$\dot{x}$ Instantaneous x-component of journal velocity, m/s

Y Nondimensional y-coordinate, y/R

y Coordinate in radial or normal direction, m; instantaneous position coordinate relative to journal center, m

$\dot{y}$ Instantaneous y-component of journal velocity, m/s

$\bar{y}$ Instantaneous position coordinate relative to bearing center, m

y_s Horizontal displacement of journal center relative to bearing center, m

Z Nondimensional z-coordinate, z/L'

z Coordinate in axial direction, m

z_c Location of bubble, m

z_e Axial location of the cavitation boundary, m

z_m 1/2 Bearing width, m

α Inclination of unit normal (n) to direction of sliding, rad; non-Newtonian material parameter, $N \cdot s/m^2$

β Liquid bulk modulus, N/m^2; non-Newtonian material parameter, $N \cdot s^2/m^2$

γ Nondimensioned counterpart to the material parameter α, $(\alpha U/\mu R)$

δ Central difference operator; nondimensioned counterpart to the material parameter β, $(6\beta U^2/\mu C^2)$

ε Eccentricity ratio of bearing (e/C)

ζ Position of upstream cavitation boundary at any axial position, m

η Unwrapped circumferential coordinate along the cylindrical bearing surface, m

θ Nondimensional density in full film, (ρ/ρ_c); fractional film content in cavitation region

θ_n Fill factor of adhered layer on sliding surface

θ_B Bridged fill factor

θ_C Fill factor of layer clung to stationary surface

λ Ratio of bearing half length to bearing radius, (L'/R_o)

μ Viscosity, $N \cdot s/m^2$

μ_a Artificial viscosity, $N \cdot s/m^2$

ξ Positional variable, m; Axial coordinate of the cylindrical bearing surface, m

ρ Density of saturated oil vapor, kg/m^3

τ Period of dynamic load; the instant the adhered film was formed at the breakup point; former instant in time, s

τ_{xy} Shear stress, N/m^2

ϕ Attitude angle, rad.

$\vec{\phi}$ Film flux, m^2/s

X Inverse function for the spatial position x, m

Xt Relative deformation function

$\tilde{\Psi}$ Liquid phase transport flux, m^2/s

Ψ_θ Circumferential transport flow, m^3/s

Ψ_z Axial pressure flow, m^3/s

ω Angular velocity of shaft, rad/s

Subscripts

a Surface a

b Surface b

B Bearing

c Cavitation

d Dynamic

F Full fluid film

j Journal

max Maximum

min Minimum

S Starvation

s Static, supply

w Waist

DEVELOPMENT AND EVALUATION OF A CAVITATION ALGORITHM

T.G. KEITH[1] AND D. VIJAYARAGHAVAN[1]

The effects of cavitation on performance have largely been disregarded in bearing performance calculations. For years, common practice was to modify full-film results in load calculations by setting all predicted negative pressures to the cavitation pressure (the half-Sommerfeld or GÜmbel boundary conditions). Albeit this produced reasonable load values, it is also well known that the results violated the conservation of mass principle. In more recent procedures the film pressure is assumed to develop from the point of maximum film thickness and end where the pressure derivative vanisnes (the Reynolds or Swift-Stieber boundary condition). Film rupture is more appropriately treated, but reformation of the film is essentially neglected.

Jacobsson and Floberg (1) and Olsson (7), proposed a set of self-consistent boundary conditions for cavitation to be applied to the Reynolds equation. The boundary conditions properly account for mass conservation in the cavitation region. The collective procedure is now generally termed JFO theory. This theory, when applied to moderately to heavily loaded journal bearings, produced values that were in satisfactory agreement with experimental values. The theory markedly improved the prediction of cavitation regions in bearing analyses and for transient problems.

Elrod and Adams (13) introduced a computational scheme that incorporates JFO theory in a very simple manner. This procedure avoids the complexities of locating film rupture and reformation boundaries as it automatically predicts cavitation regions. Later Elrod (14) modified the finite difference portion of the procedure to provide better results. The procedure, now generally termed the Elrod cavitation algorithm, has the following five objectives:

1. To remove the pressure contribution to the mass flow in the cavitation region

2. To observe the conservation of mass

3. To set approximately correct boundary conditions at the boundaries of the cavitation region

4. To produce a single equation for both the full film and the cavitated regions

5. To introduce the proper finite differencing of the governing equation.

The algorithm is based on a control volume formulation and uses the unit step (or switch) function to eliminate the pressure term in the cavitation region. Elrod pointed out that the algorithm was developed "after considerable experimentation" and therefore does not present development details. Accordingly, it does not readily lend itself to improvement.

An attempt is made here to develop an algorithm that is as effective as the Elrod algorithm in predicting cavitation in bearings. The proposed algorithm has the same objectives as the Elrod algorithm but is developed without resorting to trial and error. Hopefully, this development will serve as a platform upon which further algorithm improvement can occur.

ANALYTICAL FORMULATION

The two-dimensional, transient form of Reynolds equation for a Newtonian lubricant in laminar flow, allowing for compressibility effects, can be written as

$$\frac{\partial ph}{\partial t} + \frac{\partial}{\partial x}\left(\frac{\rho hU}{2} - \frac{ph^3}{12\mu}\frac{\partial P}{\partial x}\right) + \frac{\partial}{\partial z}\left(-\frac{ph^3}{12\mu}\frac{\partial P}{\partial s}\right) = 0 \qquad [1]$$

This is an expression of the conservation of mass: the first term on the left is the squeeze term; the second is the net mass flow rate in the x (flow) direction; and the third is the net mass flow rate in the z (axial) direction. Note that the flow rate in the x direction consists of a contribution due to shear (Couette flow) and a contribution due to pressure gradient (Poiseuille flow); whereas, the flow rate in the z-direction is solely due to pressure.

The density of the lubricant is related to the film pressure through the definition of the bulk modulus, β, i.e.,

$$\beta = \rho(\partial p/\partial \rho) \qquad [2]$$

This relation suggests that it is easier to work in terms of density in Eq. [1] than in terms of pressure. Accordingly, we can define a non-dimensional density variable

$$\Theta = \rho = \rho c \qquad [3]$$

where ρ_c is the density of the lubricant at the cavitation pressure.

For moderate to heavily loaded bearings, the pressure-induced flow within cavitated regions is small. Thus, the striated flow existing in these regions is primarily driven by shear, and the pressure is essentially constant. To reflect this feature, a so-called switch function is introduced into the pressure-density relation of Eq. [2], i.e.,

$$g\beta = \rho(\partial p/\partial \rho) = \Theta(\partial p/\partial \rho) \qquad [4]$$

[1]Department of Mechanical Engineering, University of Toledo, Toledo, OH.

where

$$g = \begin{cases} 1 \text{ in the full film region} \\ 0 \text{ in the cavitated region} \end{cases}$$

Equation [4] can be directly integrated to yield

$$p = p_c + g\beta(\ln \theta) \qquad [5]$$

Using Eqs. [1], [3], and [4] allows use to write a single expression for the conservation of mass in the bearing

$$\frac{\partial \rho_c h\theta}{\partial t} + \frac{\partial}{\partial x}\left(\frac{\rho_c hu}{2}\theta - \frac{\rho_c \beta h^3 g}{12\mu}\frac{\partial \theta}{\partial x}\right) + \frac{\partial}{\partial z}\left(-\frac{\rho_c \beta h^3 g}{12\mu}\frac{\partial \theta}{\partial z}\right) = 0 \qquad [6]$$

In the cavitated region Eqs. (5) and (6) are

$$\frac{\partial \rho_c h\theta}{\partial t} + \frac{\partial}{\partial x}\left(\rho_c hU\theta\right) = 0 \qquad p = p_c \qquad [7]$$

The variable θ warrants some discussion, for, although it is defined as the ratio of densities, it carries a somewhat different interpretation in the full film than in the cavitation region. In the former $\theta > 1$ and $\rho > \rho_c$ because of the compression of the lubricant. In cavitation regions $\theta < 1$ for another reason: The density of the lubricant is uniformly ρ_c, but, because of the vaporization, the film is not completely occupied with lubricant. Thus, θ is termed the fractional film content and $1 - \theta$ represents the void fraction.

NUMERICAL FORMULATION

Examination of the steady-state version of Eq. [6] for the full film ($g = 1$) reveals that it is an elliptic partial-differential equation. Hence, the numerical scheme adopted for its solution should reflect the fact that the dependent variable at any point in the full film depends on all neighboring variables. This permits the use of central differences. On the other hand, in the cavitated region ($g = 0$), Eq. [6] is of the hyperbolic type. Accordingly, downstream influences are not signalled upstream, and thus one-sided or upwind differencing should be used.

In the following discussion, the shear flow and the pressure-induced flow components will be treated separately. A one-dimensional flow will be used in order not to obscure the details of the development. Extension to multidimensional flow is not difficult.

Shear Flow

For simplicity the shear flow term will be written as

$$\frac{\partial}{\partial x}\left(\frac{U\rho_c}{2} h\theta\right) = \frac{\partial E}{\partial x} \qquad [8]$$

In order to reflect the correct physics of the flow, we desire a central difference of this term in the full-film portion of the bearing and a one-sided backwards difference in the cavitated region. This can be accomplished automatically by the insertion of an artificial viscosity term into Eq. [8]. This procedure is called type differencing (27) when used for similar purposes in transonic flow computations. Thus, Eq. [8] is written as

$$\frac{\partial}{\partial x}\left(\frac{U}{2}\rho_c h\theta\right) = \frac{\partial}{\partial x}\left(E - \mu_a \frac{\partial E}{\partial x}\frac{\Delta x}{2}\right) \qquad [9]$$

where μ_a, the artificial viscosity switch function, is defined as

$$\mu_a = \begin{cases} 0 \text{ in the full film region} \\ 1 \text{ in the cavitated region} \end{cases}$$

The use of the switch function permits Eq. [9] to be centrally differenced to yield

$$\frac{\delta}{\delta x}\left(\frac{U}{2}\rho_c h\theta\right)_i = \frac{E_{i+1/2} - E_{i-1/2}}{\Delta x} - \frac{1}{2}\left[\left(\mu_a \frac{\partial E}{\partial x}\right)_{i+1/2} - \left(\mu_a \frac{\partial E}{\partial x}\right)_{i-1/2}\right] \qquad [10]$$

Values of the variables on the half step may be computed from

$$\left(\quad\right)_{i\pm 1/2} = \frac{\left(\quad\right)_{i+1/2} + \left(\quad\right)_i}{2} \qquad [11]$$

Using Eq. [11], performing central differencing on the remaining derivatives in Eq. [10], and rearranging produce

$$\frac{\delta}{\delta x}\left(\frac{U}{2}\rho_c h\theta\right)_i = \frac{aE_{i+1} + bE_i + cE_{i-1}}{2\,\Delta x} \qquad [12]$$

where

$$a = 1 - (\mu_a)_{i+1/2}$$

$$b = (\mu_a)_{i+1/2} + (\mu_a)_{i-1/2} \qquad [13]$$

$$c = -[1 + (\mu_a)_{i-1/2}]$$

Comparison of the definition of μ_a and the switch function introduced to cancel the pressure term in the cavitated region, via Eq. [4], reveals that

$$g = 1 - \mu_a \qquad [14]$$

Thus, the coefficient in Eq. [13] are

$$\left.\begin{aligned} a &= (g_{i+1} + g_i)/2 \\ b &= 2 - (g_{i+1} + 2g_i + g_{i-1})/2 \\ c &= -[2 - (g_i + g_{i-1})/2] \end{aligned}\right\} \quad [15]$$

Now, if all grid points are within the full film, all g's are unity; therefore, a = 1, b = 0, and c = -1. Hence,

$$\frac{\partial}{\partial x}\left(\frac{U}{2}\rho_c h\theta\right)_i = \frac{E_{i+1} - E_{i-1}}{2\,\Delta x}$$

$$= \frac{\rho_c U}{2}\left[\frac{(h\theta)_{i+1} - (h\theta)_{i-1}}{2\,\Delta x}\right] \quad [16]$$

which is the desired central difference form. On the other hand, if all grid points are within the cavitated region, all g's vanish so that a = 0, b = 2 and c = -2. Hence,

$$\frac{\delta}{\delta x}\left(\frac{U}{2}\rho_c h\theta\right)_i = \frac{E_i - E_{i-1}}{\Delta x} = \frac{\rho_c U}{2}\left[\frac{(h\theta)_i - (h\theta)_{i-1}}{\Delta x}\right] \quad [17]$$

and the desired upwind difference version is obtained.

The foregoing may be contrasted to Elrod's (15) shear flow expression, which is written as

$$\frac{\delta}{\delta x}\left(\frac{U}{2}\rho_c h\theta\right)_i = -\frac{\rho_c U}{2\Delta x}\Big[h_{i+1}(1 - g_{i-1})\theta_{i-1} - h_i(1 - g_i)\theta_i + \frac{g_{i-1}h_{i-1}}{2}(2 - g_i) + \frac{g_i h_i}{2}(g_{i-1} - 2 + g_{i+1}) - \frac{g_{i+1}h_{i+1}\,g_i}{2}\Big] \quad [18]$$

If all grid points are within the full film, this yields

$$\frac{\delta}{\delta x}\left(\frac{U}{2}\rho_c h\theta\right) = \frac{\rho_c U}{2}\left(\frac{h_{i+1} - h_{i-1}}{2\,\Delta x}\right) \quad [19]$$

which, curiously, does not account for compressibility effects. In the cavitation region, Eq. [18] produces

$$\frac{\delta}{\delta x}\left(\frac{U}{2}\rho_c h\theta\right)_i = \frac{\rho_c U}{2}\left[\frac{(h\theta)_i - (h\theta)_{i-1}}{\Delta x}\right] \quad [20]$$

which agrees with Eq. [17].

Pressure Induced Flow

The pressure induced flow, written in terms of θ is

$$\frac{\partial}{\partial x}\left(\frac{h^3}{12\mu}\beta g\frac{\partial\theta}{\partial x}\right) \quad [21]$$

This term exists in the full film region ($\theta > 1$), but vanishes in cavitated regions ($\theta < 1$). The switch function g adequately removes the term and, therefore, no artificial viscosity term need be added for this purpose. Also, when this term exists, the governing equation is elliptic and thus can be centrally differenced.

Equation [21] can be treated in a variety of ways which will ensure that it is central differenced in the full-film and made to vanish in the cavitated regions. However, depending on the manner in which the switch function is handled and the particular differencing scheme adopted, the results vary significantly at the cavitation boundaries. Several alternative versions to the above were examined. The version that provided the most adequate and consistent results is one in which the derivative of g is not explicitly differenced. In particular, we may write that

$$g\frac{\partial\theta}{\partial x} = g\frac{\partial(\theta - 1)}{\partial x} = \frac{\partial g(\theta - 1)}{\partial x} - (\theta - 1)\frac{\partial g}{\partial x} \quad [22]$$

The last term on the right hand side vanishes for all values of θ because the spatial derivative of g vanishes for all θ except at $\theta = 1$; however, at this point, obviously, $\theta - 1$ is zero. Hence, we have

$$g\frac{\partial\theta}{\partial x} = \frac{\partial g\,(\theta - 1)}{\partial x} \quad [23]$$

Now inserting Eq. [23] into Eq. [21] and central differencing yields

$$-\frac{\delta}{\delta x}\left(\frac{h^3\beta}{12\mu}g(\theta)\frac{\delta\theta}{\delta x}\right)_i = -\frac{\delta}{\delta x}\left(\frac{h^3\beta}{12\mu}\frac{\delta g\,(\theta - 1)}{\delta x}\right)_i$$

$$= -\frac{\beta}{12\,\mu\,\Delta x^2}\Big[h^3_{i+1/2}g_{i+1}(\theta_{i+1} - 1) - \left(h^3_{i+1/2} + h^3_{i-1/2}\right)g_i(\theta_i - 1) \times h^3_{i-1/2}\,g_{i-1}(\theta_{i-1} - 1)\Big] \quad [24]$$

which is the same pressure term expression used by Elrod (15).

SOLUTION PROCEDURE

In this study cavitation in both slider and journal bearings was examined. All sliders were assumed to be one dimensional, whereas both finite and infinite length journal bearings were considered. Because the procedures for solving one- and two- dimensional problems in these configurations differed, details of each will be briefly described in the following sections.

One-Dimensional Problems

A purely implicit finite-difference scheme was used to numerically determine the distribution of θ for all one-dimensional problems. By this method, the finite difference version of Eq. [6], which incorporates Eqs. [12], [15], and [24], can be written at each node in a general form as

$$a_i\theta_{i-1}^{n+1} + b_i\theta_i^{n+1} + c_i\theta_{i+1}^{n+1} = d_i \qquad [25]$$

where the coefficients a_i, b_i, c_i, and d_i are functions of Δx, Δt, β, μ, h, g, and the form of the boundary conditions applied. Consequently, the coefficients vary throughout the grid and change with time. Initially, all nodes are assumed to be in the full film, and at all nonboundary nodes $\theta = 1$ and $g = 1$. The switch function distribution was updated after every time step.

Boundary conditions for slider bearings were taken to be of the Dirichlet type in which θ was set either greater than one (flooded) or less than one (starved) on the boundary nodes. Because the inlet and exit values of θ were specified, the entire collection of nodal equations could be arranged into the following tridiagonal matrix form:

$$\begin{bmatrix} b_1 & c_1 & & & 0 \\ a_2 & b_2 & c_2 & & \\ & \ddots & \ddots & \ddots & \\ & & \ddots & \ddots & \ddots \\ 0 & & & a_{I-1} & b_{I-1} \end{bmatrix} \begin{bmatrix} \theta_1^{n+1} \\ \theta_2^{n+1} \\ \vdots \\ \theta_{I-1}^{n+1} \end{bmatrix} = \begin{bmatrix} d_1 - a_1\theta_0 \\ d_2 \\ \vdots \\ d_{I-1} - c_{I-1}\theta_{I-1} \end{bmatrix} \qquad [26]$$

In this form the collection of equations may be readily solved by application of the Thomas algorithm (27).

For journal bearings the boundary conditions depend on the means of lubricant supply. At oil grooves, values of θ are assumed which correspond to the given supply pressure and are calculated from Eq. [5]. The procedure remains the same as for slider bearings. If, however, the bearing is submerged, periodic or continuous boundary conditions must be employed. Application of these conditions produce the following matrix form of nodal equations

$$\begin{bmatrix} b_1 & c_1 & 0 & a_1 \\ a_2 & b_2 & c_2 & \\ & & & \\ c_{I-1} & 0 & a_{I-1} & b_{I-1} \end{bmatrix} \begin{bmatrix} \theta_1^{n+1} \\ \theta_2^{n+1} \\ \vdots \\ \theta_{I-1}^{n+1} \end{bmatrix} = \begin{bmatrix} d_1 \\ d_2 \\ \vdots \\ d_{I-1} \end{bmatrix} \qquad [27]$$

The coefficient matrix in Eq. [27] is not tridiagonal and therefore the Thomas algorithm cannot be directly used in the solution. Brewe (7) has used the Gauss-Jordan procedure for this purpose, but found it to be extremely slow. To circumvent this problem, the two off-diagonal terms were lagged during the computations. By this procedure the following replacements were made:

$$a_1\ \theta_{I-1}^{n+1} = a_1\ \theta_{I-1}^{n}$$
$$c_{I-1}\ \theta_1^{n+1} = c_{I-1}\ \theta_1^{n} \qquad [28]$$

Thus, the terms were evaluated one time step behind the actual computations and, therefore, are known during the $(n+1)^{st}$ time step. Accordingly, they were incorporated into the right hand side of Eq. [27], and the Thomas algorithm applied.

The time march process was continued until the change in θ_i between two time intervals was less than 10^{-4}. At this point, it was assumed that a converged steady state had been reached.

Two-Dimensional Problems

An alternating direction implicit (ADI) finite difference scheme (7) was used to determine the distribution of θ for all finite journal bearing problems. By this method, the time step is split into two parts: in the first half, changes in the flow or x direction are calculated while old θ values are used to determine the gradients in the axial or z direction; in the second half, the recently calculated θ distribution is used to evaluate the flow direction gradients while the axial changes are updated.

The Thomas algorithm can be used in each part of the time step, if again, the appropriate variables are lagged for the submerged journal bearings case. In accordance with Brewe's (7) suggestion, the switch function was updated after every half time step. Calculations were performed over half the length of bearing due to symmetry with resepct to the axial center.

On occasion an oscillation of the θ distribution was encountered. This oscillation was triggered at the cavitation node and has been reported elsewhere (e.g., (7)). To remedy this problem, a variable time step was implemented according to the following scheme:

$$\Delta t_k = \Delta t_{min}\left(\frac{\Delta t_{max}}{\Delta t_{min}}\right)^{(k-1)/(N-1)} \qquad k = 1, 2, \ldots, N \qquad [29]$$

where Δt_{min} and Δt_{max} are grid dependent and N is normally taken to be 8.

Not only did the variable time step help reduce the oscillation, it also reduced by approximately 15 percent the number of time steps required for the solution to reach steady state.

Reference 28 examines the details of the current approach for both slider and journal bearings in one and two dimensions. The principal purpose of that effort was to compare the computed results with the published values of Elrod (14,15): The two algotithms produced comparable results. A second purpose of that work was to examine a few modifications to the basic flow terms used in the Elrod algorithm. In particular, Elrod neglects in the shear flow term the compressibility effects in the full film region. Also, an approximate equation relating the pressure to the fractional film content is sometimes used. This approximate relation uses the first two terms of a series expansion of the logarithmic term in Eq. [5], i.e.,

$$p = p_c + \beta(\theta - 1) \qquad [30]$$

CONCLUSIONS

A cavitation algorithm that automatically alters the form of finite differencing used for the shear induced flow has been developed. The algorithm is an outgrowth of the Elrod cavitation algorithm. The two algorithms produce comparable results (28). However, the newer version may lend itself more readily to improvement. The effects of film compressibility, equation of state of the lubricant, and grid spacing near cavitation boundaries on the pressure distribution were investigated (28).

FUNDAMENTAL ISSUES CONCERNING THE MOVING BOUNDARY

CODA H.T. PAN[2] AND JEAN FRENE[3]

This discussion deals with the motion of an internal cavitation boundary of an incomplete film, with emphasis on applications in which the dynamic load component overshadows the magnitude of the static load. In such applications one is concerned with supplying lubricant to the region where the surfaces are approaching each other, while voids should dominate the region of separating surfaces such that viscous friction may be kept minimal. The commonly accepted model of the π film is an attempt to approximate the extent of filling of the bearing gap. As engineers desire to refine the design art, a more precise description of the internal boundary of an incomplete film in a bearing gap is sought.

THE MODELING VIEWPOINT

A predominant concern in the analysis of an incomplete film is related to how flow continuity is maintained across the entire perimeter of the film, which comprises:

1. Inlet film edge or edges.

2. Boundaries fixed by the geometry of the bearing.

3. Internal boundary or boundries.

Suppose, that at any instant, such delineation of the film perimeter can be asserted. Then one can assign the value of the film pressure at the film inlet to be that of the lubricant supply pressure; the geometrical boundaries can be represented by the ambient pressure; and the "cavity" pressure can be assumed to prevail near the internal boundary or boundries. Consistent with this set of pressure boundary conditions, a Dirichlet type problem is prescribed by the lubrication theory and may be completely solved to yield, not only the film pressure distribution, but also the normal film flux at all points of the film perimeter.

While the film continuity condition is inherent in the interior of the bearing film as dictated by the lubrication theory, the transboundary continuity condition is more subtle. One may borrow from gas dynamics the notion of the Rankine-Hugoniot conditions to allow for abrupt changes of state properties while preserving continuity of lubricant transport. As Rankine-Hugoniot jumps are approximations of the diffused transport processes across a moving shock wave, the analogy for a moving cavitation boundary is the change of flow structure that takes place within a distance of the scale of the bearing gap.

[2]Digital Equipment Corp., Shrewsbury, MA.
[3]Professor, University of Poitiers, 86022 Poiters Cedex, France.

SOME EXPERIMENTAL FACTS

Before attempting to examine the equivalent Rankine-Hugoniot problem at the internal boundary of an incomplete film, it is instructive to recall some representative experimental facts of incomplete films. Two photographs (Fig. 1) which first appeared in the first Leeds-Lyon symposium (29), reveal that the notion of a smooth internal boundary which separates a filled gap from a void region is at best an approximation. In reality, the void region has a textured two-phase flow structure. The border between the filled gap and a void region exhibits irregularities associated with the two-phase flow structure. To circumvent such complicated details, it is convenient to deal with spatially averaged quantities of the two-phase region in modeling.

It is clearly revealed that a portion of the void-dominated region is locally filled with liquid bridging both surfaces. Less visually evident, but not to be overlooked, are the possibilities that a thin liquid layer may be attached to either but not both surfaces. Thus, a complete morphological description of the void dominated region must include the following distinct liquid states:

State A - A thin layer of liquid that adheres to the sliding (journal) surface.

State B - A liquid streak or spot that bridges both surfaces.

State C - A thin layer of liquid that clings to the stationary surface.

Excluded from present consideration are minute liquid droplets that move freely between the two surfaces.

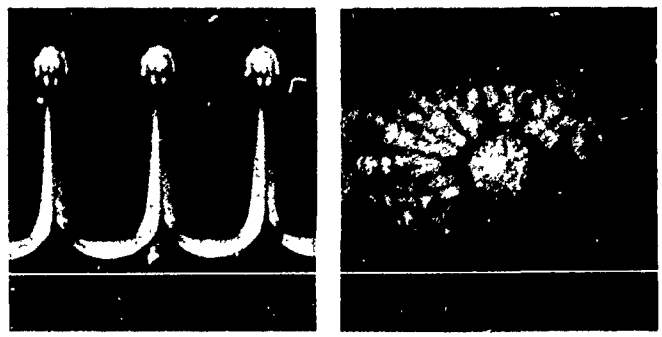

Fig. 1. - Appearance of high void content flow structures (29). (a) Divergent gap between rotating cylinder near stationary plane. (b) Separation of sphere from submerged stationary plane.

EQUIVALENT RANKINE-HUGONIOT

The equivalent Rankine-Hugoniot is concerned with the abrupt changes across a moving internal boundary. It deals with the conservation of the liquid phase as related to the thin-film flow on one side, liquid-phase transport on the other side, and the motion of the boundary.

Figure 2 shows that the normal unit vector of the internal boundary at E is directed into the void region and is inclined from the sliding vector by angle α. The film flux, according to the lubrication theory, is

$$\phi = -(12\mu)^{-1}h^3 \text{grad } p + 1/2\ Uh \qquad [31]$$

In the void dominated region liquid content is given by the volumetric fraction or the fill factor for each of the three morphological states; namely, θ_A, θ_B, θ_C. The velocity of the internal boundary is orthogonal to itself. Therefore, the "sweeping flux vector" is

$$Q = Vh\{1 - (\theta_A + \theta_B + \theta_C)\} \qquad [32]$$

The transvoid liquid transport flux is

$$\psi = Uh\ (\theta_A + 1/2\ \theta_B) \qquad [33]$$

Conservation of the liquid phase requires

$$(\phi - \psi - Q) \cdot n = 0 \qquad [34]$$

Substituting Eqs. [31] to [33] into Eq. [34], one obtains

$$-(12\mu)^{-1}\ h^2[(\cos\alpha)(\partial p/\partial x) + (\sin\alpha)(\partial p/\partial z)]$$
$$+ U(\cos\alpha)[1/2 - (\theta_A + 1/2\ \theta_B)]$$
$$- V\{1 - (\theta_A + \theta_B + \theta_C)\} = 0 \qquad [35]$$

Rearranging, one finds

$$V[1 - (\theta_A + \theta_B + \theta_C)] = U\cos\alpha\left[\frac{1}{2} - (\theta_A + \frac{1}{2}\theta_B)\right]$$
$$- (12\mu)^{-1}h^2\left(\cos\alpha\frac{\partial p}{\partial x} + \sin\alpha\frac{\partial p}{\partial z}\right) \qquad [36]$$

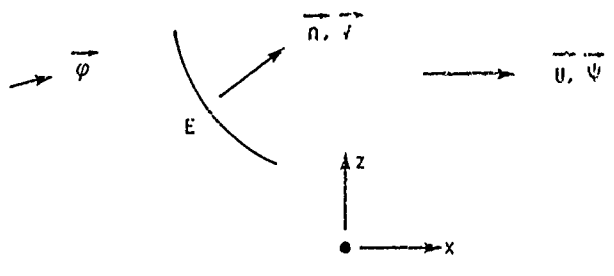

Fig. 2. - Vector diagram.

This is the equivalent Rankine-Hugoniot condition. It shows that the sweeping speed of the internal boundary depends on the neighboring film flux and the adjacent morphological states. A more restrictive form of this equation was originally presented by Olsson (8).

IMPLICATIONS OF THE EQUIVALENT RANKINE-HUGONIOT CONDITION

Equation [36] applies to both the breakup boundary, where $\cos\alpha > 0$, and to the reformation boundary, where $\cos\alpha < 0$. It must be satisfied by all valid solutions of incomplete films.

One of the solutions of the Olsson-Rankine-Hugoniot condition is the breakup line of a stationary, incomplete film. This corresponds to the Stationary breakup point:

$$\text{grad } p = 0 \qquad [37a]$$

$$\theta_A + 1/2\ \theta_B = 1/2 \qquad [37b]$$

The first of these is well known, but the second one is rarely cited.

Another solution of the stationary incomplete film refers to a point on the reformation line or Stationary reformation point:

$$-(12\mu)^{-1}h^2\{(\cos\alpha)(\partial p/\partial x) + (\sin\alpha)(\partial p/\partial z)\}$$
$$+ U(\cos\alpha)\{1/2 - (\theta_A + 1/2\ \theta_B)\} = 0 \qquad [38]$$

This relation was used by Jakobsson and Floberg (1) to find the shape of an enclosed cavity of a submerged journal bearing.

For a moving internal boundary, the Olsson-Rankine-Hugoniot condition serves as a link between an elliptic field of the fully filled domain and a hyperbolic field of liquid phase transport. In this context one may observe that, because the normal flux is a unique consequence of the Dirichlet problem, one can not rule out the possibilities that it may be inwardly directed, and that the film pressure may be less than the boundary value.

UNRESOLVED ISSUES

In order to use the Olsson-Rankine-Hugoniot condition, the three morphological state parameters θ_A, θ_B, and θ_C must be given. The θ_C probably can be neglected unless there are special chemical causes for a biased affinity of the lubricant to the stationary bearing surface. Another plausible hypothesis is to impose Eq. [37b] at the breakup point, irrespective of whether the internal boundary may be in motion. One is thus left with the remaining question of how liquid transport beyond the meniscus may be divided between an adhered film θ_A and streamers θ_B. Suppose that they are given initial values at

point E; then subsequent liquid-phase transport due to sliding can be stated as

$$(\partial/\partial t)[(\theta_A - \theta_B)h] + U(\partial/\partial x)[(\theta_A + 1/2\ \theta_B)h] = 0 \qquad [39]$$

And, if one is willing to neglect "cross flowing" between the two constituents, the streamer transport is given by

$$(\partial/\partial t)(\theta_B h) + 1/2\ U(\partial/\partial x)(\theta_B h) = 0 \qquad [39a]$$

and the adhered film transport is given by

$$(\partial/\partial t)(\theta_A h) + U\ (\partial/\partial x)\ (\theta_A h) = 0 \qquad [39b]$$

Clearly, a physically permissible initial morphological condition at E is in the range

$$0 \leq (\theta_A)_E \leq 1/2 \qquad [40]$$

If one wishes to improve the speculative aspects of these ideas, details of the three-dimensional, viscous, free surface flow with a moving surface and a moving attachment line must be studied.

The implementation of the Olsson-Rankine-Hugoniot condition in a numerical computation scheme is not trivial. It refers to the film flux at the boundary, which in turn shifts with time. It is quite clear that the computation scheme must be capable of dealing with oblique mesh lines.

GEOMETRY AND MOTION OF THE MENISCUS

JEAN FRENE,[4] LUC LAUNAY,[4] AND CODA H.T. PAN[5]

Dynamic loading is the primary concern in the design for journal bearings of automotive engines. Oil supply is to be optimized to ensure that the minimum gap is adequate while friction is to be kept as low as possible. Operation with an incomplete film is typical in such bearings.

In the past the π-film model is commonly used in analytical studies. As engineers strive for more accurate modeling tools, a more precise treatment of the dynamics of the incomplete film is in order. The π-film model, as applied to the steady-state, plain journal bearing, is equivalent to the Gümbel approximation in rejecting the subambient portion of the pressure field. In conjunction with the short bearing approximation, the π-film model yields simple, closed-form analytical results for both static (eccentricity) and dynamic (radial velocity) effects. This combination of analytical tools has been the backbone for the study of journal bearings in automotive engines. The Reynolds-Swift-Stieber cavitation model (RSS) has been regarded to be more precise. Because it requires a null condition of the pressure gradient at the cavitation boundary, it had been thought to be intrinsically contradictory to the short bearing approximation and had been used primarily in "FDM type" numerical computations. More recently, a modified Reynolds-Swift-Stieber model was used to improve the short bearing approximation. Cavities of both vented and enclosed types have been successfully modeled.

The Reynolds-Swift-Stieber model, which is restricted to the steady-state condition only, is thus, valid for either a static load or a rotating load. As it was applied with the short bearing approximation, the results are appropriate for static-load considerations of the journal bearing or for high rotating loads of the squeeze-film damper. The bearings of the automotive engine experience oscillatory loads which are not of the pure rotating type, and the static load component is not totally negligible. These applications motivate us to consider the more complicated problem of a truly time-dependent incomplete film. The short bearing approximation was retained for this work, so that one may direct full attention to issues related to the moving cavitation boundary.

ANALYTICAL APPROACH

The time-dependent, incomplete film problem requires the simultaneous treatment of an elliptical domain and a hyperbolic domain, which are joined at the moving internal boundary where the Olsson-Rankine-Hugoniot condition is to be satisfied. A centrally fed short journal bearing will serve as the specific model in the present work. The dimensionless film thickness of a dynamically loaded journal bearing, neglecting angular misalignment, is

$$H = 1 + \varepsilon \cos(\Theta - \phi) \qquad [41]$$

In Eq. [41] both ε and ϕ, may be time-dependent. employing the short bearing approximation of Ocvirk, the Poiseuille component of the circumferential flux is neglected; thus,

$$\Psi_\Theta \approx 1/2\ \omega RCH \qquad [42]$$

$$\Psi_Z = -(12\mu)^{-1}(CH)^3(\partial p/\partial z) \qquad [43]$$

The continuity condition, with allowance for motion of the journal, is

$$(\partial \Psi_\Theta/\partial\Theta) + R(\partial \Psi_Z/\partial z) + RC(\partial H/\partial t) = 0 \qquad [44]$$

Upon making use of Eqs. [41] and [42], one finds

$$(\partial^2 p/\partial z^2) = (12\mu C^{-2})H^{-3}\left[\frac{d\varepsilon}{dt}\cos\Theta - \phi - \frac{1}{2}\omega - \frac{d\phi}{dt}\sin\Theta - \phi\right] \qquad [45]$$

Boundary conditions for the chosen problem are of the Dirichlet type. At the lubricant supply plane

$$p(z = 0,\Theta) = p_s \qquad [46]$$

and at the end of the film

$$p(z_e,\Theta) = 0 \qquad [47]$$

The end of the film may be at either the discharge end of the bearing or at the internal boundary of the incomplete film; i.e.,

$$z_e \leqq L/2 \qquad [48]$$

The elliptic problem can thus be determined by integrating Eq. [45] with the constants of integration chosen to satisfy Eqs. [46] and [47], to yield

$$p(z,\Theta) = p_s(1 - 2z/L) - 1/2\ z(L/2 - z)(12\mu/C^2)H^{-3}[\dot{\varepsilon}\cos(\Theta - \phi) - (1/2\ \omega - \dot{\phi})\sin(\Theta - \phi)] \qquad [49]$$

---

[4]Professor, University of Poiters, 86022 Poitiers Cedx, France.

[5]Digital Equipment Corp., Shrewsbury, MA.

LIQUID TRANSPORT IN THE DISCHARGE CAVITY

In the discharge cavity liquid phase is assumed to be in the state of an adhered film. The liquid content is given by the adhered-film fill factor f_A. Transportation of the adhered film is described by the equation

$$(\partial/\partial t + \omega\, \partial/\partial\theta)\, H_A = 0 \qquad [50]$$

where $H_A = f_A H$. The time-stepped representation of this solution is

$$H_A(\theta,z;t) = H_A(\theta - \omega\Delta t,\ z;\ t - \Delta t)$$

$$= 1/2\ H(\theta - \omega t + \omega\tau,\ z;\ \tau) \qquad [51]$$

for $t > \tau$, where τ is the instant the adhered film was formed at the breakup point.

MOTION OF THE INTERNAL BOUNDARY

The condition of Olsson-Rankine-Hugoniot gives the sweeping speed at an internal boundary to be

$$V = (1 - f_A)^{-1}\ 1/2\ U(1 - 2f_A)\ \cos\alpha$$

$$- (CH)^2(12\mu)^{-1}\left(\frac{\cos\alpha}{R}\frac{\partial p}{\partial\theta} + \sin\alpha\,\frac{\partial p}{\partial z}\right) \qquad [52]$$

The sweeping speed V is aimed along the cavity, pointing normal to the periphery. The boundary at any instant is described by

$$z_e(\theta,t) \leqq L/2 \qquad [53]$$

which has a waist at θ_w such that

$$(\partial/\partial\theta)z_e|_{\theta_w} = 0 \qquad [54]$$

The inclination of the periphery normal is

$$\alpha = \tan^{-1}\left(\frac{\partial}{R\,\partial\theta}z_e\right) - \pi/2 \qquad [55]$$

Branches on either side of the waist are joined with null slope. But analytic continuation from one to the other across the waist point can not be assured because computation of Eq. [51] would follow different rules for the two branches. In the breakup ($\theta < \theta_w$), the Reynolds-Swift-Stieber law applies so that

$$f_A = 1/2 \qquad [56]$$

and

$$V_{breakup} = -(CH)^2(6\mu)^{-1}\left(\frac{\cos\alpha}{R}\frac{\partial p}{\partial\theta} + \sin\alpha\,\frac{\partial p}{\partial z}\right) \qquad [57]$$

But in the reformation branch f_A is computed according to Eq. [51], so that Eq. [52] would be used in its full form. It is convenient to represent the sweeping motion by

$$\left(\frac{\partial}{\partial t}\right)z_e = \csc\alpha\ V$$

$$= (1 - f_A)^{-1}\left[1/2\ U\ (1 - 2f_A)\ \mathrm{ctn}\ \alpha\right.$$

$$\left. - (CH)^2(12\mu)^{-1}\left(\frac{\mathrm{ctn}\ \alpha}{R}\frac{\partial p}{\partial\theta} + \sin + \frac{\partial p}{\partial z}\right)\right] \qquad [58]$$

Then updating of the boundary geometry can be executed by computing

$$z_e(\theta,t) = z_e(\theta,\ t - \Delta t) + \int_{t-\Delta t}^{t} (\partial/\partial t)z_e\ dt \qquad [59]$$

at all inner points of the internal boundary. The end points move along $z = L/2$ and can be calculated from

$$(\partial/\partial t)x_e\Big|_{z=L/2} = \sec\alpha\ V\Big|_{z=L/2}$$

$$= (1 - f_A)^{-1}\ 1/2\ U(1 - 2f_A)$$

$$- (CH)^2(12\mu)^{-1}\left(\frac{\partial p}{R\,\partial\theta} + \tan\alpha\frac{\partial p}{\partial z}\right)_{z=L/2} \qquad [60]$$

Again, f_A would be set to 1/2 for the breakup point but would be computed according to Eq. [50] from the prior history of the reformation point.

EQUATION OF MOTION

The journal mass may experience an acceleration as the bearing film force may not cancel the applied force completely. This acceleration can be integrated in time to determine the varying velocity of the journal center. The corresponding squeeze-film terms would necessitate recalculation of the fluid film forces with the new cavity boundary.

PERIODICITY

In the automotive application the periodic state of the constant speed operation of the engine is of interest. The character of the above procedure of calculation does not assure this periodicity in advance. Therefore, it is necessary to perform the computation for more than a full cycle, until the results demonstrate complete attenuation of the initial transient caused by the assumed initial values of ε and ϕ.

CLASSIC CAVITATION MODELS FOR FINITE ELEMENT ANALYSIS

J.F. BOOKER[6]

A review of several mathematical models commonly used to incorporate cavitation in the finite-element analysis of lubrication is presented. The various mathematical models are completely equivalent in the limit, but they differ in physical interpretation and numerical implementation. The models are classic in the sense that they are not flow preserving. For clarity we review the development of finite-element lubrication analysis both with and without the complication of cavitation.

CAVITATION EXCLUDED

Transient lubrication analysis is usually based on a boundary-value problem in which the pressure satisfies the Reynolds differential equation (30) over a complete film region, and either pressure value or normal pressure gradient, respectively, satisfy "essential and natural" conditions everywhere on its boundary, whose location is fixed in the absence of cavitation. In an equivalent variational (extremum) problem (31), a pressure distribution is sought which minimizes a functional (integral) involving variants of the Reynolds operators over the region and "essential" boundary conditions on its boundary.

Following finite-element discretization of the pressure field, the functional can be expressed in terms of nodal pressure values. Necessary conditions for the resulting unconstrained minimization (quadratic programming) problem give a linear algebraic equation set. The set can also be obtained through application of Galerkin's method to the boundary value problem.

Solution of the linear equation set commonly accomplished by either direct decomposition (e.g., Gauss, Choleski, LUD (lower and upper decomposition)) or indirect iteration (e.g., Gauss-Seidel, and SOR) methods.

CAVITATION INCLUDED

In the classical view of transient cavitation analysis, the complete film region has one or more free boundaries on which both pressure value and normal pressure gradient satisfy so-called Reynolds boundary conditions (usually null). In a second view, a nonnegative solution (over the entire film region) is sought for the variational problem. The resulting constrained minimization (quadratic programming) problem no longer admits a simple linear algebraic solution. Third, we can choose to apply a mixture law view of two-phase (cavitating) fluids (15). Applied here, a complete film region is characterized by positive pressure and constant (mixture) density value (unity volume fraction); an incomplete (incipiently cavitating) region is characterized by null pressure and negative density time rate of change. The physical interpretation is obviously that of vaporization. It can be shown that the three viewpoints are equivalent in the limit. Any one is sufficient in principle to fix the (instantaneous) division of complete and incomplete film regions and/or the positions of their (free) boundaries. In practice, however, all three viewpoints introduce nonlinear complexities to the problem and a consequent layer of iteration to its numerical solution.

Focusing on boundary location, as in the first view, is particularly awkward for finite-element analysis. Since locations of free boundaries are unknown a priori, they must be selected in iterative trials (with attendant nodal discretization) followed by solution of a well-posed problem over the complete film region (with only one of the two Reynolds boundary conditions fixed and the other evaluated for iterative closure).

Focusing on local behavior is particularly convenient for finite-element analysis, since it allows a fixed nodal discretization. The constrained quadratic programming problem of the second view can be solved in a number of ways, all iterative. Physically appealing is Christopherson's method, in which the linear equation set is solved by Gauss-Seidel (or SOR) iteration, after which any computed negative pressures are set to zero, and the process repeated until satisfactory convergence is achieved. (One can imagine an analogous physical process in which quantities of liquid are converted to vapor.) The scheme has been used with success (32,33); its main drawback is its reliance on the iterative convergence of real variables. An alternative to the constrained quadratic programming problem is the linear complementarily problem (equivalent in the limit). Its numerical application (34-36) appears identical to that of the mixture law (37), in which one seeks to partition nodes as cavitating (or not), depending on whether particular equality and inequality constraints are satisfied.

A metaphor would be a "porcupine bearing" in which all interior nodes communicate via feed/bleed check-valves to an ambient pressure source. Although no cavitation at all would occur in such a preposterous arrangement, the mathematical problem is identical to those above.

Solution of all such problems is a matter of integer programming (guesswork) combined with direct solution of linear equation sets for pressures and direct evaluation for flow terms. In Murty's method (analogous to Christopherson's method) nodes at which constraint violations occur are shifted to the opposite partition for the next iteration. The great advantage of such integer iteration is that convergence is abrupt and unam-

[6]School of Mechanical and Aerospace Engineering, Cornell University, Ithaca, NY.

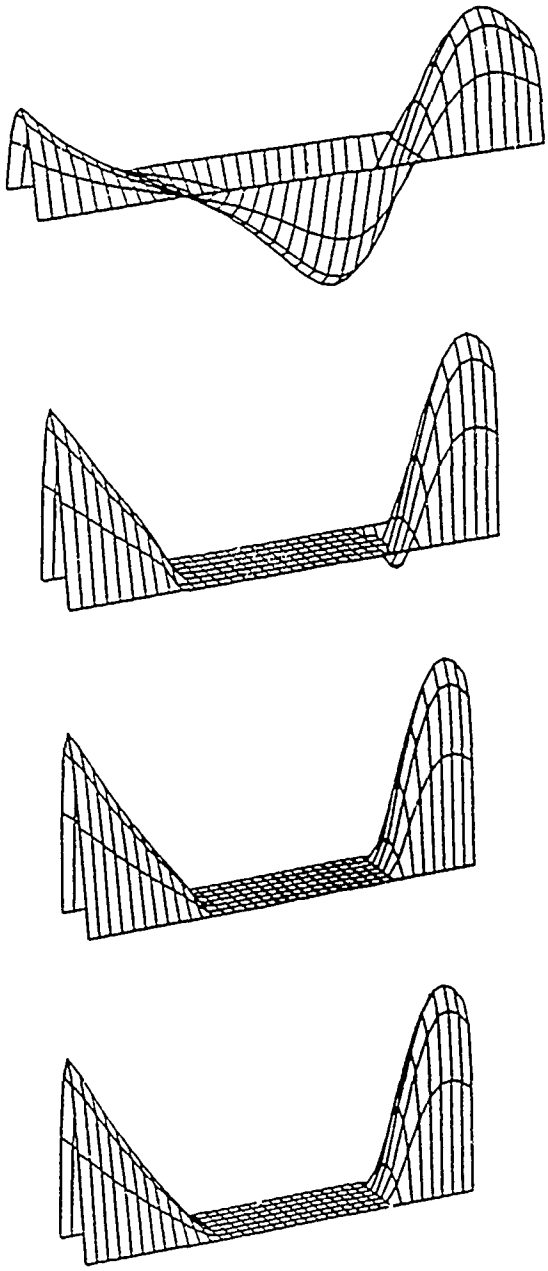

Fig. 3 . - Convergence of a pressure profile with integer iteration.

biguous; with a bit of luck, it is also fast. Figure 3 shows pressure distributions from a series of such steps, starting with the assumption of no cavitated nodes whatsoever. It should be noted that such a blind start is unnecessary in practice; reasonable first iterates result in convergence in one or two steps. (Corresponding nodal flow quantities do not provide for a meaningful plot in this previously unpublished study by LaBouff.)

SUMMARY

Several mathematical models commonly used to incorporate cavitation in the finite-element analysis of lubrication and suggested both physical interpretation and numerical implementation. These classic models, which are equivalent in the limit of discretization, describe incipient (quasistatic),nonevolving (flow-preserving) transient cavitation, in the sense that vapor only begins to form before the liquid is replenished. Though they are physically unrealistic in a really most basic way, the fact that they fix the cavitation situation quasistatically in instantaneous response to bearing kinematics means that the degrees of freedom of the problem are hundreds of times fewer than if nodal density (volume fraction) must be called on to reflect evolutionary history. The models thus lead to computationally efficient algorithms and are, therefore, likely to persist for a long time to come, whatever their departures from realism.

MATHEMATICAL MODELS AND RELATED ALGORITHMS IN CAVITATION PROBLEMS

G. BAYADA,[7] M. CHAMBAT,[8] M. EL ALAOUI[9]

We concern ourselves with gaseous cavitation operating under both the steady-state and transient conditions. Applications to circumferentially supplied bearings and to seals are given. We describe first the widely used cavitation algorithms and the related mathematical problems especially in view of the output flow computation. We propose new algorithms using the finite elements variational approach whose reliability has been theoretically proved. For unsteady problems, a time discretization procedure using the characteristic lines allows us to introduce a set of stationary like problems for which equality between input and output flows is preserved.

STEADY STATE PROBLEMS

Classical Models

The Gümbel (or Half-Sommerfeld) model of cavitation is widely used because it is easy to implement, but it is associated to a false boundary condition on the free boundary surface. The situation is much more confusing for the Swift-Stieber or Reynolds models. The validity of this last model has been supported in various ways:

a. The regularity condition is required to hold at the free rupture boundary (38):

$$p = \partial p/\partial n = 0 \qquad [61]$$

b. In numerous papers condition [61] is generalized to any free boundary (39).

c. In a more mathematical formulation, condition (61) is deduced from a minimization argument (40): Through all positive smooth functions satisfying the external boundary conditions, the pressure is the function that minimizes the energy integral.

d. The pressure is the solution of a variational inequality (41,42).

e. The pressure is the solution of a complementary problem (43).

f. The pressure is obtained by the Christopherson procedure.

There are two types of unpleasant problems that appear both analytically or numerically:

1. For a journal bearing with an axial supply line located in the convergent part of the gap, a strange pressure distribution has been obtained numerically with nonconnected active areas (44).

2. The balance between the input flow and output flow is not always satisfied, especially for seals (45).

Theoretical studies lead to the following conclusions (46):

- Formulations c, d, e, f are equivalent. They are associated with a well-posed problem which has a unique solution that fulfills the conditions of Eq. [61]. This solution is such that the cavitation area is located only in the divergent part of the mechanism.

A New Model

Various interpretations of the model are described in references (1) and (14). A summary of those interpretations is given here. The pressure is not a unique parameter governing the cavitation phenomenon; and we must introduce another parameter θ which can be viewed as a saturation function or a fractional film content (the percentage of oil contained in an elementary volume) or the result of the homogenization of the oil fingers. In any case, the cavitated area is not empty as it contains some lubricant.
The flow is now defined by

$$\phi = h^3/(12\mu)\nabla p - \theta U\, h/2 \qquad [62]$$

assuming ($p \geq 0$ and $0 < \theta < 1$), with the constraint that ($\theta = 1$ if $p > 0$) then the condition div (ϕ) = 0, in a weak variational sense, gives the equations for the problem.

Numerical Method and Applications

Elrod proposed an iterative procedure (15) well adapted for finite difference discretization. We propose a new procedure using the finite-element discretization, whose accuracy and convergence have been rigorously proved (46).

It is possible to express the problem in terms of one single unknown X which is a solution of a nonlinear equation

$$X = B(X) \qquad [63]$$

This equation can be solved using the fixed-point method starting from zero. Once X is known, it is easy to recover the initial functions p and θ.

We consider a bearing with a circumferential supply line. We compute the load, the attitude

[7]Centre Math 403, INSA 69621 Villeurbanne, Cedex, France.
[8]Lan Math, University of Lyon 1, 69622 Villeurbanne, Cedex, France.
[9]University of Caddi Ayyad Fac Sciences, Marrakech, Morocco.

angle, and the input/output flow rates for various supply pressures, various eccentricities, and three length to diameter ratios. The first computation is related to the Reynolds model solved using the Christopherson numerical procedure, and the second one to the Elrod-Jacobson-Floberg model using the new procedure. Both computations involved finite elements. Results demonstrate little discrepancy for the load between the two models, but gave more discrepancy for the eccentricity angle. The equality between output flow and input flow is very well preserved for the second model. However, it is not true for the first model for which the discrepancy increases with eccentricity and length to diameter ratio.

TRANSIENT PROBLEMS

Classical Models

The same analysis can be made for steady-state problems from both the theoretical and numerical aspects. The Christopherson procedure is commonly used with an explicit or implicit time descretization. Bad results are usually reported for the balance of the flow, especially for seals. These will be illustrated as a prime example.

New Model

We describe it first in the particular case of an infinitely long mechanism. However, the generalization to real two-dimensional geometry is straightforward.

As in the steady-state problem, a unique equation in a weak or distributional sense is well suited for numerical procedure:

$$\frac{\partial(\theta h)}{\partial t} - \frac{\partial}{\partial h}\left(\frac{h^3}{12\mu}\frac{\partial p}{\partial x}\right) + \frac{1}{2}\frac{\partial(\theta h U)}{\partial x} = 0 \qquad [64]$$

This equation includes all the above equations, especially the condition on the free boundary, which appears exactly as the classical Rankine Hugoniot condition for shocks in hyperbolic equations and is equivalent to those proposed by Elrod (14). Supplementary data involve (1) boundary conditions on the pressure and (2) initial data for θ.

Numerical Procedure (47)

The starting point is to substitute the total derivative $D(\theta h)/Dt$ for $1/2[\partial(\theta hu)/\partial x] + (\partial\theta h/\partial t)$ with the meaning that the derivative in t is taken along the direction U so that the equation becomes

$$\frac{D(\theta h)}{Dt} - \frac{\partial}{\partial x}\left(\frac{h^3}{12\mu}\frac{\partial p}{\partial x}\right) = 0 \qquad \theta = 1 \text{ if } p > 0 \qquad [65]$$

and then discretize the first term of the equation in time along the characteristic line.

CONCLUSIONS

An application to a seal was made in (47). Rectangular finite elements were used.

1. The discrepancy between input mass flow and output mass flow never exceeds 4 percent in each period.

2. Periodicity of the load and of the flows is obtained in four periods. The cavity follows the rotor movement when $x_2 = 2x_1$.

NON-NEWTONIAN EFFECTS IN FILM CAVITATION

A.Z. SZERI[10], K.R. RAJAGOPAL[10], AND ZHANG[10]

There exist in engineering usage a vast number of fluids, both naturally occurring and man made, the behavior of which cannot adequately be described by classical, linearly viscous theory. Though such fluids also abound in tribological practice, we have accumulated only scant knowledge of the effects non-Newtonian behavior might have on tribological performance. The principal problem we are faced with in the area of non-Newtonian fluid mechanics is our inability to successfully model the stress-deformation relationship of a particular material. But, in part, we can also blame the lack of reliable experimental data and, thus, the absence of guidance to theoretical research.

Viscoelastic fluids differ from Newtonian fluids in one main aspect, viz., viscoelastic fluids possess memory. Having memory, for the fluid, means that the stress presently experienced by a fluid particle is no longer determined by existing conditions alone but depends on deformation history of the material in the neighborhood of that particle. The principal practical manifestations of non-Newtonian behavior are normal stress effects and shear thinning. We have recently noted another strong effect on the velocity profile in a thrust bearing-like geometry (48) (Fig. 4). Velocity profiles were measured using laser Doppler anemometry, in a flow between rotating parallel disks. Figure 4 displays the tangential velocity field at a fixed radial position, with the top disk stationary and the bottom disk rotated at constant angular velocity. The profile in (a) was obtained in water, and that in part (b) was measured in a viscoelastic fluid (0.029 percent polyacrylamide solution). It is easy to discern the qualitative difference between the two profiles: Shear thinning occurs at a certain axial position, the separation distance of which from the bottom plate depends on various parameters, resulting in large velocity gradients. The cause for this localized action is not known to us.

We have also noted recently (49-51) that journal bearings lubricated with non-Newtonian lubricants could be less susceptible to thermal effects when compared with bearings lubricated with Newtonian fluids.

In this note we wish to further explore lubrication with viscoelastic fluids and focus our attention on cavitation, first wishing to place the constitutive relationship of the class of fluids we employ, in proper perspective. To this end we define the motion of a fluid particle as follows. If fluid particle X at time t occupies the spatial position x, we write

$$x = \chi(X, t) \qquad t > 0 \qquad [66]$$

As t varies, so will vary the position x of the particle X. We insist that this relationship (Eq. [66]) be invertible; i.e., that two particles do not at the same time occupy the same spatial position, and write for the inverse of Eq. [66]

$$X = \chi^{-1}(x,t) \qquad [67]$$

This is just mathematical shorthand for the statement that spatial position x at time t has the

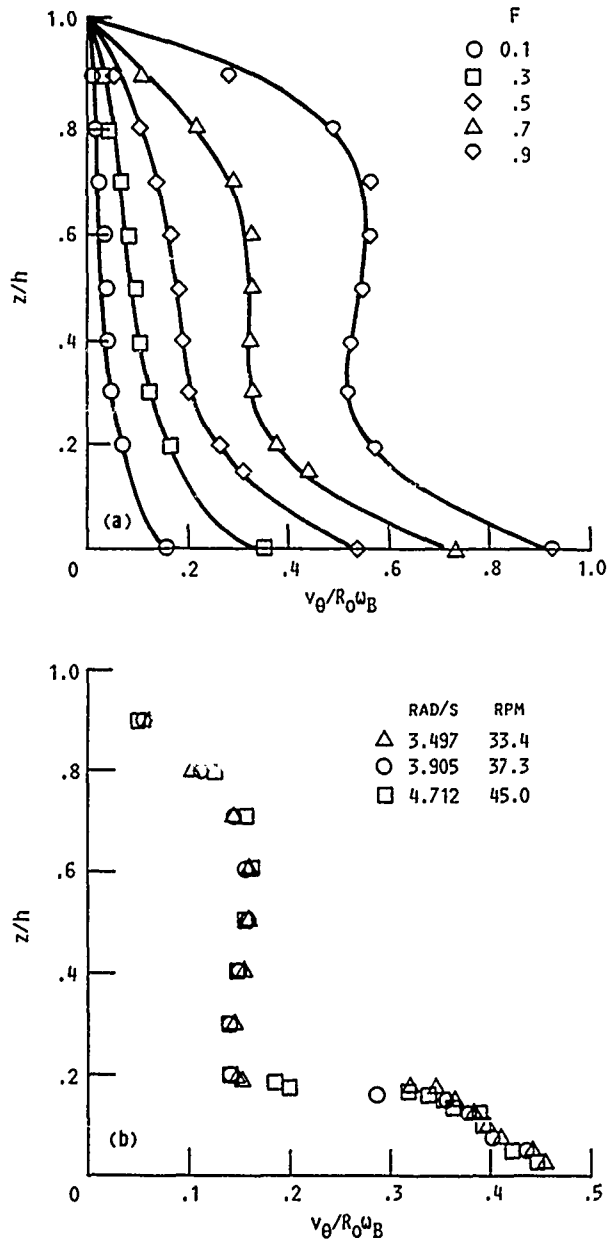

Fig. 4. - Azimuthal velocity between parallel, rotating disks. (a) Newtonian. (b) Viscoelastic fluid.

[10]Department of Mechanical Engineering, University of Pittsburgh, Pittsburgh, PA.

fluid particle X as its temporary resident.

Consider now another time instant $\tau < t$, at which time our fluid particle X was resident at the position ξ. Hence, we have

$$\xi = \chi(X,\tau) \qquad [68]$$

But we can substitute for X from Eq. (67) into Eq. [68] and have

$$\xi = \chi[\chi^{-1}(x,t),\tau] \equiv \chi_t(x,\tau) \qquad [69]$$

The relationship $\xi = \chi_t(x,t)$ states that the fluid particle that is in position x at the present time t, was in position ξ at some former time instant we call τ. If we now let $\tau \geqq 0$ vary while calling t the present time and keeping it fixed, we are looking backwards in time and tracing the history of motion of the fluid particle X.

The vector valued function χ_t occurring in Eq. [68] is called the relative deformation function. If the deformation χ_t described is smooth and the material has no microstructure (and this applies to most deformations and most materials in engineering practice), we can define the gradient of χ_t, called $F(s)$, through (52).

$$d\xi = F(s)\,dx; \quad F(s) \equiv \partial\xi/\partial x; \quad s = t - \tau \qquad [70]$$

Equation [70] shows that the gradient of χ_t, in our notation $F(s)$, is indicative of how an infinitesimal line element $d\xi$ at the instant of time τ had to be stretched and rotated so as to become the line element dx of the present time t. As we let $s > 0$ increase, the equality here signifying present time, we have the history of deformation characterized by $F(s)$.

The deformation gradient history $F(s)$ is used in the definition of a class of fluids called "simple fluids". Simple fluids (and the adjective "simple" refers to the lack of microstructure and does not imply that the fluid is elementary in any sense) are those in which the stress T at a point depends on the history of deformation of a neighborhood of that point, or

$$\tilde{T} = \overset{s=\infty}{\underset{s=0}{f}}(F(s)) \qquad [71]$$

There is a fairly good agreement among practitioners of non-Newtonian fluid mechanics concerning the validity of Eq. [71] and the assumptions leading up to it. But, there is disagreement on how to proceed further, for Eq. [70] is hardly a practicaily usefui statement.

There are many ways to approximate the functional f in Eq.[71]. Integral representations are well received by the rheology community in general but have to be as yet handled numerically in a practical application. Differential representations, on the other hand, yield to numerical treat ment but allow only for infinitesimal memory.

It has been shown that under certain conditions Eq. [71] has an expansion in terms of certain differential quantities. When this expansion is terminated at a low order and when account is made of the particular geometry common to most lubricant films, we essentially obtain that the stress has the following structure (cf. (50))

$$\tilde{T} = -p\tilde{I} + [\mu + \beta(\mathrm{tr}\,\tilde{A}_1^2)]\,\tilde{A}_1 + \alpha\tilde{A}_2 \qquad [72]$$

Here, μ is the molecular viscosity, α and β are non-Newtonian parameters, and A_1 and A_2 are the first and second Rivlin-Ericksen tensors, respectively, defined by

$$\tilde{A}_1 = (\mathrm{grad}\,\vec{v}) + (\mathrm{grad}\,\vec{v})^T$$

$$\tilde{A}_2 = d\tilde{A}_1/dt + \tilde{A}_1(\mathrm{grad}\,\vec{v}) + (\mathrm{grad}\,\vec{v})^T\tilde{A}_1 \qquad [73]$$

The material parameter α promotes normal stress effects while a $\beta < 0$ portrays shear thinning and a $\beta > 0$ will make the fluid shear thicken. This is easily seen when Eq. [72] is written for simple shear flow, for then

$$\tau_{xy} = [\mu + \beta(du/dy)^2](du/dy) \qquad [74]$$

Models of this type (Eq. [72]) h e been used by several researchers (53-55). We have applied it to journal bearings (50,51) and demonstrated that even a slight departure from Newtonion behavior, as measured by the numerical values of α and β, renders bearing performance relatively insensitive to changes in lubricant temperature.

In a continuation of previous effort, we looked at non-Newtonian effects on cavitation in a journal bearing. Figure 5 shows the slow, gradual change in the pressure profile as the material

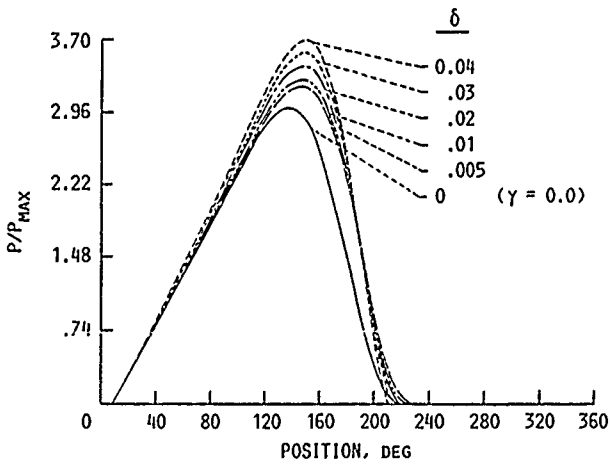

Fig. 5. - Pressure profiles in shear thickening fluid ($\gamma = -0.1$).

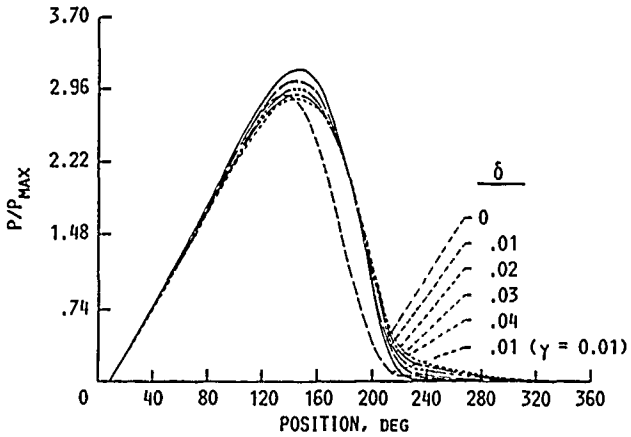

Fig. 6. - Pressure profiles in shear thinning fluid ($\gamma = -0.1$).

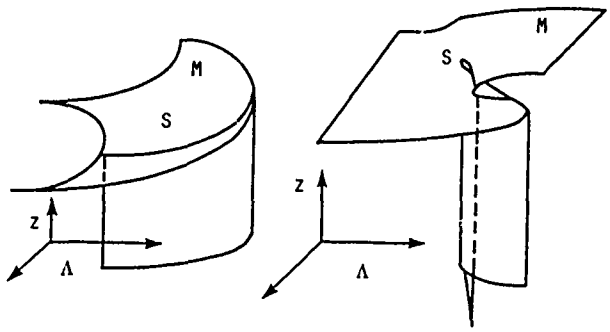

Fig. 7. - Foldlines (S) on solution manifolds (M).

parameter β is made progressively smaller while α is kept constant. To be precise, it is not α and β that are used as the parameters of the problem but their nondimensional counterparts γ and δ, defined by

$$\gamma \equiv \frac{\alpha U}{\mu R} \qquad \delta \equiv \frac{6\beta U^2}{\mu C^2} \qquad [75]$$

Here, U is the surface velocity of a shaft of radius R, and C is the radial clearance in the bearing.

Figure 5 shows pressure profiles for shear thickening fluid, $\delta > 0$, at $\gamma = -0.1$. As the value of δ decreases from $\delta = 0.004$, the maximum pressure, gradually decreases, otherwise the profile seems to change little.

Figure 6 shows pressure profiles again at $\gamma = -0.1$ but, now, for a shear thinning fluid. Starting at $\delta = -0.004$, the pressure curve shows no cavitation. Increasing the value of δ slowly increases the maximum pressure, but, otherwise, the shape remains invariant, still showing no cavitation. This phenomenon persists up to the value $\delta = 0.0025$, a slightly shear thickening fluid. But at a somewhat larger value of $\delta = 0.005$, Fig. 5 already shows cavitation.

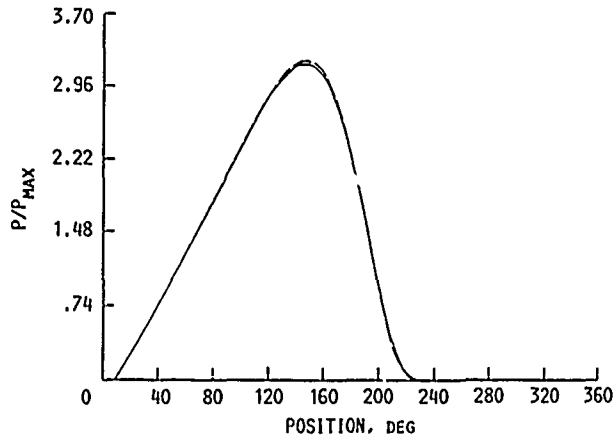

Fig. 8. - Pressure profiles at $\gamma = -0.1$.

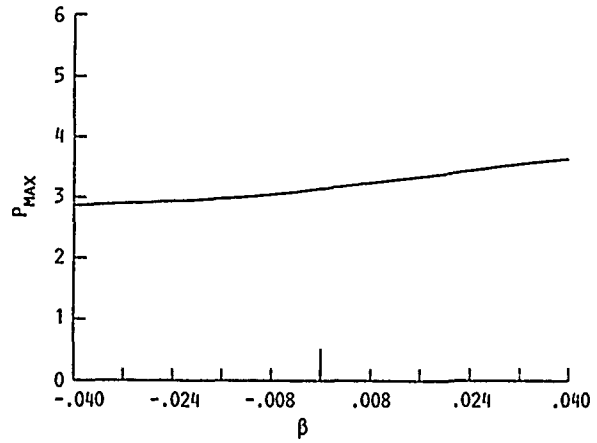

Fig. 9. - Pressure maxima at $\gamma = -0.1$.

Our investigations are incomplete at this stage, and conclusions are not well founded. But they suggest the presence of a fold line on the solution manifold at $0.0025 < \delta < 0.005$ when $\gamma = -0.1$. Here, the two solutions, one with cavitation and one without, join. Of course it is possible, or even likely, that the noncavitating solution, if it at all exists, represents an unstable branch and is therefore not reproducible in the laboratory. All we suggest at this juncture is, that there might be an other than the classical, cavitating solution to the problem. Our next task is to trace the fold line on the solution manifold using continuation methods. Figure 7 illustrates some possible fold lines of an equilibrium surface.

Figure 8 shows two pressure profiles, one obtained with $\beta = 0.0025$ exhibiting noncavitation; while the other, calculated with $\beta = 0.005$, exhibiting a classical, cavitating profile. Except for the presence or absence of cavitation, the profiles are virtually identical. Figure 9 displays the pressure maxima at $\gamma = -0.1$ as the parameter β is varied.

It is well known that nonlinear problems often yield a rich multiplicity of solutions, supported on identical steady-state boundary conditions. As an example we may quote the work of Bejamin and Mullin (56), who found 21 solutions in the flow between short, concentric rotating cylinders. Their work was experimental and thus shows much more than idle mathematical curiosity. This of course, constitutes no proof that what we have here in the non-Newtonian journal bearing is also multiplicity of solutions; but it perhaps suggests that our findings should not be discarded out of hand.

CAVITATION MODELING FOR ANALYSIS OF FLUID FILM JOURNAL BEARINGS

L.E. BARRETT[1] AND L.A. BRANAGAN[1]

A reasonable description of the cavitation phenomenon in thin fluid films is critical to the accurate prediction of the pressure distribution, and hence forces, in fluid-film journal bearings. Cavitation occurs when the fluid film is subjected to conditions of tension which tend to produce negative pressures within the film. Usually, under these circumstances, the pressure falls to essentially the vapor pressure of the lubricant, but no lower. Gaseous components of the lubricant come out of solution and, together with vaporized lubricant, form a two-phase flow field of bubbles and streamers. Cavitation usually occurs in regions of diverging film thickness within the bearing and depends on the supply pressure of the lubricant to the bearing. Hence, cavitation regions can be drastically altered by changes in bearing geometry and supply pressure, and for a given bearing they are dependent on operating parameters such as shaft speed and bearing load. Figure 10 shows a comparison by Tonnesen of predicted and measured pressures obtained in a two-axial-groove journal bearing. This figure clearly shows the cavitated region of low pressure that occurs in the top pad of the bearing in which a diverging film thickness occurs. It should be noted that cavitation within bearing fluid films is not considered to be inherently bad. Only rarely has cavitation been cited as the primary cause of bearing damage or failure due to surface pitting, and cavitation control is rarely a goal of bearing design except in the case of squeeze-film bearings.

The fluid mechanics and chemistry of cavitation is very complex. Fortunately, for most practical design considerations, a detailed description of the phenomenon is not required. What is required is an accurate prediction of the cavitation region boundaries and the pressure, temperature, and shear heat generation within the region. This is usually accomplished by applying reasonable auxiliary conditions on the fluid film pressures and temperatures obtained from a coupled iterative solution of the governing equations, the Reynolds equation for pressure, and the energy equation for temperature. The solutions are dependent on boundary conditions of supply pressure and temperatures and may include the heat conduction effects in the bearing and shaft. The simplest solution is to solve the governing equations independent of the existence of cavitation and to set any predicted negative pressures to the cavitation pressure using a forward solution for the pressure starting at the leading edge of the film. It is easily shown that this approach violates mass flow continuity, but it does provide a reasonable approach to defining the cavitation region for many bearing applications, particularly if certain simplifying approximations to Reynolds equation are used, such as the short bearing approximation. It is called the half-Sommerfeld pressure boundary condition.

For finite-length solutions, this approach has usually been used to avoid an iterative solution for the trailing boundary of cavitated region where the pressure is the cavitation pressure and the pressure gradient is zero, thus ensuring mass flow conservation. This is referred to as the Reynolds boundary condition. Actually, the trailing cavitation boundary can be easily found without iteration by back solving for the pressure, starting from the trailing edge of the fluid film and substituting the cavitation pressure whenever the solution predicts a subcavitation pressure. If coupled pressure-temperature solutions are being sought, the problem is already highly iterative, so there is no advantage to be gained by using the half-Sommerfeld cavitation boundary condition, even if a forward substitution scheme is employed.

Once the cavitation boundaries are known, the heat generation within the cavitated region must be calculated. The heat generated has an indirect effect on the cavitation boundaries and no effect on the pressure within the cavitated region. The effect on the boundaries comes about because the heat generation alters the temperature within the fluid film in the cavitated region. Thus, the temperature of the lubricant exiting the trailing edge of the film is altered. In turn, it affects the temperature of the film at the leading edge of the following pad.

The usual theoretical approach is to use what is called hot oil carry over calculations. In this method the lubricant exiting the trailing

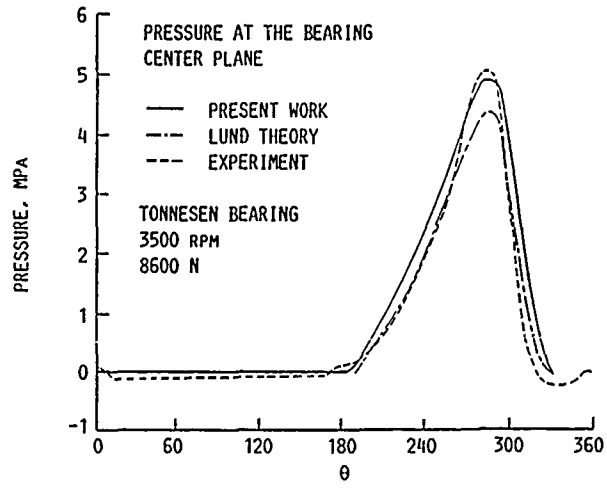

Fig. 10. - Predicted and measured pressures in a two-axial-groove bearing.

[1]Department of Mechanical and Aerospace Engineering, School of Engineering and Applied Science, University of Virginia, Charlottesville, VA.

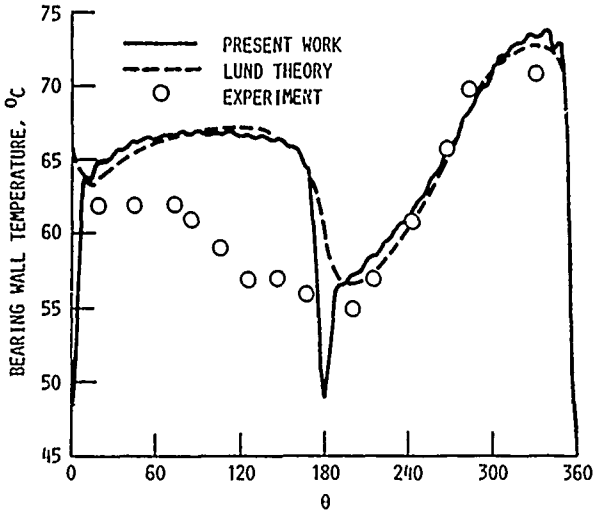

Fig. 11. - Predicted and measured pressures in a two-axial-groove bearing. Experiemnt conditions: Tonnesen bearing; 3500 rpm; 5600 N; T_S = 50 °C. Present work used 2° elements and 30 harmonics.

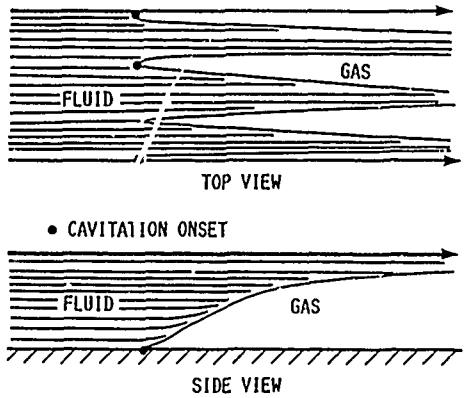

Fig. 12. - Model for two-phase flow in cavitated lubricant films.

edge of a pad is assumed to cling to the shaft and to be carried into the inlet of the following pad. If this volume of lubricant is insufficient to fully supply the following pad, the remaining volume is made up of lubricant supplied through the inlet supply groove. The temperature of the inlet lubricant is determined by the ratios of the carry over and the supply groove volumes at their respective temperatures.

A detailed theoretical model of the two-phase flow in the cavitated region is usually not conducted. Some assumption of the flow field is therefore made, and the shear heating of the lubricant in this region is determined by supplemental calculations. The simplest model is to assume that the lubricant film extends from the bearing surface to the pad surface. The axial film width decreases in the diverging circumferential direction since there is a constant volume of lubricant and because there is no pressure gradient developed in the cavitated region. This model treats the cavitated region as one with a central streamer of lubricant flowing along the bearing centerline. The heat generation is easily calculated since the velocity gradient across the film is essentially constant, at least for laminar flow, being approximately $R\omega/2$, where R is the shaft radius and ω is the shaft angular velocity.

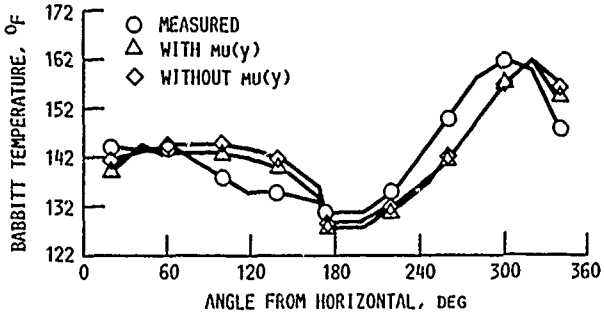

Fig. 13. - Predicted and measured temperatures in a two axial groove bearing with two-phase flow model used in cavitated region. Effect of cross-film bearing; Tonnesen bearing; 3500 rpm; Babbitt temperature profile; 1289.5 lbf load; w/ thermal cav.

Calculations performed using this model are shown in Fig. 11 for a two-axial-groove bearing. This figure shows the circumferential temperature variation of the bearing surface in both the loaded pad and cavitated pad. Measured temperatures made by Tonnesen are shown. Although heat conduction into the shaft and bearing surface is included in the theoretical calculations, the analysis predicts significantly higher temperatures in the cavitated region than those measured. This suggests that the heat generation model is predicting larger shear heating than actually occurs.

Figure 12 shows a two-phase lubricant-gas model for heat transfer in the cavitated region in which the lubricant adherence to the shaft surface can be assumed. Further, it is assumed that the height of the film diminishes along the diverging portion of the gap rather than have the film decrease in width. This model has been developed by observations of flow fields in transparent bearings, which suggest that this type of flow pattern exists. Because the viscosity of the gaseous portion of the film is considerably lower than that of the lubricant, most of the shearing occurs in the gaseous region. Thus, this model generates less shear heating in the cavitated region. The heat conduction to the shaft and bearing surfaces is also modified because of the difference in thermal properties of the two fields.

Figure 13 shows the results of calculations performed on the same two-axial-groove bearing as presented in Fig. 11. The results show better correlation with the measured temperatures in the cavitated region, suggesting that the two-phase model used is reasonably good.

A MODEL FOR CAVITATION IN DYNAMIC BEARINGS

JOHN A. TICHY[1,2] AND C.P. KU[1,2]

In fluid film lubrication problems, pressure often seeks a level lower than lubricant vapor pressure in the divergent region of the bearing, in which case gas or vapor forms a cavity. For the steadily loaded bearing, the cavity is usually formed due to ventilation from the surrounding atmosphere or the emission of dissolved gases from the lubricant. For the dynamically loaded bearing, the cavity is composed mostly of lubricant vapor.

For the heavily and moderately loaded bearing, the Jakobsson-Floberg-Olsson cavitation model seems to be correct to predict the extent of the cavitation region and to specify proper pressure boundary conditions on the interface. However, this model is difficult to apply due to the nonlinearity of the reformation boundary conditions. It requires extreme numerical effort in guessing the shape of the cavitation region and checking the flow balance (57).

In the proposed model we assume the shape of the pressure axial profile, and the Floberg boundary conditions are maintained. After integrating the Reynolds equation across the axial direction, a nonlinear ordinary differential equation for the distance of the cavitation boundary from the bearing centerline as a function of the circumferential coordinate is obtained. In the present study we consider the circular-centered orbit squeeze-film damper bearing with two circumferential oil supply grooves at the bearing ends (Fig. 14). The lubricant properties and temperature are assumed to be constant, and the fluid is laminar and inertialess. The unwrapped dimensionless bearing surface and pressure boundary conditions are shown in Fig. 15, where $Z = 0$ is the centerline and $W(X)$ is the width of the cavity.

ANALYSIS

The dimensionless Reynolds equation and the Floberg boundary conditions are

$$\frac{\partial}{\partial X}\left(H^3 \frac{\partial P}{\partial X}\right) + \frac{1}{\lambda^2}\frac{\partial}{\partial Z}\left(H^3 \frac{\partial P}{\partial Z}\right) = 12\frac{dH}{dX} \qquad [76]$$

For $X_1 \leqq X \leqq X_m$, $Z = W(X)$,

$$\frac{\partial P}{\partial X} = \frac{\partial P}{\partial Z} = 0 \qquad [77a]$$

For $X_m \leqq X \leqq X_2$, $Z = W(X)$,

$$\frac{H^3}{12}\left(\frac{1}{\lambda^2}\frac{\partial P}{\partial Z} - \frac{dW}{dX}\frac{\partial P}{\partial X}\right) = \frac{dW}{dX}[H(\zeta) - H(X)] \qquad [77b]$$

where ζ is shown in Fig. 15 $\lambda = L'/R_0$, and X_1, X_2, X_m, $W(X)$ are unknowns. The $P(X,Z)$ is a periodic function in the X direction and global mass conservation requires

$$\int_0^{2\pi} Q_{ZL(X)} = \int_0^{2\pi} -\frac{H^2}{12\lambda}\frac{\partial P}{\partial Z}(X,1)\, dX = 0 \qquad [78]$$

After integrating the Reynolds equation across the Z direction and applying boundary conditions at $Z = 0$ and $Z = 1$ or $W(X)$, an integral Reynolds equation in regions I, II, and III is obtained:

Region I:

$$\frac{d}{dX}\left(H^3 \frac{d\bar{P}}{dX}\right) = 12\frac{dH}{dX} + \frac{12}{\lambda}Q_{ZL} \qquad [79]$$

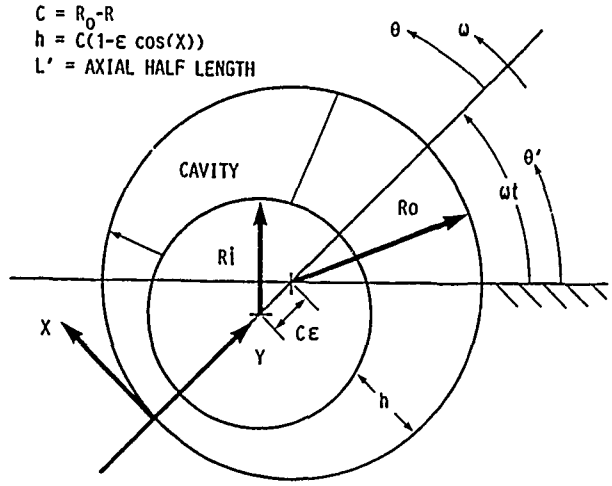

Fig. 14. - Squeeze-film damper schematic.

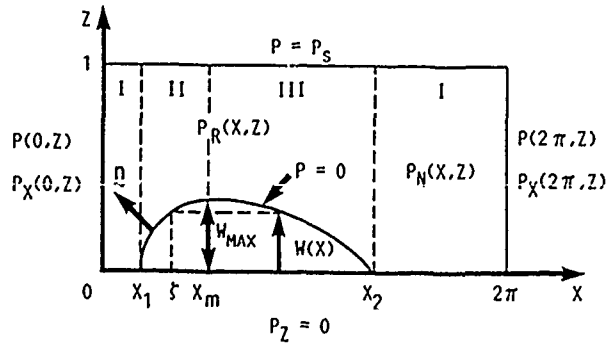

Fig. 15. - Bearing surface.

[1,2]Department of Mechanical Engineering, Aeronautical Engineering and Mechanics, Rensselaer Polytechnic Institute, Troy, NY.

Region II:

$$\frac{d}{dX}\left(H^3 \frac{d\bar{P}}{dX}\right) = 12(1 - W)\frac{dH}{dX} + \frac{12}{\lambda}Q_{ZL} \qquad [80]$$

Region III:

$$\frac{d}{dX}\left(H^3 \frac{d\bar{P}}{dX}\right) = 12(1 - W)\frac{dH}{dX} + \frac{12}{\lambda}Q_{ZL} + 12[H(\zeta) - H]\frac{dW}{dX}$$

[81]

where the integral pressure $P(X)$ is defined as the integral of $P(X,Z)$ across the Z direction.

Equations [82] and [83] are pressure profile assumptions in the noncavitation and rupture regions, respectively. These pressure profiles satisfy all boundary conditions at $Z = 0,1$ and $Z = W$.

$$P_N(X,Z) = P_s Z^2 + P_c(X)(1 - Z^2) \qquad [82]$$

$$P_R(X,Z) = P_s\left(\frac{Z - W}{1 - W}\right)^2 + (1 - W)\frac{\partial P}{\partial Z}(X,W)\left[\left(\frac{Z - W}{1 - W}\right) - \left(\frac{Z - W}{1 - W}\right)^2\right] - 2\lambda^2(1 - W)\frac{dW}{dX}\frac{\partial P}{\partial X}(X,W)\left[\left(\frac{Z - W}{1 - W}\right)^2 - \left(\frac{Z - W}{1 - W}\right)^3\right]$$

[83]

$$\frac{\partial P}{\partial X}(X,W) + \frac{\partial P}{\partial Z}(X,W)\frac{dW}{dX} = 0 \qquad [84]$$

Calculating the integral pressure of Eqs. [82] and [83] and applying the chain rule (Eq. [84]), we substitute these equations into Eqs. [79] to [81] and apply the boundary conditions at X_1, X_m, and X_2 on the interface to obtain the following ordinary differential equations:

Region I:

$$\frac{d^2P_c}{dX^2} + \frac{3}{H}\frac{dH}{dX}\frac{dP_c}{dX} - \frac{3}{\lambda^2}(P_c - P_s) = \frac{18}{H^3}\frac{dH}{dX} \qquad [85]$$

$$P_c(X_1) = \frac{dP_c}{dX}(X_1) = P_c(X_2) = 0 \qquad [86]$$

Region II:

$$\frac{d^2W}{dX^2} + \frac{3}{H}\frac{dH}{dX}\frac{dW}{dX} - \frac{6}{\lambda^2}\frac{1}{1 - W} + \frac{36(1 - W)}{P_s H^3}\frac{dH}{dX} = 0 \qquad [87]$$

$$W(X_1) = \frac{dW}{dX}(X_m) = 0, \quad \frac{dW}{dX}(X_1) = DWI \qquad [88]$$

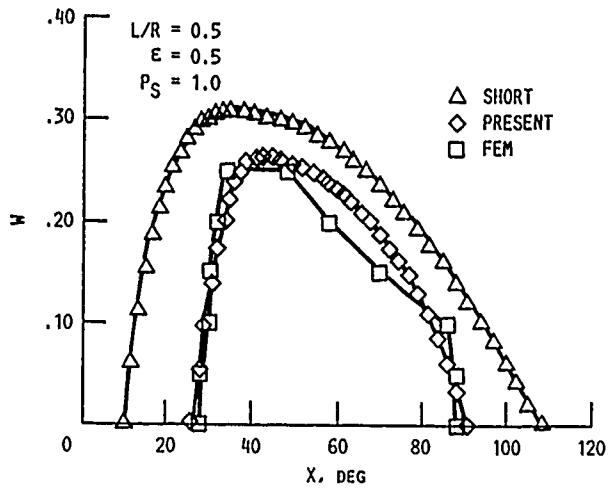

Fig. 16. - Cavity shape.

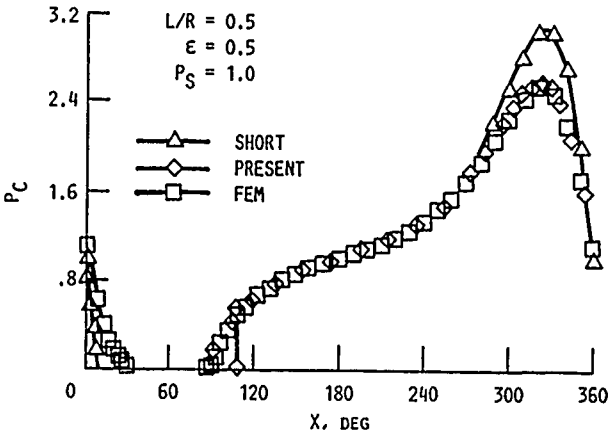

Fig. 17. - Centerline pressure.

Region III:

$$\bar{P} = \frac{1}{3}P_S(1 - W) + 2\lambda^2[H(\zeta) - H](1 - W)^2\frac{1}{h^3}\frac{dW}{dX} \qquad [89]$$

$$\frac{d}{dW}\left(H^3 \frac{d\bar{P}}{dX}\right) = 12(1 - W)\frac{dH}{dX} - \frac{2P_S H^3}{(1 - W)\lambda^2} + 12[H(\zeta) - H]\frac{dW}{dX}\left[\frac{2 + 3\left(\lambda\frac{dW}{dW}\right)^2}{1 + \left(\lambda\frac{dW}{dX}\right)^2}\right] \qquad [90]$$

$$W(X_2) = 0 \qquad [91]$$

In Eqs. [85] to [91], the independent variable is X; the dependent variables in the three regions are P_C, W, and $\bar{P}$; and H is a known function. Known parameters are P_S and λ. Unknown parameters to be determined from the solution procedure are the locations X_1, X_m, X_2 (see Fig. 15) and the slope dW/dX at X_1 (= DWI).

SOLUTION PROCEDURE

First we guess the values of X_1 and DW1. Equations [85] and [87] are solved with the initial conditions at $X = X_1$, and the values of X_2 and X_m are determined with extra boundary conditions in Eqs. [86] and [88]. In principle, only one boundary equation is needed for each interface. With the initial conditions obtained from Eq. [87] at $X = X_m$, we solve Eqs. [89] and [90]. The guessing values of X_1 and DW1 are adjusted until Eq. [91] and Eq. [78] are satisfied.

RESULT

The typical cavity shapes and the centerline pressure distributions are shown in Figs. 16 and 17. Compared with the numerical schemes, with the current model we only need to guess two values rather than the whole cavity shape, and the partial differentail equation reduces to odinary differential equations. A large amount of numerical work is saved and not too much accuracy is lost. We are currently obtaining the numerical results by finite-element methods. Compared with the short bearing model (58), the present model obtains better results when correlated with the finite-element-method model.

THE INFLUENCE OF CAVITATION ON JOURNAL-BEARING ROTORDYNAMIC CHARACTERISTICS

M.L. ADAMS[13]

Even under the smoothest running conditions, the journal always exhibits some orbital vibration about its equilibrium position with respect to the bearing. Provided this vibration is sufficiently small, one can justify characterization of the resulting fluid-film interactive dynamic force between journal and bearing by a linear mathematical model. The essential ingredients of this model are the linearized stiffness and damping coefficients for the journal bearing, i.e., a 2 by 2 stiffness matrix and a 2 by 2 damping matrix. These rotordynamic coefficients for the interactive dynamic force between the journal and bearing are delineated in the following equation:

$$\begin{bmatrix} f_x \\ f_y \end{bmatrix} = -\begin{bmatrix} K_{xx} & K_{xy} \\ K_{yx} & K_{yy} \end{bmatrix} \begin{bmatrix} x \\ y \end{bmatrix} - \begin{bmatrix} C_{xx} & C_{xy} \\ C_{yx} & C_{yy} \end{bmatrix} \begin{bmatrix} \dot{x} \\ \dot{y} \end{bmatrix} \qquad [92]$$

The radial dynamic force f exerted on the journal is the vector sum of the applied static force W and the total fluid-film force F, as illustrated in Fig. 18.

In the simplest of cases, the flow field between the rotating and nonrotating members has no memory. This would be the situation for the hydrodynamic pressure distribution produced in a purely viscous, fully developed, incompressible fluid-film journal bearing in the absence of cavitation (film rupture) as characterized by the following classical lubrication equation of Reynolds combined with pressure boundary conditions:

$$\frac{\partial}{\partial \eta}\left(\frac{h^3}{\mu}\frac{\partial p}{\partial \eta}\right) + \frac{\partial}{\partial \xi}\left(\frac{h^3}{\mu}\frac{\partial p}{\partial \xi}\right) - 6\omega R\frac{dh}{d\eta} + 12\frac{dh}{dt} \qquad [93]$$

where η is the unwrapped circumferential coordinate and ξ is the axial coordinate map of the cylindrical bearing surface.

The lubricant fluid film pressure distribution $p(\eta,\beta,t)$ embodies an interactive radial force vector which acts to separate the journal and the bearing. This pressure distribution is functionally related to the radial-orbit position and velocity vectors of the journal center relative to the bearing center; that is, the film thickness distribution h separating the journal and the bearing is a function of the relative position of the journal with respect to the bearing as follows:

$$h = C - \bar{x}\cos(\eta/R) - \bar{y}\sin(\eta/R) \qquad [94]$$

where $\bar{x} = x_s + x$ and $\bar{y} = y_s + y$ (see Fig. 18). Equation [94] is applicable to the typically assumed condition that bearing clearance is much smaller than bearing radius ($C \ll R$) and that the bearing and the journal axial centerlines are parallel; i.e., no misalignment, as given by $\partial h/\partial \xi = 0$. Consistent with Eq. [94], the following derivatives of h, which appear in Eq. [93], are

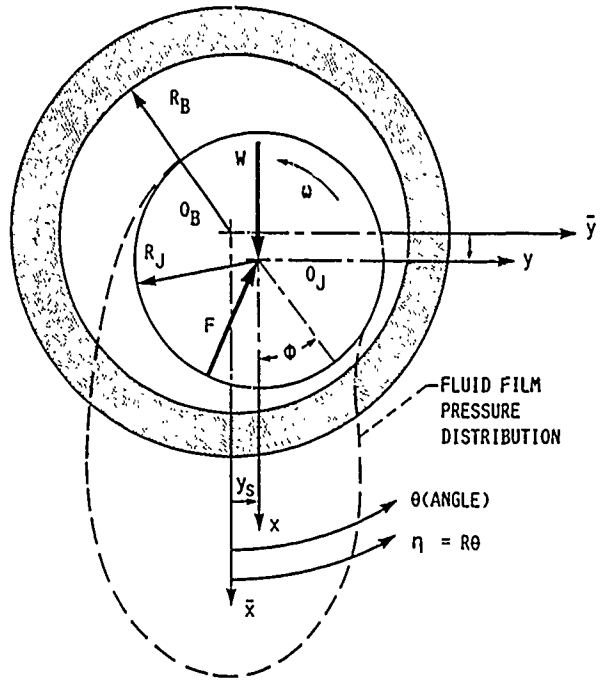

(a)

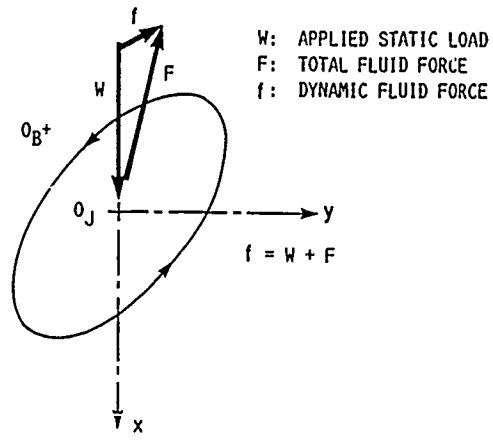

(b)

Fig. 18. - (a) Radial motion coordinates of journal relative to bearing, referenced to static equilibrium state (W = static load); (b) Harmonic orbital motion of journal relative to bearing; $x = x_O \sin(\Omega t + \Theta_X)$; $y = y_O \sin(\Omega t + \Theta_Y)$.

[13]Department of Mechanical and Aerospace Engineering, Case Western Reserve University, Cleveland, OH.

written as

$$dh/d\eta = [(\bar{x} \sin(\eta/R) - \bar{y} \cos(\eta/R)]/R \quad [95]$$

$$dh/d\bar{t} = -\bar{x} \cos(\eta/R) - \bar{y} \sin(\eta/R) \quad [96]$$

Clearly, in this case, the instantaneous pressure distribution and, thus, the instantaneous journal-bearing separating force are determined by the instantaneous position and velocity vectors (x, y) and $(\dot{x}, \dot{y})$, respectively, and thus, has no memory feature. With no memory, the eight stiffness and damping coefficients are functions only of the static equilibrium flow field, e.g., for purely laminar flow, a function of bearing Sommerfeld number only.

When cavitation is admitted into the problem, the longstanding approach is to require $p = p_{vap}$ and $\bar{\nabla}p \cdot \bar{n} = 0$ (to conserve mass flow) at the interface boundary separating the full-film region, in which Eq. [93] is solved, and the cavitated region, in which all pressures are set equal to the vapor pressure, p_{vap}. With this approach to cavitating bearings, the solution again leads to rotordynamic coefficients that are functions of the static equilibrium flow field only. While this approach to cavitating bearings is probably an acceptable characterization for static load capacity predictions, it has, unfortunately, been extended, with little questioning, to the rotor-dynamic coefficients. If closely scrutinized, the approach for cavitating bearings is found to satisfy mass conservation only within the full-film region and on its boundaries but not within the cavitated or ruptured region. In essence, this approach functions within a rotordynamic context in the following loosely worded manner: whenever the right-hand side of the Reynolds equation gives the command, the left-hand side instantly becomes activated to allow the generation of local film pressures, whether or not the fluid has had time to refill the local gap.

In fact, the actual system is quite transient or memory-like, as shown by the computations of Elrod and Adams (14), who employed a time-transient solution scheme which properly accounted for mass conservation throughout the bearing clearance gap. Thus, even in the absence of fluid inertia, a dynamically loaded cavitating journal bearing can exhibit inertia-like effects. And these effects can be expected to become progressively more important as vibration frequency is increased. This is quite similar to compressibility effects.

A more complete discussion of this and related topics is given in (59). For the purpose of this discussion, it is simply concluded that the memory or frequency effects of cavitation on bearing rotordynamic characteristics is important.

CAVITATION IN JOURNAL BEARINGS AND SQUEEZE-FILM DAMPERS: ANALYTICAL

B. JACOBSON[15]

Cavitation boundary conditions for stationary and vibrating journal bearings have been discussed in the literature for more than 30 years. The Swift-Stieber condition for the start of the cavitation region has been used both for stationary bearings and whirling bearings where the minimum film thickness is constant and the speed of the cavitation zone is less than the mean value of the surface speeds. A more accurate boundary condition for the start of the cavitation zone was given by Floberg where the number of streamers per unit width in the cavitation zone determined the amount of subcavity pressure in front of the cavitation zone. The most frequently used outlet boundary condition for the cavitation zone is the JFO (Jakobsson, Floberg, Olsson) condition, which says that the oil flow going into the cavitation region is transported straight through it without side flow and that there is continuity of mass flow at the end of the cavitation region.

THE DIFFERENCE BETWEEN VAPOR AND GAS CAVITATION

Whereas the pressure in a vapor bubble is almost totally given by the temperature, the pressure in a gas bubble increases rapidly according to the gas law as the volume of the bubble decreases. The transport of gas into and away from a bubble is a slow process, as can be clearly seen from the cavitation films where it often takes hundreds of vibrations before the gas cavitation pattern stabilizes. If the gas transport into and out of the bubble is neglected, the bubble pressure can easily be calculated using a polytropic compression, i.e., midway between an isothermal and an adiabatic compression. This gives a radius ratio of 0.2 for a flat bubble when its pressure is increased 100 times. Therefore, if the bubble contains air, it will be visible in the high-pressure zone of the bearing. Vapor bubbles, on the other hand, collapse within milliseconds of formation.

ANALYSIS OF VAPOR CAVITATION

A simple model of the vapor cavitation behavior in dynamically loaded journal bearings is to assume the pressure to be constant during the collapse of the bubble. This means that the vapor condenses at the same rate as the bubble wall moves. For a spherical bubble, this gives the collapse velocity as

$$V = \frac{h_c \Delta T_{v,l}}{\ell_v \rho} \qquad [97]$$

and for a flat bubble with the radius r in an oil film of the thickness h,

$$V = \frac{h_c \Delta T_{v,l}(h + r)}{\ell_v \rho h} \qquad [98]$$

where h_c is the film coefficient of heat transfer for condensing oil vapor at low flow velocity, ℓ_v is the heat of evaporation for oil, and $\Delta T_{v,l}$ is the temperature drop from vapor to liquid oil.

For a 10-mm-diameter, flat bubble in a 20-μm oil film and with $\rho = 6\times10^{-6}$ kg/m^3, $h_c = 600$ W/m^2·°C, $\ell_v = 350$ kJ/kg, and the collapse velocity $V = 5$ m/s, the temperature drop needed from the vapor to the oil $\Delta T_{v,l} = 7.0\times10^{-5}$ °C. This means that the vapor bubbles collapse almost without any resistance.

CAVITATION FORMATION

By changing the coordinate system for the vibrating bearing to a system rotating with the same speed as the minimum oil film thickness, the right-hand side of the Reynolds equation can be simplified for times close to the instant the minimum oil film thickness has its lowest value. The right-hand side of the Reynolds equation for the geometry of the vibrating bearing is then simplified to

$$\lambda = C \cdot \sin\theta \left[\frac{\omega_s(\varepsilon_s + \varepsilon_d)}{2} - \varepsilon_d \omega_d\right] \qquad [99]$$

For close to zero minimum oil film thickness, $\varepsilon_s + \varepsilon_d \to 1$, and the criterion for the formation of vapor cavitation is simply

$$\varepsilon_d > \frac{\omega_s}{2\omega_d} \qquad [100]$$

Just as was mentioned in the experimental results, a high rotating speed ω_s of the journal stops the vapor cavitation (see also (24)). This is easily seen as ε_d must always be less than 1.

CAVITATION COLLAPSE

Once vapor cavitation has been formed and some time has passed, the minimum oil film thickness increases, and the atmospheric pressure at the edges of the bearing becomes important for consideration of the collapse of the vapor cavitation bubbles. The side flow induced by the atmospheric pressure at the bearing edges increases with the third power of the oil film thickness. The high-speed films showed that the bubble collapse is mainly governed by this side flow. A simple short bearing type of analysis can give the criterion for when the bubble reaches its maximum width and starts to collapse. This happens when

[15]Chalmers University of Technology, Göteborg, Sweden, and SKF Engineering and Research Centre, Nieuwegein, The Netherlands.

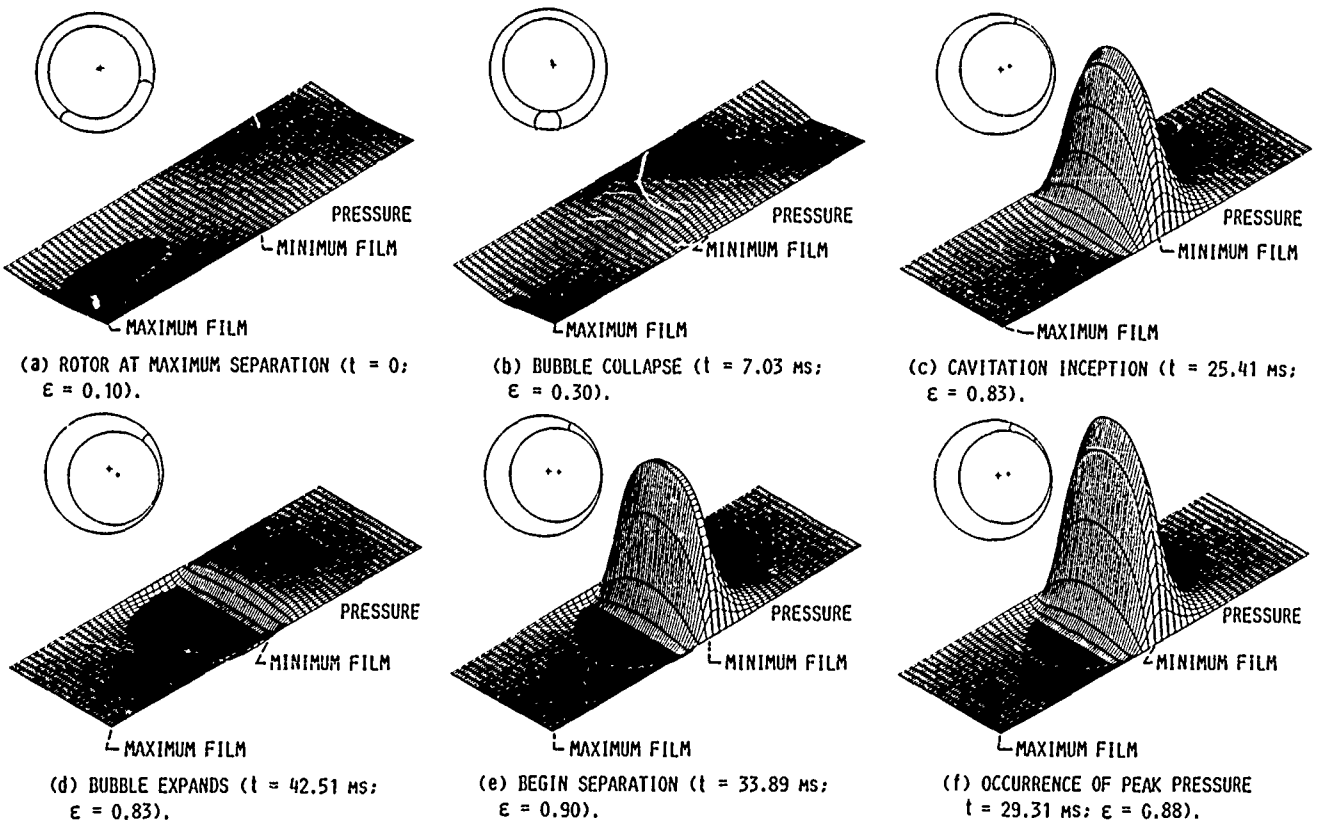

(a) ROTOR AT MAXIMUM SEPARATION (t = 0; ε = 0.10).

(b) BUBBLE COLLAPSE (t = 7.03 ms; ε = 0.30).

(c) CAVITATION INCEPTION (t = 25.41 ms; ε = 0.83).

(d) BUBBLE EXPANDS (t = 42.51 ms; ε = 0.83).

(e) BEGIN SEPARATION (t = 33.89 ms; ε = 0.90).

(f) OCCURRENCE OF PEAK PRESSURE t = 29.31 ms; ε = 0.88).

Fig. 19. - Pressure distribution and bearing configuration for a full period of shaft whirl ($0.1 \leqq \varepsilon \leqq 0.9$). Figures (a) to (f) viewed clockwise are consecutive in time.

$$\frac{(U_a + U_b)}{2} \frac{\partial h}{\partial x} + \frac{\partial h}{\partial t} < \frac{h^3}{6\mu} \frac{(p_o - p_c)}{(z_m - z_c)^2} \qquad [101]$$

If the cavitation collapse takes place in the same location many times, it will result in cavitation erosion damage on the journal and the bearing.

NUMERICAL-THEORETICAL CALCULATIONS OF VAPOR CAVITATION

The appearance and motion of the cavitation zone and its boundaries can be studied using numerical methods. This was done using a computer program (7) in which Elrod's algorithm for the continuity of mass flow into, through, and out of the vapor cavitation zone was used. This program makes it possible to predict the dynamic behavior of the vapor cavitation zone. The Cray computer at NASA Lewis Research Center was used to do the computations. The boundary condition for the vapor cavitation zone was the pressure equal to zero, which is consistent with the earlier experimental results. This was used together with Elrod's algorithm to make sure that the continuity of mass flow was maintained, both in the full oil film and in the cavitation zone, during the whole vibration cycle. Some numerically calculated pressure distributions and cavitation regions (23) are shown in Fig. 19. A comparison with the experimental results shows similar behavior for the experimental cavitation zone and the theoretically calculated zone, even if the size of the experimental cavitation zone is slightly smaller. This can be partly explained by elastic distortion of the PMMA tube.

CONCLUSIONS

Vapor cavitation occurs when the tensile stress applied to the oil exceeds the tensile strength of the oil or the binding of the oil to the surface. The physical situation necessary for vapor cavitation to exist is a squeezing and sliding motion in a bearing. The implication of the results as they apply to squeeze film dampers is that if the sliding velocity is increased, the occurrence of vapor cavitation is decreased (see also (24)).

Vapor cavitation bubbles collapse at pressures lower than the atmospheric pressure, and they cannot be transported through a high pressure zone of the bearing, unlike gas cavitation bubbles.

The numerical calculations (23) of the cavitation bubble dynamics show that an increasing vibration amplitude gives:

- Longer vapor bubble life
- Larger maximum vapor bubble size
- Earlier start and later collapse of the vapor bubble.

REFERENCES

1. Jakobsson, B., and Floberg, L., "The Finite Journal Bearing, Considering Vaporization", Trans. Chalmers Univ. Technology, 190, Göteborg, Sweden (1957).

2. Dowson, D., and Taylor, C.M., "Cavitation in Bearings," Annual Reviews of Fluid Mechanics, Vol. 11, edited by M. Van Dyke, J.V. Wehausen, and J.L. Lumley, Annual Reviews Inc., Palo Alto, CA, pp. 35-66(1979).

3. Horsnell, R., and McCallion, H., "Prediction of Some Journal-Bearing Characteristics Under Static and Dynamic Loading," Lubrication and Wear, Institute of MechanicalEngineers, New York, pp. 126-138 (1963).

4. Newkirk, B.L., "Shaft Whipping," General Electric Review, 27, pp. 169-178 (1924).

5. Badgley, R.H., and Booker, J.F., "Turborotor Instability: Effect of Initial Transients on Plane Motion," J. Lubr. Technol., 91, pp. 624-633 (1969).

6. Kirk, R.G., and Gunter, E.J., "Short Bearing Analysis Applied to Rotor Dynamics, Part I: Theory," J. Lubr. Technol., 98, pp. 47-56 (1976).

7. Brewe, D.E., "Theoretical Modeling of the Vapor Caviation in Dynamically Loaded Journal Bearings," J. Tribology, 108, pp. 628-638 (1986) and NASA TM-87076 or USAAVSCOM-TR-85-C-15.

8. Olsson, K., "Cavitation in Dynamically Loaded Bearings," Trans. Chalmers Univ. Technology, Göteborg, Sweden, 308, (1965).

9. Olsson, K.O., "On Hydrodynamic Lubrication with Special Reference to Nonstationary Cavitation," Trans. Chalmers Univ. Technology, Göteborg, Sweden, 1974.

10. Coyne, J.C., and Elrod, H.G., Jr., "Conditions for the Rupture of a Lubricating Film - Part II: New Boundary Conditions for Reynolds Equation," J. Lubr. Technol., 93, pp. 156-167 (1971).

11. Etsion, I., and Ludwig, L.P., "Observation of Pressure Variation in the Cavitation Region of Submerged Journal Bearings," J. Lubr. Technol., 104, pp. 157-163 (1982).

12. Pan, C.H.T., "Dynamic Analysis of Rupture in Thin Fluid Films. I - A Noninertial Theory," J. Lubr. Technol., 105, pp. 96-104 (1983).

13. Jacobson, B.O., and Hamrock, B.J., "Vapor Cavitation in Dynamically Loaded Journal Bearings," NASA TM-83366 (1983).

14. Elrod, H.G., and Adams, M.L., "A Computer Program for Cavitation and Starvation Prob Cavitation and Related Phenomena in Lubr tion, edited by D. Dowson, M. Godet, and C.M. Taylor, Mechanical Engineering Publications, England, pp. 37-41 (1974).

15. Elrod H.G., "A Cavitation Algorithm," J. Lubr. Technol., 103, pp. 350-354 (1981).

16. Rowe, W.B., and Chong, F.S., "A Computational Algorithm for Cavitating Bearings," TRIBOLOGY INTERNATIONAL, Vol. 17, No. 5, October (1984), pp. 243-250.

17. Miranda, A.A.S., "Oil Flow, Cavitation and Film Reformation in Journal Bearings Including Interactive Computer-Aided Design Study," Ph.D. Thesis, Univ. of Leeds, U.K. (1983).

18. Dowson, D., Taylor, C.M., and Miranda, A.A.S., "The Prediction of Liquid Film Journal Bearing Performance with a Consideration of Lubricant Film Reformation, Part I: Theoretical Results," Proc. Inst. Mech. Eng. C - Mech. Eng. Sci., 199, pp. 95-102 (1985).

19. Dowson, D., Miranda, A.A.S., and Taylor, C.M., "Implementation of an Algorithm Enabling the Determination of Film Rupture and Reformation Boundaries in a Liquid-Film Bearing," Developments in Numerical and Experimental Methods Applied to Tribology, D. Dowson, C.M. Taylor, M. Godet, and D. Berthe, Butterworths, pp. 60-70 (1984).

20. Vaidyanathan, K., and Keith, T.G., "Numerical Prediction of Cavitation in Noncircular Journal Bearings," STLE Preprint 88-AM-1D-2 (1988).

21. Lebeck, A.O., Teale, J.L., and Pierce, R.E., "Hydrodynamic Lubrication with Wear and Asperity Contact in Mechanical Face Seals," ME-86(78), ONR-414-1, Bureau of Engineering Research, Univ. of New Mexico, Albuquerque, NM (1978) (Avail. NTIS, AD-A050783).

22. Brewe, D.E., Hamrock, B.J., and Jacobson, B.O., "Theoretical and Experimental Comparison of Vapor Cavitation in Dynamically Loaded Journal Bearings," NASA TM-87121 USAAVSCOM-TR-85-C-19 (1986).

23. Brewe, D.E., and Jacobson, B.O., "The Effect of Vibration Amplitude on Vapor Cavitation in Journal Bearings," Wear, 115, pp. 63-73 (1987) (also, NASA TM-88826 or USAAVSCOM-TR-86-C-26).

24. Brewe, D.E., and Khonsari, M.M., "Effect of Shaft Frequency on Cavitation in a Journal

Bearing for Noncentered Circular Whirl," Tribology Trans., 31, pp. 54-60 (1988). (Also, NASA TM-88925 or USAAVSCOM-TR-86-C-41).

25. Woods, C.M. and Brewe, D.E., "The Solution of the Elrod Algorithm for a Dynamically Loaded Journal Bearing Using Multigrid Techniques," J. Tribology, 111, pp. 302-308 (1989). (Also, NASA TM-120941 or AVSCOM-TR-88-C-006).

26. Brewe, D.E., "Elasticity Effects on Cavitation in a Squeeze Film Damper Undergoing Non-Centered Circular Whirl," Wear, 130, pp. 69-80 (1989).

27. Anderson, D.A., Tannehill, J.C., and Pletcher, R.H., Computational Fluid Mechanics and Heat Transfer, Hemisphere Publishing Corp , pp. 302-305 (1984).

28. Vijayaraghavan, D., and Keith, T.G., Jr., "Development and Evaluation of a Cavitation Algorithm," Tribology Trans., 32, pp. 225-233 (1989).

29. Dowson, D., Godet, M., and Taylor, C.M., Cavitation and Related Phenomena in Lubrication, Mechanical Engineering Publication Ltd., England (1974).

30. Booker, J.F., "Basic Equations for Fluid Films with Variable Properties," J. Tribology, in press, 1989.

31. Booker, J.F., and Huebner, K.H., "Application of the Finite Element Methods to Lubrication: An Engineering Approach," J. Lubr. Technol., 94, pp. 313-323 (1972).

32. Goenka, P.K., and Booker, J.F., "Effect of Surface Ellipticity on Dynamically Loaded Cylindrical Bearings," J. Lubr. Technol., 105, pp. 1-12 (1983).

33. Goenka, P.K., and Booker, J.F., "Spherical Bearings: Static and Dynamic Analysis via the Finite Element Method," J. Lubr. Technol., 102, pp. 308-319 (1980).

34. Kostreva, M.M., "Elasto-Hydrodynamic Lubrication: A Nonlinear Complementarity Approach," Int. J. Numer. Methods Fluids, 4, pp. 377-397 (1984).

35. Oh, K.P., "The Numerical Solution of Dynamically Loaded Elastohydrodynamic Contact as a Nonlinear Complementarity Problem," J. Tribology, 106, pp. 88-95 (1984).

36. Goenka, P.K., "Dynamically Loaded Journal Bearings: Finite Element Method Analysis," J. Tribology, 106, pp. 429-439 (1984).

37. LaBouff, G.A., and Booker, J.F., "Dynamically Loaded Journal Bearings: A Finite Element Treatment for Rigid and Elastic Surfaces," J. Tribology, 107, pp. 505-515 (1985).

38. Swift, H.W., "Fluctuating Loads in Sleeve Bearings," J. Inst. Civ. Eng., No. 4, pp. 161-195 (1937).

39. Lohou, J., "Hydrodynamique des Joints d'Etancheite du Type Radial," Thesis, Mecanique, Univ. Lyon 1, 1970.

40. Rhode, S.M., and McAllister, G.T., "A Variational Formulation for a Class of Free Boundary Problem Arising in Hydrodynamic Lubrication," Int. J. Eng. Sci., 13, pp. 841-850 (1975).

41. Cimatti, G., and Menchi, O., "On the Numerical Solution of a Variational Inequality Connected with the Hydrodynamic Lubrication of a Finite Journal Bearing," Calcolo, 15, pp. 249-258 (1978).

42. Bayada, G., and Du Parquet, J., "The Influence of the Operating Parameters on the Cavitation Frontiers in a Dynamically Loaded Narrow Journal Bearing," Cavitation and Related Phenomena in Lubrication, edited by D. Dowson, M. Godet, and C.M. Taylor, Mechanical Engineering Publications, England, pp. 101-108 (1974).

43. Strozzi, A., "Formulation of Three Lubrication Problems in Terms of Complementarity," Wear, 104, pp. 103-119 (1985).

44. Bayada, G., and Chambat, M., "Analysis of a Free Boundary Problem in Partial Lubrication," Quart. Appl. Math., 40, pp. 369-375 (1983).

45. Findlay, J.A., "Cavitation in Mechanical Face Seal," J. Lubr. Technol., 90, pp. 356-364 (1968).

46. Bayada, G., and Chambat, M., "Sur Quelques Modelisations de la Zone de Cavitation en Lubrification Hydrodynamique," J. Mec. Theor. Appl., 5, pp. 703-729 (1986).

47. El Alaoui Talibi, M., "Sur un Probleme a Frontiere Libre en Mecanique des Films Minces," Thesis, Math Univ. Lyon 1, 1986.

48. Sirivat, A., Rajagopal, K.R., and Szeri, A.Z., "An Experimental Investigation of the Flow of Non-Newtonian Fluids Between Rotating Disks," J. Fluid Mech., 186, pp. 243-256 (1988).

49. Szeri, A.Z., and Rajagopal, K.R., "Flow of a Non-Newtonian Fluid Between Heated Parallel Plates," Int. J. Non-Linear Mech., 20, pp. 91-101 (1985).

50. Kacou, A., Rajagopal, K.R., and Szeri, A.Z., "Flow of a Fluid of the Differential Type in a Journal Bearing," J. Tribology, 109, pp. 100-107 (1987).

51. Kacou, A., Rajagopal, K.R., and Szeri, A.Z.A., "A Thermodynamic Analysis of Journal Bearings Lubricated by a Non-Newtonian Fluid," J. Tribology, 110, pp. 414-420 (1988).

52. Truesdell, C., and Noll, W., Handbuch der Physik, Vol. 3, Pt. 3, Non-Linear Field Theories of Mechanics, edited by S. Flugge, Springer-Verlag (1965).

53. Ng, C.W., and Saibel, E., "Nonlinear Viscosity Effects in Slider Bearing Lubrication," J. Basic Eng., 84, pp. 192-196 (1962).

54. Bourgin, P., and Gay, B., "Determination of the Load Capacity of a Finite Width Journal Bearing by a Finite-Element Method in the Case of a Non-Newtonian Lubricant," J. Tribology, 106, pp. 285-290 (1984).

55. Buckholz, R.H., "Effects of Power-Law, Non-Newtonian Lubricants on Load Capacity and Friction for Plane Slider Bearings," J. Tribology, 108, pp. 86-91 (1986).

56. Benjamin, T.B., and Mullin, T., "Anomalous Modes in the Taylor Experiment," Proc. Roy. Soc. Lond. A, 377, pp. 221-249 (1981).

57. Dowson, D., Ruddy, A.V., Sharp, R.S., and Taylor, C.M., "An Analysis of the Circumferentially Grooved Journal Bearing With Consideration of Lubricant Film Reformation," Proc. Inst. Mech. Eng. C - Mech. Eng. Sci., 199, pp. 27-34 (1985).

58. Pan, C.H.T., "An Improved Short Bearing Analysis for the Submerged Operation of Plain Journal Bearings and Squeeze-Film Dampers," J. Lubr. Technol., 102,pp. 320-332 (1980).

59. Adams, M.L., "Insights Into Linearized Rotor Dynamics, Pt. 2," J. Sound Vibration, 112, pp. 97-110 (1987).

60. Kumar, A., and Booker, J.F., "A Finite Element Cavitation Algorithm," to be published in ASME J. of Tribology.

PART III

EDITORS SUMMARY

The following discussion summarizes the major issues brought out by the contributors as these issues relate to present technological requirements. At the risk of appearing myopic, the editors have taken the liberty to occasionally emphasize the importance of the work, what has been resolved, and what needs to be done.

Many of the articles focused on cavitation as it pertained to a broad list of applications in crankshaft bearings, rotordynamics, slider bearings, and seals. The key issue is the dynamic loading. As pointed out in the introduction to Part II, dynamic loading causes changes in the local film thickness, which leads to nonstationary cavitation. This certainly plays an important role in determining rotordynamic characteristics. Adams' discussion amplifies this topic, especially concerning the effect of frequency. Adams draws the analogy that nonstationary cavitation can exhibit "inertia-like effects" and that these effects can be expected to become progressively more important as vibration frequency is increased. Of course, this is only one example of many where nonstationary cavitation is likely to have a significant effect on the rotordynamic characteristics. Jacobson discusses the effect of deformation, vibrational amplitude, surface tension, and sliding velocity on vapor bubble inception, size, life, and collapse. Both inception and collapse play an important role in the bubble dynamics which, in turn, affects rotordynamic behavior.

As pointed out by Launay, dynamic loading is the primary concern in the design of journal bearings of automotive engines. Here, operation with an incomplete film is typical in such bearings, and one strives to maintain an adequate film while keeping the friction as low as possible. In the case of diesel engines, the combustion conditions can become more severe (i.e., higher rates of change of cylinder pressure), resulting in cavitation erosion damage to the bearings. Martin discusses the work on this subject by Garner, James, and Warriner (52). He includes examples of typical cavitation erosion damage, together with a plausible mechanism of damage. Commonly applied paliiatives and their effectiveness, based on engine experience, are also discussed. It was concluded that cavitation erosion damage resulted from three main causes. Two were related to oil-column inertia effects in the connecting rod drillings, crankshaft drillings, and bearing oil feed features. These were obviated by simple modifications to the detail design. The third, related to journal movements within the bearing clearance space, posed a more difficult problem. Martin indicated that a more detailed theory than that used in their analysis was needed to reliably predict damage for the design stage.

Of course, cavitation effects are not limited to journal bearings and squeeze-film dampers. In a seal or slider application, Lebeck describes a mechanism in which cavitation is used to advantage. The asperities in parallel sliders were hypothesized to produced load support by virtue of the fact that cavitation developed at the downstream side of the asperity. In the presence of cavitation there is a net load support for individual asperities and, hence, for the parallel slider.

The above articles dealt mainly with cavitation effects in various applications, especially where it concerned dynamic operating conditions. In order to gain insight and provide better design through numerical modeling for these applications, we must identify the modes of cavitation associated with different dynamical conditions. For example, in the introduction to Part I we distinguished between gaseous and vaporous cavitation, but in actual practice both may occur together unless definitive steps are taken to preclude one or the other (i.e., degassing the fluid so that only vapor cavitation can occur or pressurizing the fluid so that vapor pressures are not possible). Jacobson elaborates on some of the noted differences between vapor and gaseous cavitation in Part II. Parkins' article on the "Categorization of Cavitation Types and Onset Conditions" is a beginning in understanding the conditions under which one or the other might dominate. The categorizations in this article were based on sustained oscillatory squeeze motion - simplified by removing the translational component. Three cavitation regimes - including subregimes - were identified and characterized according to the method of feeding the bubble. It was noted that cavitation bubbles fed from within the film could be either gaseous or vapor. Cavitation bubbles fed from outside the film obviously were gaseous (e.g., refer to the proposition of "side entrainment of gas," by Heshmat) and took several forms. Three of these forms were leaf type patterns, and the fourth appeared as smoothly curved bubbles entering from all sides of the square plate. Certain regimes were observed to coexist. Parkins indicates that "a limited knowledge is available about the conditions which determine the onset of a particular regime or subregime and its transformation into another subregime. The large number of possible forms of behavior make a confused picture when observed over a small range of variables, which renders it difficult to formulate classifications." In the editors' opinions, this work deserves an expanded effort in which classification according to methods of feeding the bubble should be looked at with the translational component as well. It is only through the classification procedure that we can hope to bring order to this "confused picture," thereby providing a basis upon which analysts can formulate appropriate models.

We have already noted the importance of bubble dynamics in rotordynamic behavior. Bubble dynamics is a complicated subject in itself. The dynamics of the bubble can be affected by

the gas and vapor content (or fractional film content within the bubble) as well as by trans-cavity flow rate or fluid propagation speed within the bubble. The propagation speed of the fluid through the bubble depends on the morphological condition of the bubble. Pan and Frene discuss this issue with regard to numerical modeling and implementing the transport process across the interface. They include the possibilities that a portion of the void-dominated region is locally filled with liquid, bridging both surfaces, or that a thin liquid layer may be attached to either but not both surfaces (also see discussions by Heshmat by Barrett and Branagan in Part I). For the first possibility, the propagation speed of the fluid is assumed to be the average of the two surface speeds. But for the latter possibility, the fluid takes on the speed of the surface to which it becomes attached. In the case of the journal bearing, one might argue that fluid transport through the cavity influences the position, size, and life of the bubble. Consequently, it can have an effect on the load capacity (7) and, possibly, the stiffness and damping characteristics of the bearing. Knowledge is scant on the conditions that determine whether attachment is to one or both surfaces, although it is generally accepted that load is a determining factor. More work is needed to clarify this issue and the effect it has on bubble dynamics and, consequently, on rotordynamic performance.

The temperature effects on cavitation are an important consideration both from the standpoint of bubble dynamics and heat-transfer characteristics. Both Heshmat and Barrett and Branagan discussed temperature effects as it pertained to "hot-oil carry over" in padded bearings. Not surprisingly, it was noted by both that heat generation within the cavitation region was practically nonexistant. Barrett and Branagan compared theory with experiment. They found that treating the void region as a two-phase lubricant-gas in which the fluid attaches itself to the shaft was the most suitable model for the experiment considered. Further studies involving a wider range of operating conditions would be useful information to the analyst in modeling thermal effects on cavitation. Correctly predicting the apportionment of heat transfer to the shaft and housing is partly dependent on choosing the appropriate cavitation model. One other way in which thermal effects can affect cavitation is through the indirect changes in surface energy. In this context we refer to temperature effects on the wettability of the lubricant to the surface and the consequences to fluid transport through the bubble as well as heat transfer to the bearing and shaft material. Albeit, Szeri, Rajagapol, and Zhang (Part II) noted that journal bearings lubricated with non-Newtonian lubricants could be less susceptible to thermal effects when compared with bearings lubricated with Newtonian fluids.

Non-Newtonian effects on cavitation were further discussed by Szeri and shown to be important. That is, a shear thickening fluid cavitated within a range of material parameters, whereas the shear thinning fluid did not cavitate at all for the same parameter range. Furthermore, the change in material parameter for the shear thickening fluid affected the position of th rupture boundary to some extent. Since many of the lubricants used these days are non-Newtonian, it behooves us to learn much more about this phenomena.

Using high-speed photography, Jacobson and Hamrock (Part I) noted a clear influence of the surface energy of the journal surfaces on cavitation incipience. For steel journals, cavitation bubbles start in different parts of the low-pressure region, depending on where the largest bubble or dirt particle is located. For PTFE journals, the cavitation seems to start from the same position of the journal for each vibration, which indicates a rupture of the oil-PTFE interface. Presently, analytical models do not account for this phenomena.

This calls attention to the subject of numerical modeling. Most of the contributions to this subject have dealt with flow preserving schemes, numerical expedience, and some recent advances using finite-element schemes. In flow preserving schemes, the attention is naturally drawn to the more complex cavitation boundaries. With the advent of the Elrod algorithm, much of the complexity has been reduced while retaining the flow-preserving features of the JFO theory. Keith and Vijayaraghavan (Part II) present their version of the Elrod algorithm in the context of gas dynamics. Borrowing concepts used in modeling transonic flow through a duct, an artificial viscosity term is introduced that implements the "type differencing" employed. The two schemes are equivalent, but the artificial viscosity plays an opposite role to Elrod's switch function. Their formulation was instructive and not unlike the modeling viewpoint of Pan and Frene (see discussion on Rankine-Hugoniot conditions in Part II), although Pan and Frene's treatment is more general in that it accomodates any one of three types of fluid transport within the cavitation boundary. Frene, Launay, and Pan illustrate the use of the equivalent Rankine-Hugoniot conditions for a centrally fed journal bearing using short bearing theory. The analogy drawn between the shock wave and the cavitation interface is constructive since it forms a basis of communication and progress in either field can be shared.

As our models become more complex, the search for simpler more efficient programing techniques becomes essential. Tichy and Ku (Part II) describe a solution procedure for a squeeze-film damper bearing with two circumferential oil supply grooves at the bearing ends undergoing circular-centered whirl. In this

procedure a large amount of numerical work is saved and not too much accuracy is lost. Numerical results for centerline pressure and cavity shape using finite-element methods compared favorably.

This brings us to our last topic of discussion, employing finite-element methods in lubrication problems in which cavitation occurs. Because of the ease in programing and adaptability to the high-speed super computers, finite-difference schemes are most often used. However, from the standpoint of handling irregular boundaries, the finite-element method is well suited to dealing with cavitation. In Part II Booker discusses several mathematical models commonly used to incorporate cavitation in the finite-element analysis of lubrication. The models are classic in that they are not flow-preserving. Until recently, this has been an obstacle to achieving a physically realistic solution to transient problems. Bayada (Part II) discusses a two-dimensional analysis using FEM in which mass conservation is treated in a way that is consistent with that proposed by Elrod (14) or the equivalent Rankine-Hugoniot condition at the interface. The procedure was applied to a seal (46) using rectangular finite elements. The discrepancy between input mass flow and output mass flow never exceeded 4 percent in each period. As of this writing, Booker (59) has achieved a flow-preserving FEM scheme applied to journal bearings in three dimensions.

To sum up, the experimenter must continue to help perceive the order in a very complex phenomena. This can be done by extensive classification and clarification of unresolved issues using carefully planned experiments. The numerical analyst find themselves on a tortuous journey to realism in which all of the effects of temperature, misalignment, deflections, local deformations, surface energy, and lubricant rheology, to name only a few, must eventually be included in the computational models. To make this possible, the analysts must bring to bear the latest numerical advances, keeping abreast of new developments in related fields. Algorithms that incorporate all of the latest techniques in finite differencing as well as finite elements to shorten computational times are needed. In addition, these same algorithms must lend themselves to employing the latest computer architecture, i.e., pipeline and parallel processing.

NASA
National Aeronautics and Space Administration

Report Documentation Page

1. Report No.	2. Government Accession No.	3. Recipient's Catalog No.
NASA TM-103184 AVSCOM TM 89-C-007		

4. Title and Subtitle

Current Research in Cavitating Fluid Films

5. Report Date

6. Performing Organization Code

7. Author(s)

8. Performing Organization Report No.

E-4924

9. Performing Organization Name and Address

NASA Lewis Research Center
Cleveland, Ohio 44135-3191
and
Propulsion Directorate
U.S. Army Aviation Systems Command
Cleveland, Ohio 44135-3191

10. Work Unit No.

510-01-1B

11. Contract or Grant No.

13. Type of Report and Period Covered

Technical Memorandum

12. Sponsoring Agency Name and Address

National Aeronautics and Space Administration
Washington, D.C. 20546-0001
and
U.S. Army Aviation Systems Command
St. Louis, Mo. 63120-1798

14. Sponsoring Agency Code

15. Supplementary Notes

Prepared for the Cavitation Symposium—1988 Society of Tribologists and Lubrication Engineers Annual Meeting, Cleveland, Ohio, May 9-12, 1988.
Editors: D.E. Brewe, U.S. Army Propulsion Directorate, Lewis Research Center; J.H. Ball, Waukesha Bearings Corp., Waukesha, Wisconsin; and M.M. Khonsari, University of Pittsburgh, Pittsburgh, Pennsylvania.
Also available as STLE SP-28.

16. Abstract

The 1988 Society of Tribologists and Lubrication Engineers Annual Meeting held a two session symposium on cavitation in fluid films. This paper is an edited review of the current research as discussed by the invited participants. Phenomena and experimental observations included gaseous cavitation, vapor cavitation, and gas entrainment. Cavitation in flooded, starved, and dynamically loaded journal bearings, as well as squeeze film dampers was reviewed. Observations of cavitation damage in bearings and the possibility of cavitation between parallel plates with microasperities were discussed. The session on theoretical modeling summarized the transcavity fluid transport process, meniscus motion and geometry or form of the film during rupture, and reformation. Performance effects were related to heat-transfer models in the cavitated region and hysteresis influences on rotor-dynamics coefficients. Contributors presented a number of cavitation algorithms together with solution procedures using the finite-difference and finite-element methods. Although Newtonian fluids were assumed in most of the discussions, the effect on non-Newtonian fluids on cavitation was also discussed. An executive summary is provided by the editors discussing the major issues brought out by the contributors as these relate to present technological requirements. The importance of the work, what has been resolved, and what needs to be done are discussed therein.

17. Key Words (Suggested by Author(s))	18. Distribution Statement
Cavitation; Fluid films; Vapor cavitation; Gaseous cavitation; Journal bearings; Squeeze film dampers; Bearings; Seals; Numerical modeling; Theory; Analysis	Unclassified—Unlimited Subject Category 34

19. Security Classif. (of this report)	20. Security Classif. (of this page)	21. No. of pages	22. Price*
Unclassified	Unclassified	68	A04

NASA FORM 1626 OCT 86

*For sale by the National Technical Information Service, Springfield, Virginia 22161